CSIRO Marine Laboratories
Report No. 211

Design of an Ocean Temperature Observing Network in the Seas North of Australia

Part II

Tropical Indian Ocean: Statistics

Helen Phillips
Rick Bailey
Gary Meyers

1990

CSIRO Marine Laboratories Report No. 211

Design of an Ocean Temperature Observing Network in the Seas North of Australia

Part II Tropical Indian Ocean: Statistics

Helen Phillips
Rick Bailey
Gary Meyers

CSIRO Division of Oceanography
Marine Laboratories
GPO Box 1538
Hobart, Tasmania 7001
Australia

Abstract

This report is a compilation of the statistical data required for design of an ocean temperature observing network in the Indian Ocean using the method of optimum interpolation (OI). The statistics were estimated from expendable bathythermograph observations on the shipping routes La Réunion–Red Sea; Fremantle–Red Sea; Fremantle–Persian Gulf; Fremantle–Sunda Strait; Port Hedland–Japan and Flores Sea–Banda Sea. The temporal and spatial autocorrelation function (ACF) for the sea-surface temperature and depth of the 20°C isotherm were estimated at each degree longitude on the Flores Sea–Banda Sea route and at each degree latitude for each of the other routes.

The ACF statistics permit estimation of the parameters required for OI: levels of signal and noise variance for each field and spatial/temporal decorrelation scales. The OI parameters are then summarised in large areas to represent the major currents.

National Library of Australia Cataloguing-in-Publication

Phillips, Helen.
Design of an ocean temperature observing network in the seas north of Australia. Part II, Tropical Indian Ocean: statistics.

ISBN 0 643 05033 7.

1. Ocean temperature – Indian Ocean – Measurement. 2. Ocean temperature – Indian Ocean – Statistics. I. Bailey, R. J. (Richard john). II. Meyers, Gary. III. CSIRO. Marine Laboratories. IV. Title: Tropical Indian Ocean: statistics. (Series: Report (CSIRO. Marine Laboratories); no. 211).

551.4601

I. Introduction

A network for observing ocean temperature has been established under the auspices of the World Climate Research Program/Tropical Oceans and Global Atmosphere Program (WCRP, 1985). The objectives are: to document and describe thermal variability in sufficient detail to understand the processes that control it, and to obtain the thermal data required to initialise dynamical models for prediction of climate. Ideally, the network should resolve thermal variability in the open ocean, with spatial scales larger than 100 km (meridional) by 1000 km (zonal), and time scales greater than one month. Smaller resolution is required in some boundary regions (such as the western boundaries, the equator and passages of Indonesian throughflow). The Implementation Plan prepared by the international TOGA Project Office (ITPO, 1987) requires an accuracy 0.25°C for temperature measurements at these scales. This report is the second part of a series that will assemble the statistical information required to design and optimise sampling in the area that has the greatest control over Australian climate. The first (Meyers et al., 1989) was concerned with statistical structure of the tropical Pacific Ocean. The third part develops sampling guidelines; it has been submitted for publication in *Progress in Oceanography*.

Plans for the TOGA ocean temperature observing network (ITPO, 1987) called for three methods of thermal data collection: (1) expendable bathythermograph (XBT) by ships-of-opportunity; (2) fixed temperature moorings with sensors in the upper 200–500 m; and (3) satellite-tracked drifting buoys, with sensors either in the upper 200 m or at the surface only. The first step was to make maximum use of ships-of-opportunity (i.e. voluntary observing ships from the Merchant Marine), because this is the most cost-effective method of obtaining coverage of large areas. The second step was to deploy temperature moorings wherever continuous time-series might be required, such as near the equator. Finally, drifting buoys would be deployed where prevailing currents would carry them into areas between ship-of-opportunity tracks. Some progress has been made since 1985, when TOGA began, in deploying all three methods. The network now needs to be optimised by finding the right mix of temperature sampling methods that are both cost-effective and accurate.

The standard method of determining a sampling strategy in oceanography is optimal interpolation (OI) (Gandin, 1963; Alaka and Elvander, 1972; Bretherton et al., 1976; White and Bernstein, 1979; White et al., 1982). Before this method can be applied, certain statistics of the field of interest — in this case either temperature or isotherm depth — must be known or estimated. The required statistics are: (1) variance of the signal of interest, (2) variance of the instrumental noise (usually negligible), or more importantly geophysical noise (i.e. unresolved thermal variability with scales smaller than the typical distance between XBT drops), and (3) spatial and temporal autocorrelation function (ACF) of the field of interest. If not known from theory, these statistics have to be determined from a data set — preferably one that has considerably oversampled the signals of interest.

The CSIRO Division of Oceanography started an XBT sampling network in the Indian Ocean in 1983, using volunteer merchant vessels.

This network collects XBT transects along the shipping routes Fremantle–Red Sea, Fremantle–Persian Gulf, Fremantle–Sunda Strait, Port Hedland–Japan and the east–west route across the Flores Sea–Banda Sea. By mid-1986 all of these tracks were in operation, and all were covered by at least 12 sections per year except Fremantle–Persian Gulf, which had only six. In addition to the CSIRO XBT data, data from the shipping route Réunion–Red Sea, from the TOGA Subsurface Data Centre archives, were also used for this study. Figure 1 shows the location of these tracks and the distribution of observations along each track, and Table 1 shows the number of observations made by each ship on each voyage. Note that the data available for this study covered a period of approximately two years for most of the Indian Ocean tracks. Although some of the time series are too short or sparse to fully resolve the signals being sampled, they can be used to estimate the optimum interpolation (OI) statistics, at least provisionally.

The OI statistics estimated with this data set are reported here. The mean and standard deviation of properties along each transect are presented in Section II. Estimates of the temporal/spatial ACF are presented in Section III. Decorrelation scales and signal-to-noise ratios are presented in Section IV. Finally, an attempt is made in Section V to summarise and schematicise the statistical structure across the tropical Indian Ocean.

The parameters selected for statistical analysis were: temperature at 3.5 m depth (called "sea-surface temperature" [SST]), vertically averaged temperature over 200 m and 400 m (called "T_{200}" and "T_{400}") and depth of the 25°C, 20°C and 15°C isotherms (called "D_{25}", "D_{20}" and "D_{15}"). This report presents a selection of the results, primarily as visual displays, and primarily for SST and D_{20}. Tabulated values of all the results were saved in computer-compatible format; they can be provided to interested users upon request.

It should be noted that the method used in this report differs slightly from Part I in that there were insufficient data in the Indian Ocean to exclude the 1986/1987 El Niño Southern Oscillation (ENSO) event. In Part I, for the Pacific Ocean, we estimated the statistics for both an ENSO period 1979–1983 and a non-ENSO period 1979–1982. We then used the non-ENSO statistics to provide the more stringent guidelines for network design. In the Indian Ocean, because of the problem of sparse data, all available observations were required to determine a preliminary estimate of the OI statistics. It is the intention of the authors to re-calculate the statistics once several more years' worth of observations have been collected.

II. Mean and Standard Deviation

The mean and standard deviation of temperature were calculated for each track (Figures 2–7). Relatively small gridding is needed in the Indonesian Seas to resolve small-scale boundary currents associated with the complex topography. The bins used for the Port Hedland–Japan track were half degree latitude between 10°S and 3°N and one degree latitude elsewhere; for tracks across the Flores

Sea–Banda Sea the bins were chosen to represent passages between islands, as shown in Figure 7C. For all other tracks in the open ocean one degree latitude bins were used.
Along the Port Hedland–Japan track the ships always travel northward in the open Pacific Ocean and southward in the Mindanao Current (Fig. 1). The mean sections along this track are shown for northbound and southbound voyages combined (Fig. 6a), northbound only (Fig. 6c) and southbound only voyages (Fig. 6d). As the standard deviation did not alter very much between the three alternative sets of data, only the northbound and southbound combined version is included (Fig. 6b).

It was noted by Stuart Godfrey that along the Fremantle–Persian Gulf route there was a maximum standard deviation on the equator at 120 m depth, while the Fremantle–Red Sea route showed no such maximum. This is a manifestation of the problem of sparse data on the Persian Gulf route; there were only 7 observations in the equatorial bin on this route.

III. Autocorrelation Functions

The methods used to estimate ACFs were discussed by Meyers et al., 1989.

a. Temporal Structure

The ACF for time-lags of 0.5 to 11.5 months was estimated for each degree latitude on the five meridional tracks and each degree longitude on the one zonal track. The temporal ACFs are displayed in groups of three for each degree latitude (longitude) for SST (Figs 8, 10, 12, 14, 16 and 18) and for D_{20} (Figs 9, 11, 13, 15, 17, and 19) for the six tracks. It should be noted that only northward cruises were used for the Port Hedland–Japan track in the region 5°N to 10°N so that scales estimated from these ACFs would reflect the conditions observed in the open ocean and not the Mindanao Current.

b. Spatial Structure

The meridional structure of ACFs is expected to be non-isotropic with respect to lags northward and southward as found in the Pacific Ocean (see Part I). Isotropy was not assumed in estimating the spatial ACFs so that non-isotropic structure could emerge where appropriate.

The ACF for latitude (longitude) lags of 1° to 6°, north and south (east and west), was estimated for each degree of latitude (longitude) on each track. The ACFs for SST are displayed in Figures 20–31; and for D_{20} in Figures 21, 23, 25, 27, 29 and 31 for the six tracks. Note that sparse sampling on the La Reunion–Red Sea and Fremantle–Persian Gulf routes causes more noise in the estimated ACFs for D_{20} (Figs 21 and 25) than on other routes.

IV. Signal-to-Noise Ratio and Decorrelation Scales

The statistics needed for OI can be derived from estimated ACFs presented in the previous section, after appropriate assumptions (Alaka and Elvander, 1972).

The squared signal-to-noise ratio (α^2) is the ratio of signal variance (S^2) to noise variance (N^2). It is calculated by extrapolating the estimated ACFs into the origin (Gandin, 1963, p. 30). Given the estimated value at the origin, μ_0, the ratio is:

$$\alpha^2 = \frac{\mu_0}{1-\mu_0} = \frac{S^2}{N^2}.$$

The value of μ_0 for this study was assumed to be the value of the temporal ACF (Section IIIA; Figures 8–19) in the first bin. Estimates of α for SST on each track are shown in Figure 32, and for D_{20} in Figure 33 (note that α, not α^2, is plotted). Again the noisy quality of the Fremantle–Persian Gulf route stands out.

The variance of instrumental and geophysical noise (N^2) and signal (S^2) can be estimated from α and the measured standard deviation (σ) of the parameter of interest:

$$S^2 = \mu_o \sigma^2$$
$$N^2 = \sigma^2 - S^2.$$

The instrumental noise is usually small for the temperature-sensing methods used by the TOGA network, so that N^2 is primarily associated with geophysical noise, such as eddies (which have a small space-scale) or weather events (which have a small time-scale).

The signals have scales larger than the bin sizes used in estimating the ACFs (i.e. 1 month and 1° latitude (longitude)).

The spatial structure of ACFs can be represented as a decorrelation scale, which is the typical size of coherent large-scale features. The spatial decorrelation scale was defined to be the e-folding scale measured on the estimated ACFs (Section IIIb, Figs 20–31). The scale was measured on the northward and southward (eastward and westward) sides and tabulated. The smaller of the two is the more stringent constraint in designing the network and is therefore the one presented in this report. The spatial scales for SST are presented in Figure 34, and for D_{20} in Figure 35.

The temporal structure of ACFs can also be represented as a decorrelation scale. The temporal structure of ocean-temperature variability is often found to be either oscillatory (i.e. second-order autoregressive process) (Chatfield, 1975) or characterised by increasing amplitude with longer time-scales (first-order process). The appropriate decorrelation scale for a second-order process is the first zero crossing of the ACF. For a first-order process it is the e-folding scale. The appropriate scale was measured on the temporal ACFs (Section IIIa, Figs 8–19). In most cases the e-folding scale was used. The zero-crossing was selected in cases where the ACF showed a seasonal signal. The temporal scales for SST are presented in Figure 36 and for D_{20} in Figure 37.

V. Summary of Statistical Structure

The differences in scales are in part due to statistical noise resulting from relatively short or sparse XBT time series in comparison to those of the Pacific Ocean, and in part due to real differences in the statistical structure of the Indian Ocean. We seek a simplification of the statistical structure that is homogeneous over large areas and still representative of real structure in the ocean. With this goal in mind, three summaries of the essential OI statistics (spatial and temporal decorrelation scales, signal-to-noise ratios [α] and standard deviation[σ]) were prepared, representing three levels of increasing simplification.

a. Averages in 3° Latitude (Longitude) Bands

The ACFs (Figs 8–31) were averaged over 3° latitude (longitude) bands. This summary essentially documents all of the meaningful detail in the statistics we have estimated. Table 2 presents the averages for SST along the five meridional transects, table 3 presents the averages for D_{20} along the five meridional transects and table 4 presents the averages for both SST and D_{20} along the single zonal transect. In averaging the variance-related statistics (α, α) , RMS values were calculated. The averaged meridional (zonal) scale is the shorter of the northward and southward (eastward and westward) values. Scales greater than 6° latitude (longitude) were set equal to 6°.

It should be noted that where the data were very sparse, particularly in the Fremantle–Persian Gulf transects, the signal could not be adequately resolved and the values for the signal-to-noise ratio became very large.

b. Dynamic Subregions

Geographic areas were selected to identify representative scales according to the baroclinic structure of the major zonal currents. The areas are shown in Figure 38. The equatorial wave-guide (EWG) is the region 3°N to 3°S. The North Equatorial Current (NEC) is the region 3°N to 12°N. The influence of the monsoon winds of the Indian Ocean on this current has been discussed by Wyrtki (1973). The northern edge has been cut off at 10°N to avoid the confluence of XBT routes in the narrow Somalia Current. The South Equatorial Countercurrent (SECC) is the region 3°S to 10°S. Finally the central South Equatorial Current (SEC) is the region 10°S to 20°S. Neumann and Pierson (1966) show similar divisions of the major zonal currents.

In addition to the major zonal currents, representative scales have been found for the region 3°N to 10°S; 115°E to 135°E, enclosing most of the Indonesian Seas (IS) (Fig. 38). The scales for this region were determined from the Port Hedland–Japan track between 10°S and 3°N and the Flores Sea–Banda Sea zonal track.

Because the Indian Ocean is relatively unknown, straightforward arithmetic means were used to find the scales to avoid misinterpretation of the signals by a more subjective method. The statistics are presented on maps in Figures 39 and 40. Space and time

scales representative of the structure of the thermocline (Table 3) are smaller than the scales of SST, and more critical in designing the network.

c. Uniform Scales

In some optimal mapping procedures it may be desirable to use one set of scales for the entire Indian Ocean, with the possible exclusion of boundary current regions. As an estimate of uniform scales in the open Indian Ocean, the median of all 3° latitude averages, along all tracks except Flores Sea–Banda Sea and north of the equator on the Port Hedland–Japan track, was calculated for each of the parameters λ, τ and α. The scales obtained were: Meridional Decorrelation Scale of 6° latitude for SST and 3.3° latitude for D_{20}; Temporal Decorrelation Scale of 2.7 months for SST and 2.5 months for D_{20}; Signal-to-Noise Ratio of 1.9 for SST and 1.1 for D_{20}. This leads us to believe that the scales defined for the Pacific Ocean in Part I can also be used for the Indian Ocean. The recommended scales for the Indian Ocean are therefore a meridional decorrelation scale of 3° latitude, a temporal decorrelation scale of 2 months and a signal-to-noise ratio of 1.

These scales must be considered provisional because of the relatively short duration of XBT sampling in the Indian Ocean and also because of the unknown effect that the 1986/87 ENSO event may have had on the results.

Acknowledgements

The authors wish to acknowledge the generous assistance given by all the merchant ships that have participated in the CSIRO XBT Ship-of-Opportunity program: *Act 3, Act 4, Act 6, Anro Asia, Anro Australia, Australia Star (Mahsuri), Australian Progress, Botany Bay (Nedlloyd Tasman), Encounter Bay, Flinders Bay, Iron Newcastle, Meridian, Nimos, Shearwater, Swan Reefer.*

We also wish to acknowledge the efforts of the merchant ships and research vessels in the ORSTOM (Office de la Recherche Scientifique et Technique Outre Mer) XBT program that contributed to the Réunion–Red Sea transect.

References

Alaka, M. A. and R. C. Elvander, 1972: Optimum interpolation from observations of mixed quality. *Monthly Weather Review* **100**, 612–624.

Bretherton, F. P., R. E. Davis and C. B. Fandry, 1976: A technique for objective analysis and design of oceanographic experiments applied to MODE–73. *Deep-sea Research* **23**, 559–582.

Chatfield, C., 1975: *The Analysis of Time-series: Theory and Practice.* Chapman and Hall, London, 263 pp.

Gandin, L. S. 1963: Objective analysis of Meteorological Fields, GIMI, Leningrad from Russian, Israel Program for Scientific Translations, Jerusalem, No. **1373**, 242 pp.

ITPO, 1987: *TOGA International Implementation Plan* (Second Edition). International TOGA Project Office, World Meteorological Organisation, Geneva, 118 pp, 13 appendices.

Meyers, G., J. Sprintall, H. Phillips, J. Peterson, T. Fonseca, 1989: Design of an Ocean Temperature Observing Network in the Seas North of Australia. Part I — Tropical Pacific Ocean: Statistics. *CSIRO Marine Laboratories Report* **204**, 50 pp.

Neumann, G. and W. J. Pierson, 1966: *Principles of Physical Oceanography,* Prentice-Hall, Englewood Cliffs, NJ, 545 pp.

WCRP, 1985: Scientific Plan for the Tropical Ocean and Global Atmosphere Programme, WCRP Publ. Ser. No. 3, World Meteorological Organisation, Geneva, 146 pp.

White, W. B. and R. L. Bernstein, 1979: Design of an oceanographic network in the mid-latitude north Pacific. *Journal of Physical Oceanography* **10**, 592–606.

White, W. B., G. Meyers and K. Hasunuma, 1982: Space/time statistics of short-term climatic variability in the western north Pacific. *Journal of Geophysical Research*, **87**, 1979–89.

Wyrtki, K., 1973: Physical Oceanography of the Indian Ocean. In: *Ecological Studies. Analysis and Synthesis*, vol. 3, chap. 1.3, pp. 18–36. Springer-Verlag, Berlin.

Illustrations

Figure 12A–C: Fremantle–Persian Gulf Track. Sea surface temperature temporal autocorrelation function. Details as in Fig. 8.

Figure 13 A–C: Fremantle–Persian Gulf Track. Depth of 20°C isotherm temporal autocorrelation function. Details as in Fig. 8.

Figure 14 A–B: Fremantle–Sunda Strait Track. Sea surface temperature temporal autocorrelation function. Details as in Fig. 8.

Figure 15A–B: Fremantle–Sunda Strait Track. Depth of 20°C isotherm temporal autocorrelation function. Details as in Fig. 8.

Figure 16A–C: Port Hedland–Japan Track. Sea surface temperature temporal autocorrelation function. Details as in Fig. 8.

Figure 17A–C: Port Hedland–Japan Track. Depth of 20°C isotherm temporal autocorrelation function. Details as in Fig. 8.

Figure 18A–B: Flores Sea–Banda Sea Track. Sea surface temperature temporal autocorrelation function, in 3° longitude bands. The central longitude is indicated at the top of each frame and its ACF indicated with dots. Lag is in months.

Figure 19A–B: Flores Sea–Banda Sea Track. Depth of 20°C isotherm temporal autocorrelation function. Details as in Fig. 18.

Figure 20A–B: La Réunion–Red Sea Track. Sea surface temperature meridional autocorrelation function, in 3° latitude bands. The central latitude is indicated at the top of each frame, and its ACF indicated with dots. Lag is in degrees latitude; positive indicates northward separation.

Figure 21A–B: La Réunion–Red Sea Track. Depth of 20°C isotherm meridional autocorrelation function. Details as in Fig. 20.

Figure 22A–B: Fremantle-Red Sea Track. Sea surface temperature meridional autocorrelation function. Details as in Fig. 20.

Figure 23A–B: Fremantle–Red Sea Track. Depth of 20°C isotherm meridional autocorrelation function. Details as in Fig. 20.

Figure 24A–C: Fremantle–Persian Gulf Track. Sea surface temperature meridional autocorrelation function. Details as in Fig. 20.

Figure 25A–C: Fremantle–Persian Gulf Track. Depth of 20°C isotherm meridional autocorrelation function. Details as in Fig. 20.

Figure 26A–B: Fremantle–Sunda Strait Track. Sea surface temperature meridional autocorrelation function. Details as in Fig. 20.

Figure 27A–A: Fremantle–Sunda Strait Track. Depth of 20°C isotherm meridional autocorrelation function. Details as in Fig. 20.

Figure 28A–C: Port Hedland–Japan Track. Sea surface temperature meridional autocorrelation function. Details as in Fig. 20.

Figure 29A–C: Port Hedland–Japan Track. Depth of 20°C isotherm meridional autocorrelation function.Details as in Fig. 20.

Figure 30A–B: Flores Sea–Banda Sea Track. Sea surface temperature zonal autocorrelation function in 3° longitude bands. The central longitude is indicated at the top of each frame, and its ACF indicated with dots. Lag is in degrees longitude; positive indicates eastward separation.

Figure 31A–B: Flores Sea–Banda Sea Track. Depth of 20°C isotherm zonal autocorrelation function. Details as in Fig. 30.

Figure 32 A–F: Signal to noise ratio of SST on the La Réunion–Red Sea (A), Fremantle–Red Sea (B), Fremantle–Persian Gulf (C), Fremantle–Sunda Strait (D), Port Hedland–Japan (E), and Flores Sea–Banda Sea (F) tracks.

Figure 33A–F: Signal to noise ratio of D_{20} on six tracks as in Fig. 32.

Figure 34 A–F: Meridional decorrelation scale of SST on five tracks (A-E) and zonal decorrelation scale of SST on track F, as in Fig. 32.

Figure 35A–F: Meridional decorrelation scale of D_{20} on five tracks (A-E) and zonal decorrelation scale of D_{20} on track F, as in Fig. 32.

Figure 36A–F: Temporal decorrelation scale of SST on six tracks as in Fig. 32.

Figure 37A–F: Temporal decorrelation scale of D_{20} on six tracks as in Fig. 32.

Figure 38: Geographical areas where optimum interpolation statistics were summarised. North Equatorial Current (NEC); Equatorial Wave Guide (EWG); Southern Equatorial Countercurrent (SECC); South Equatorial Current (SEC).

Figure 39: Signal to noise ratio (α), and standard deviation (α). Values for sea surface temperature (SST) and depth of 20°C isotherm (D_{20}) as in legend.

Figure 40: Meridional and temporal decorrelation scales , as in Fig. 39.

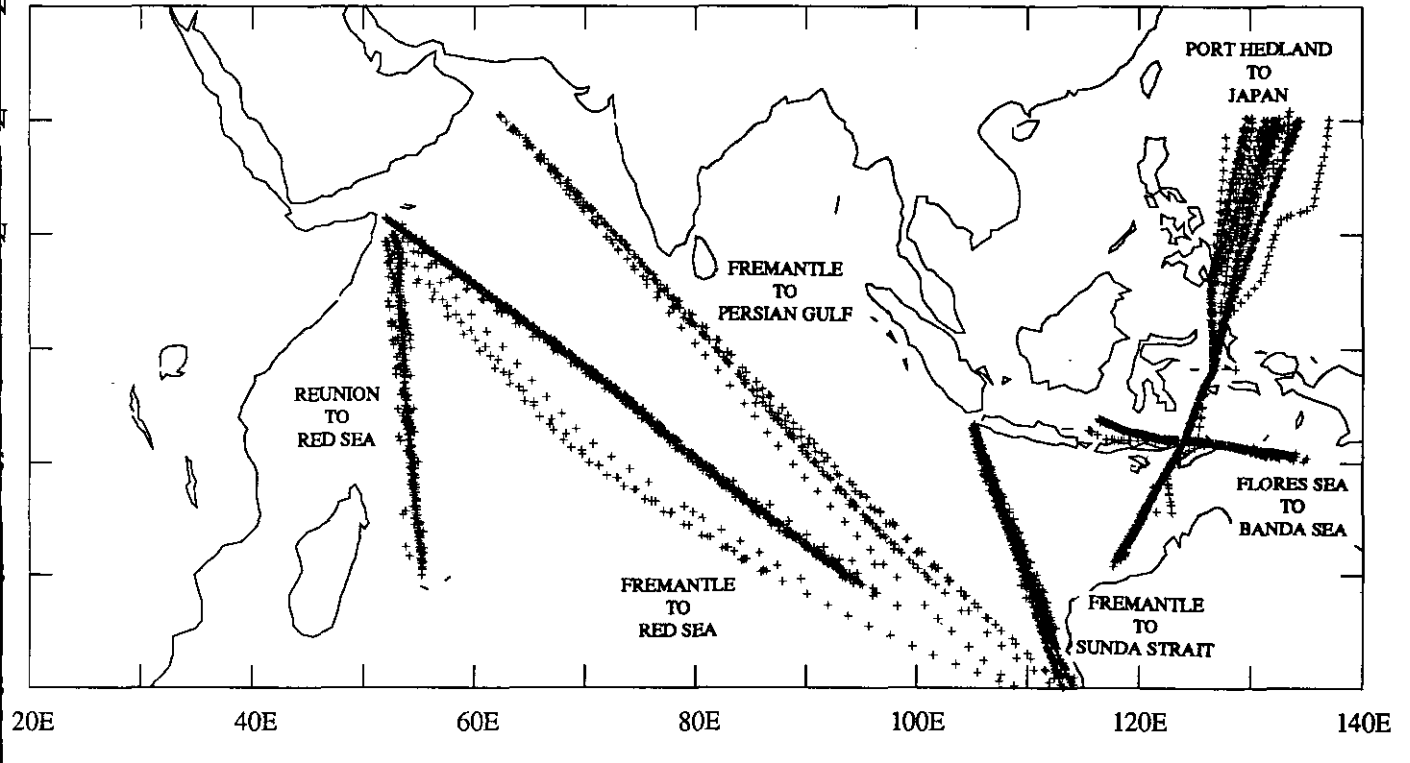

Figure 1: Indian Ocean XBT routes — geographical location.

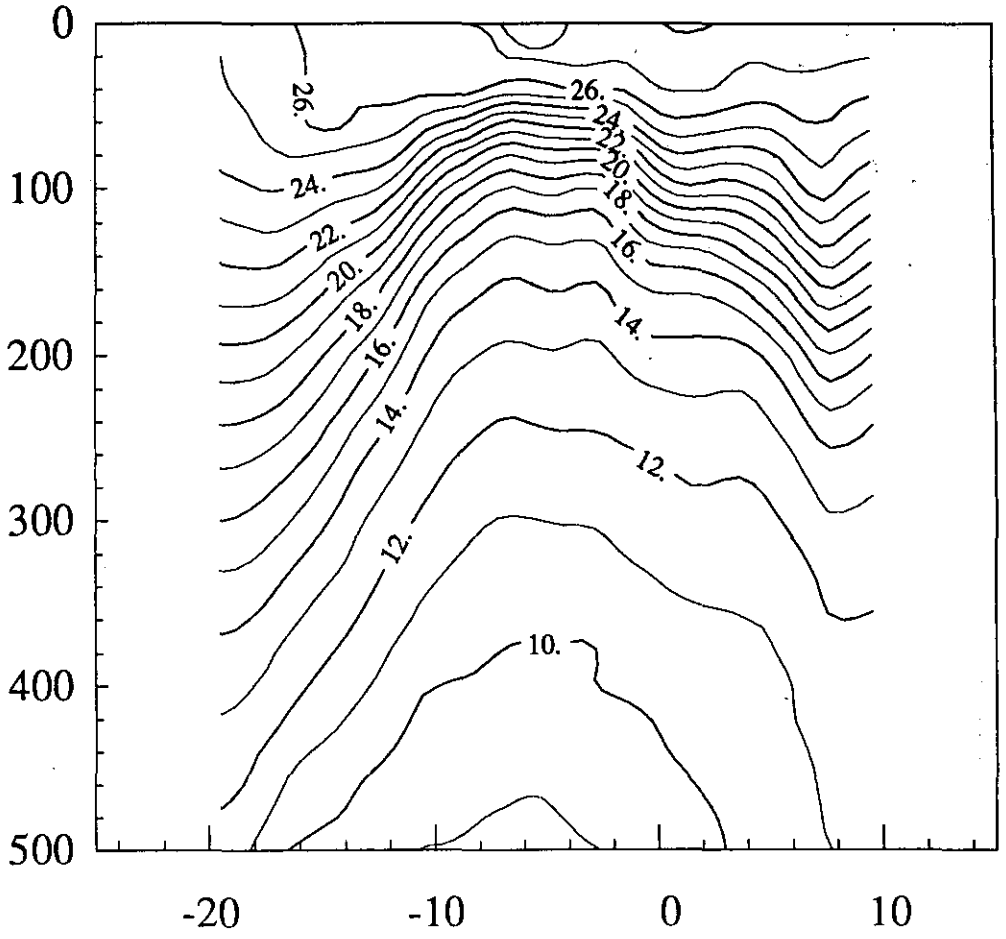

Figure 2A: Mean temperature February 1985 to February 1988.
La Réunion-Red Sea Track.

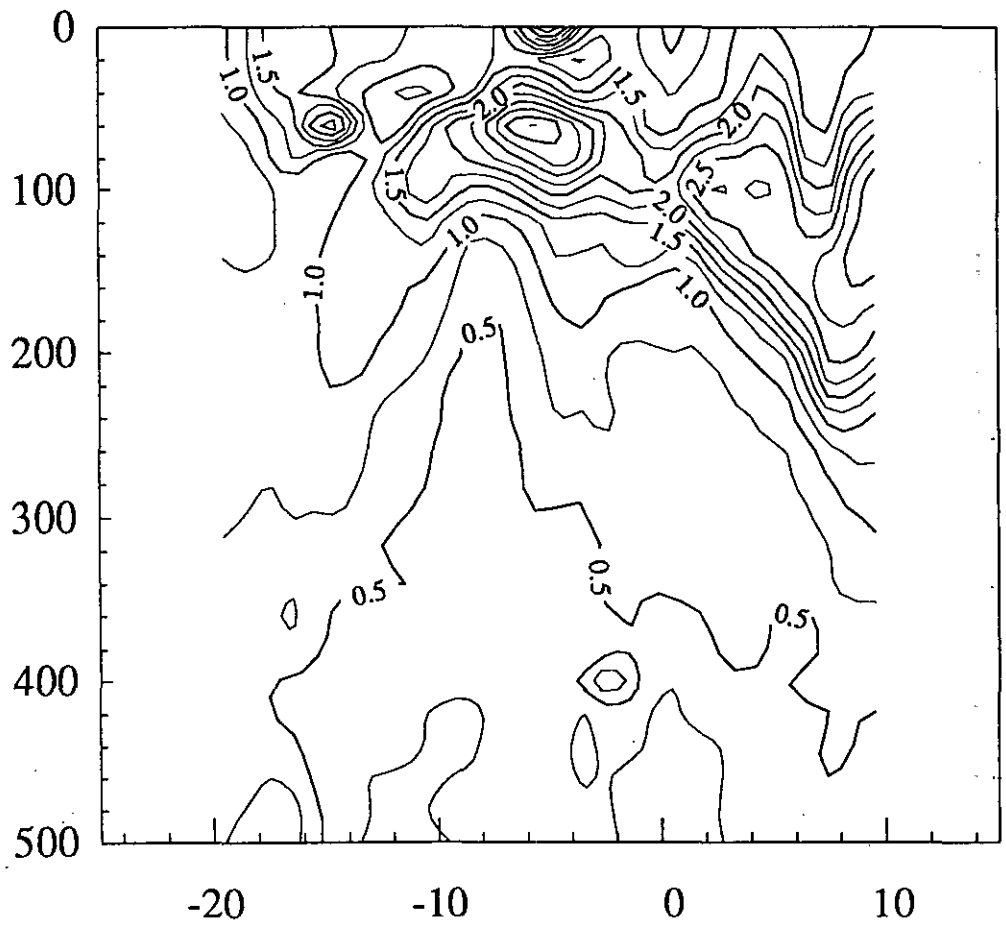

Figure 2B: Standard Deviation February 1985 to February 1988.

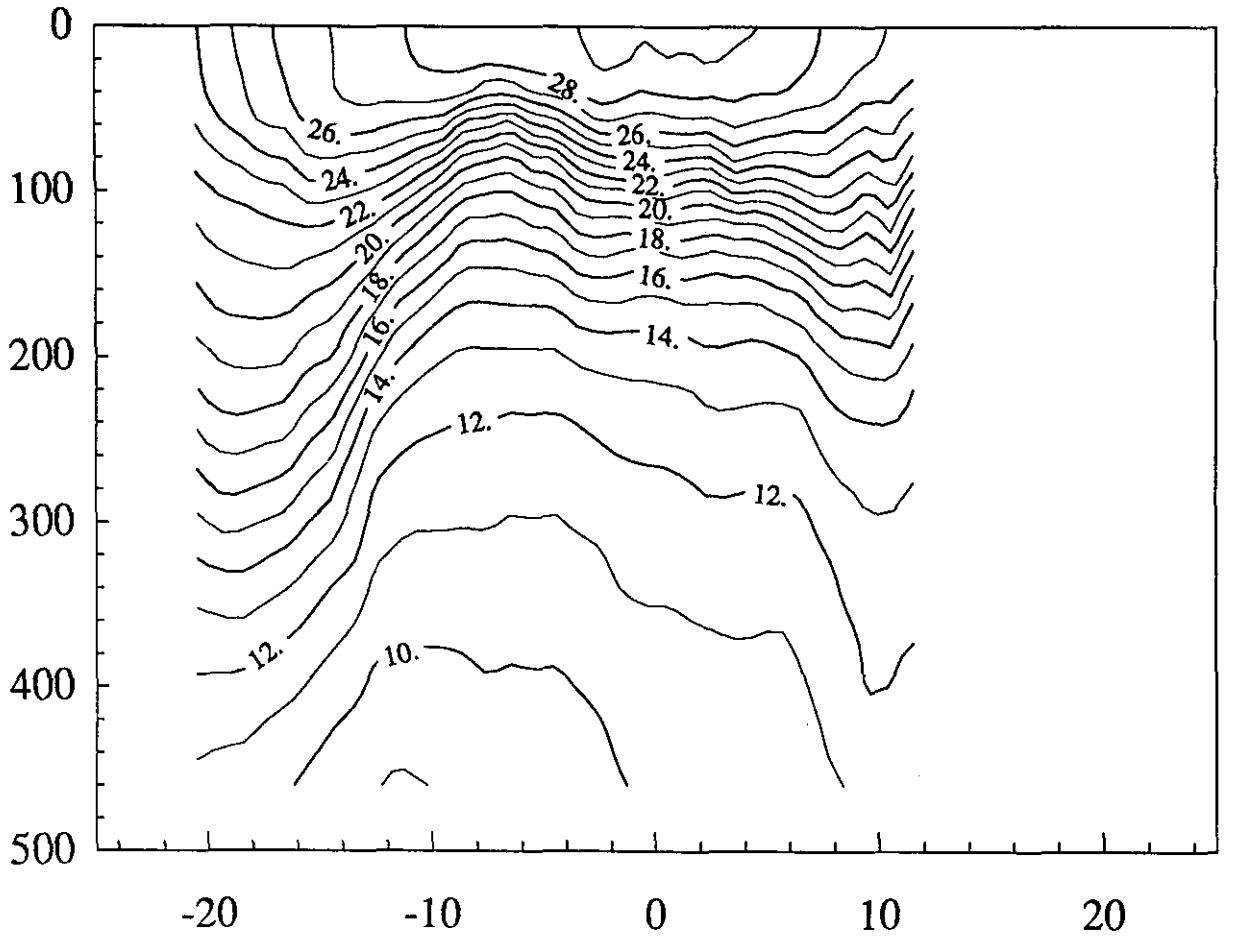

Figure 3A: Mean temperature August 1986–July 1988.
Fremantle–Red Sea track.

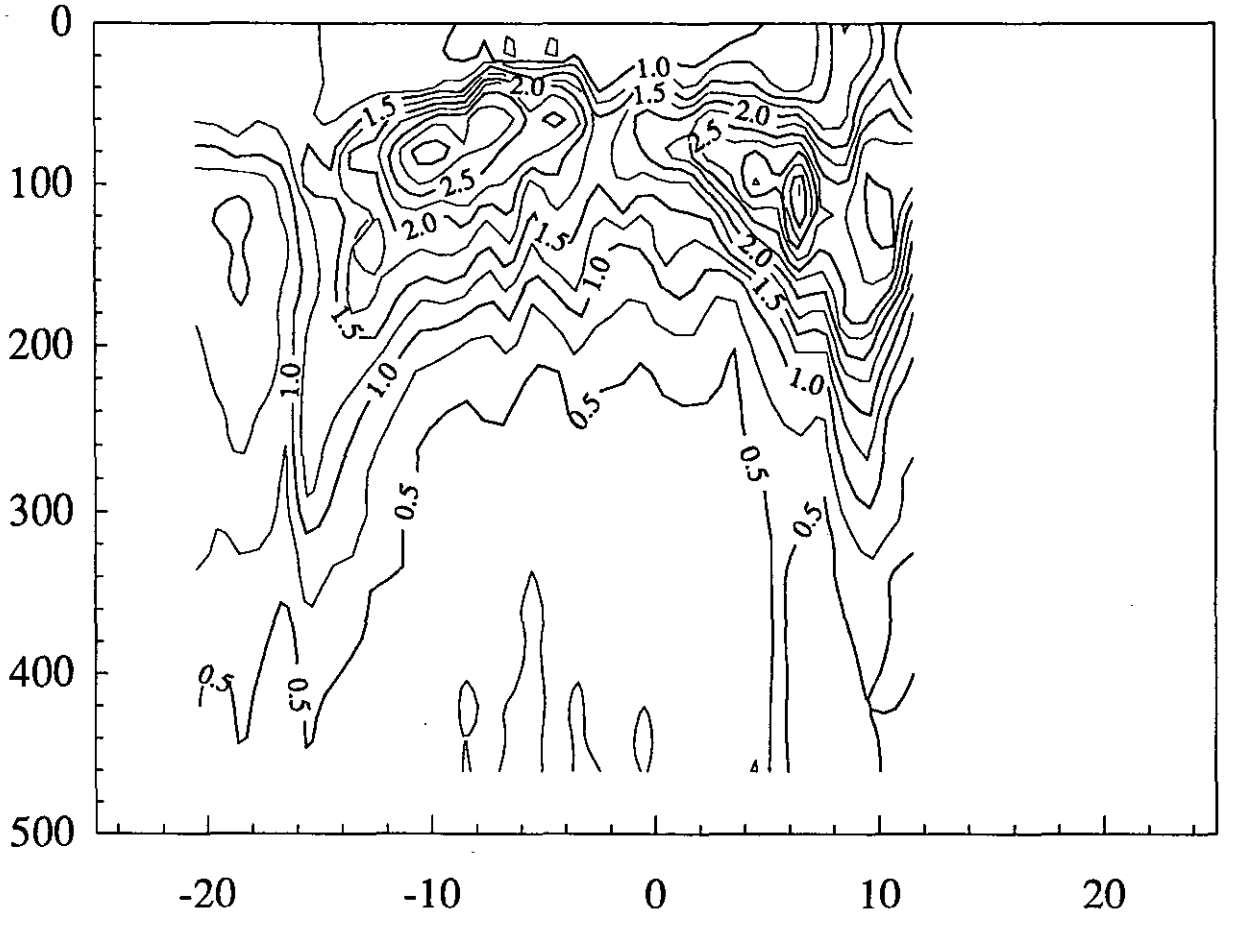

Figure 3B: Standard deviation August 1986–July 1988.

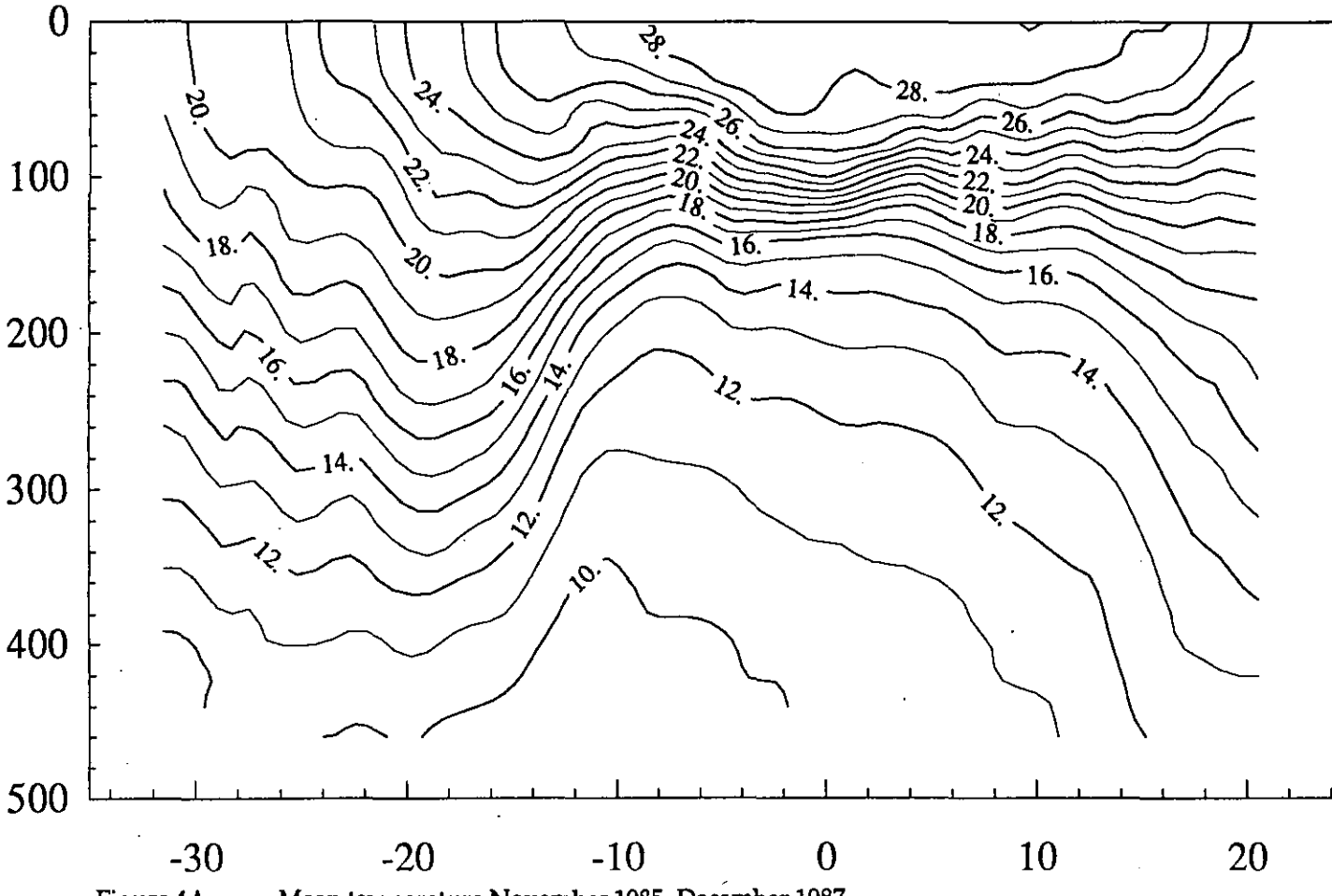

Figure 4A: Mean temperature November 1985–December 1987.
Fremantle–Persian Gulf Track.

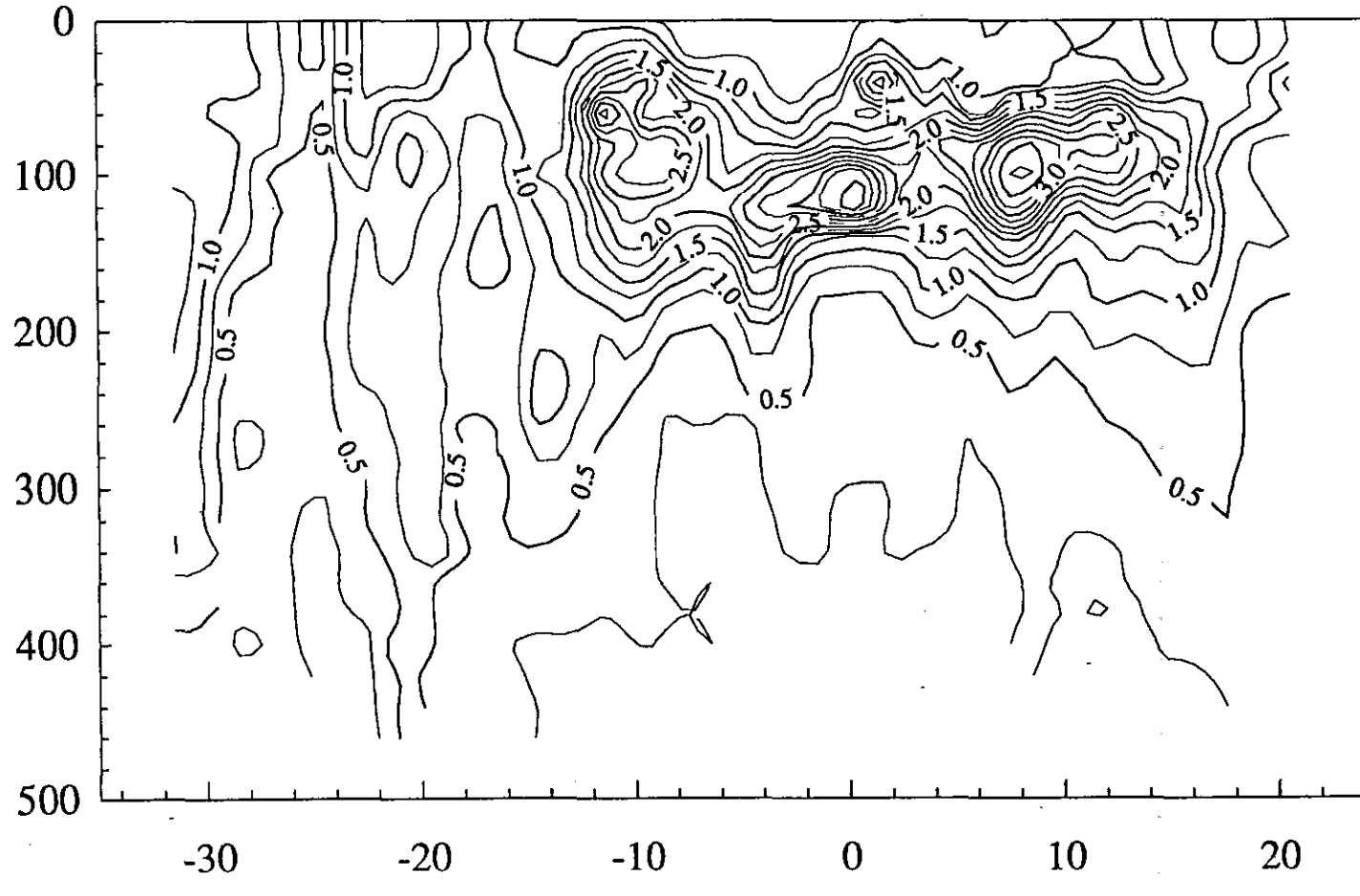

Figure 4B: Standard Deviation November 1985–December 1987.
Note: The equatorial maximum at 120 m is a result of insufficient data on this route.

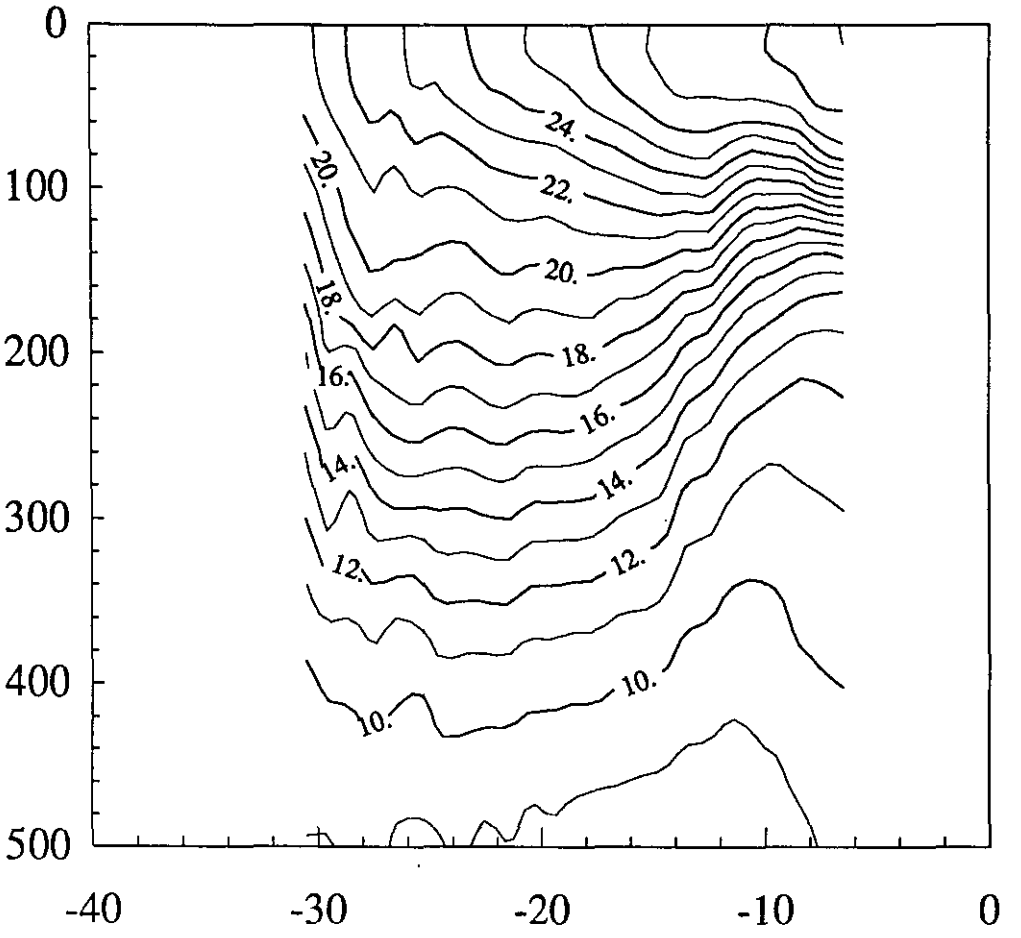

Figure 5A: Mean temperature May 1983–July 1988.
Fremantle–Sunda Strait Track.

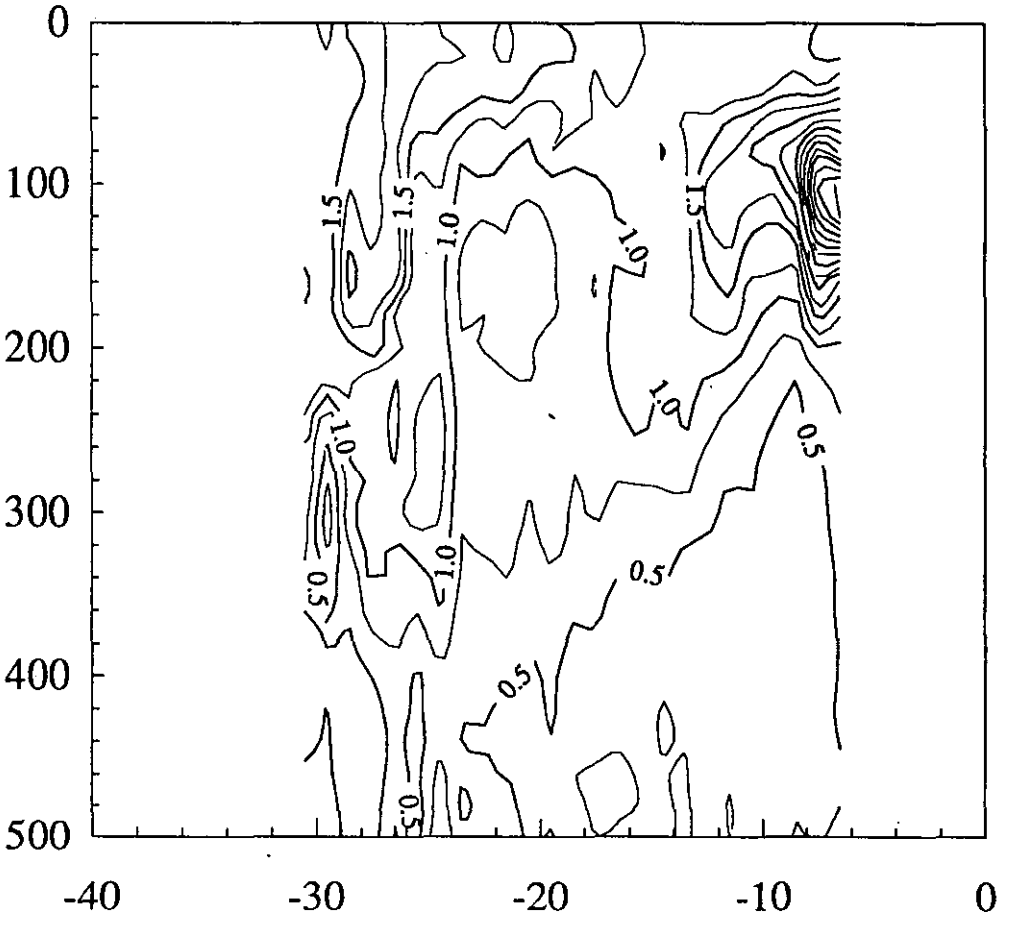

Figure 5B: Standard Deviation May 1983–July 1988.

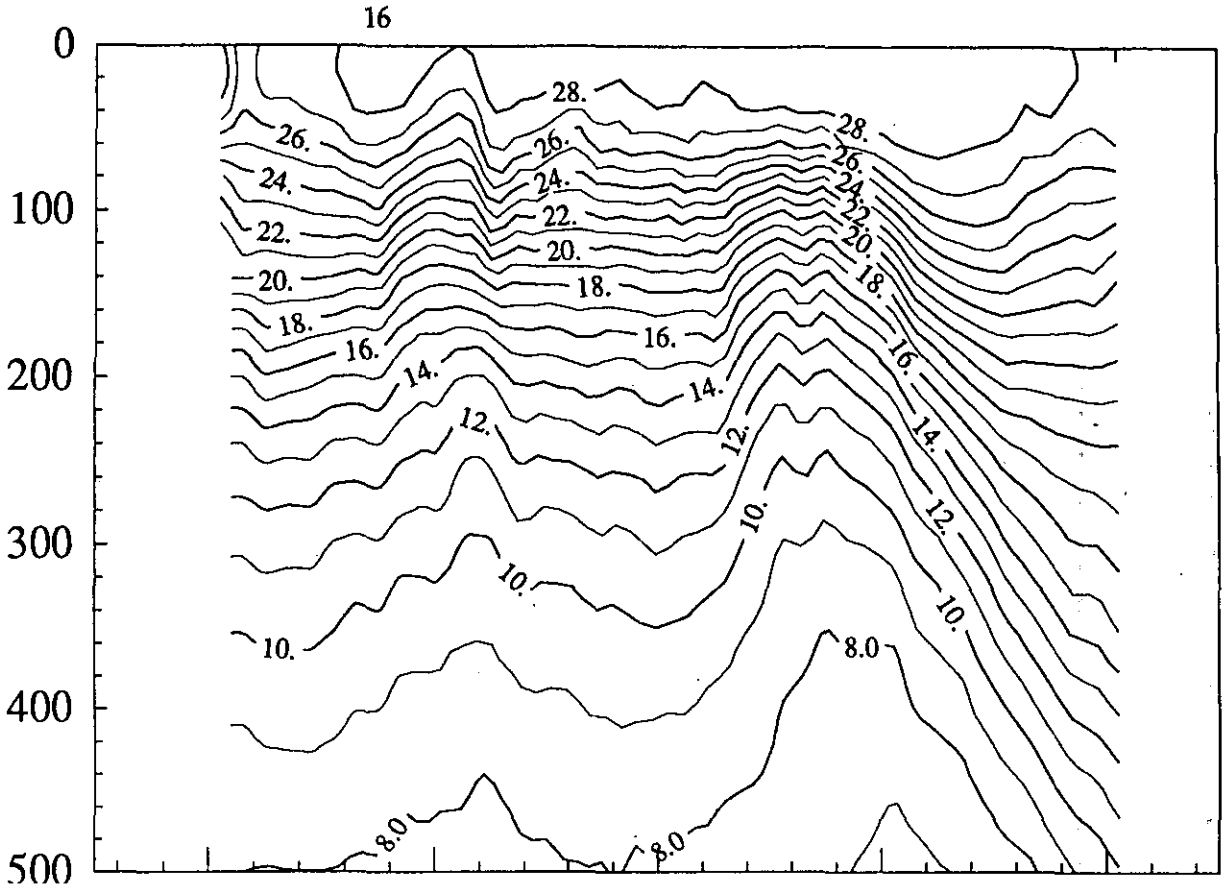

Figure 6A: Mean temperature July 1986–June 1988.
Port Hedland–Japan Track. Northbound + southbound voyages.

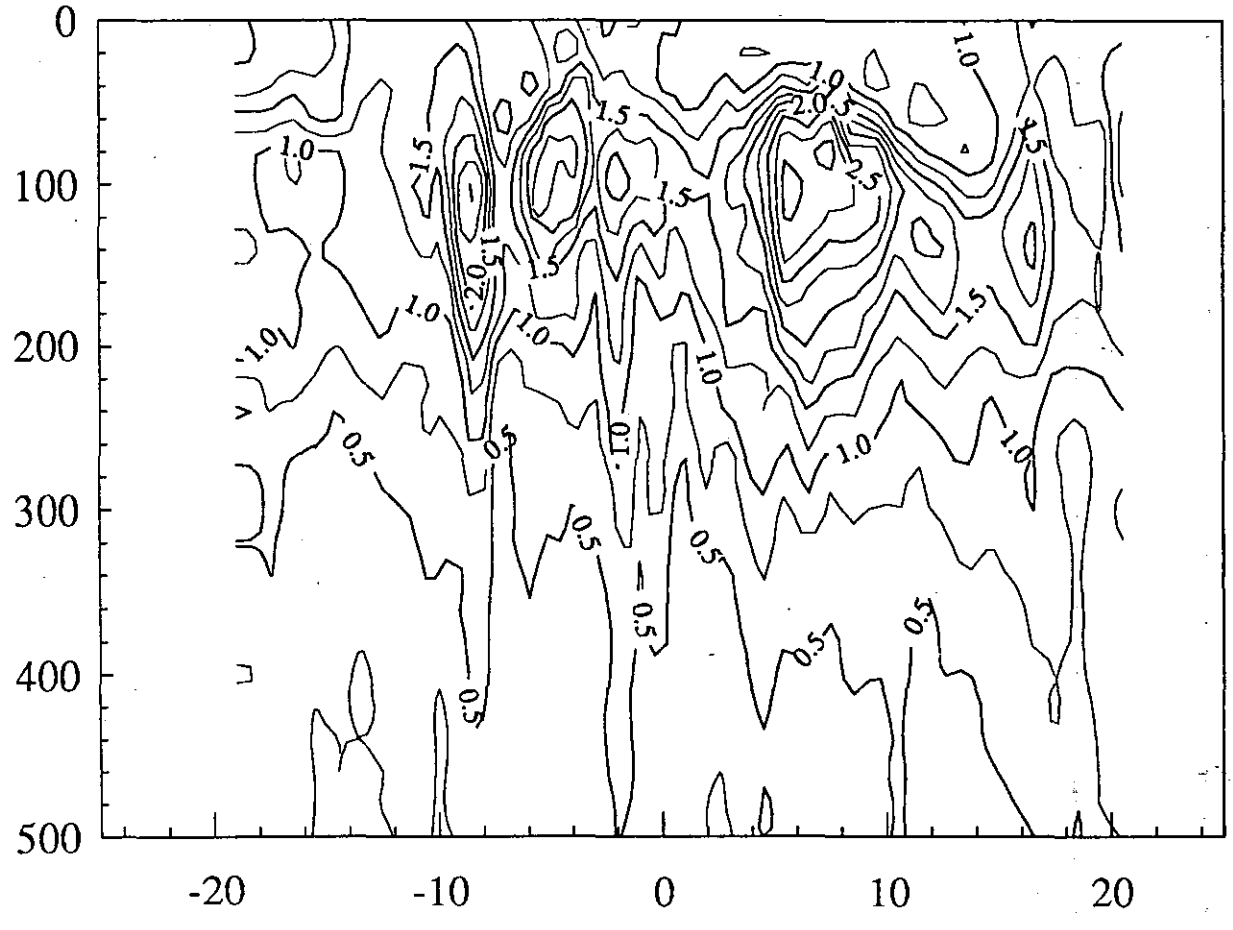

Figure 6B: Standard Deviation July 1986–June 1988.

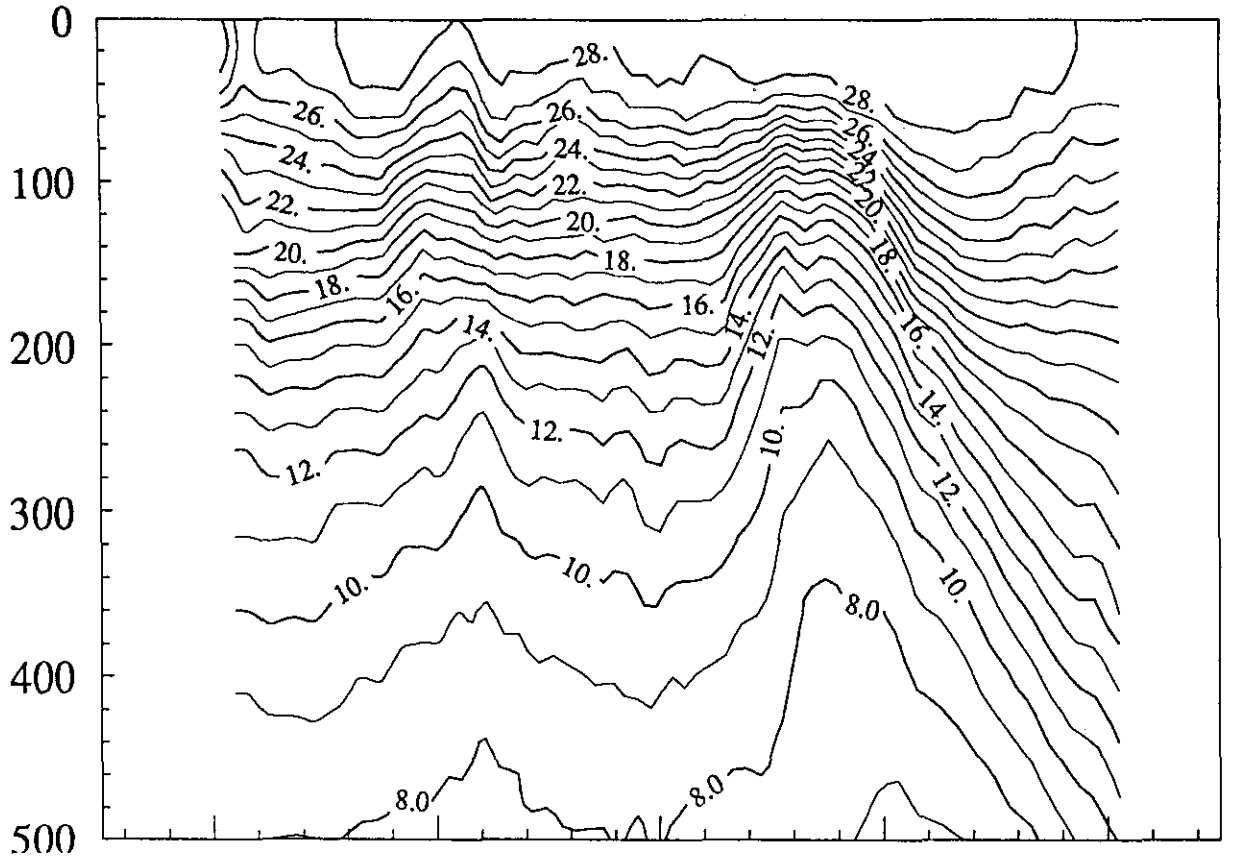

Figure 6C: Mean temperature July 1986–June 1988. Northbound only voyages

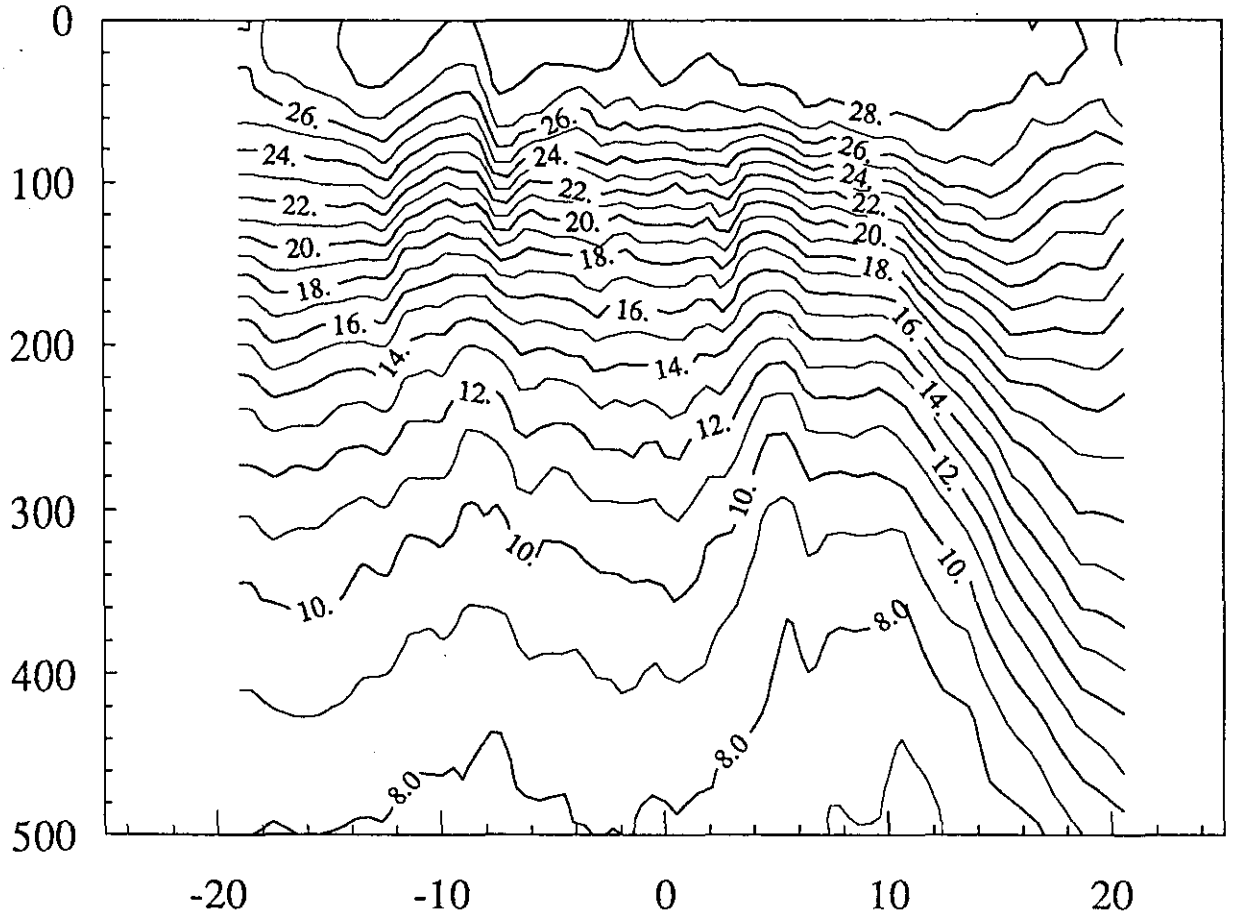

Figure 6D: Mean Temperature July 1986–June 1988. Southbound only voyages.

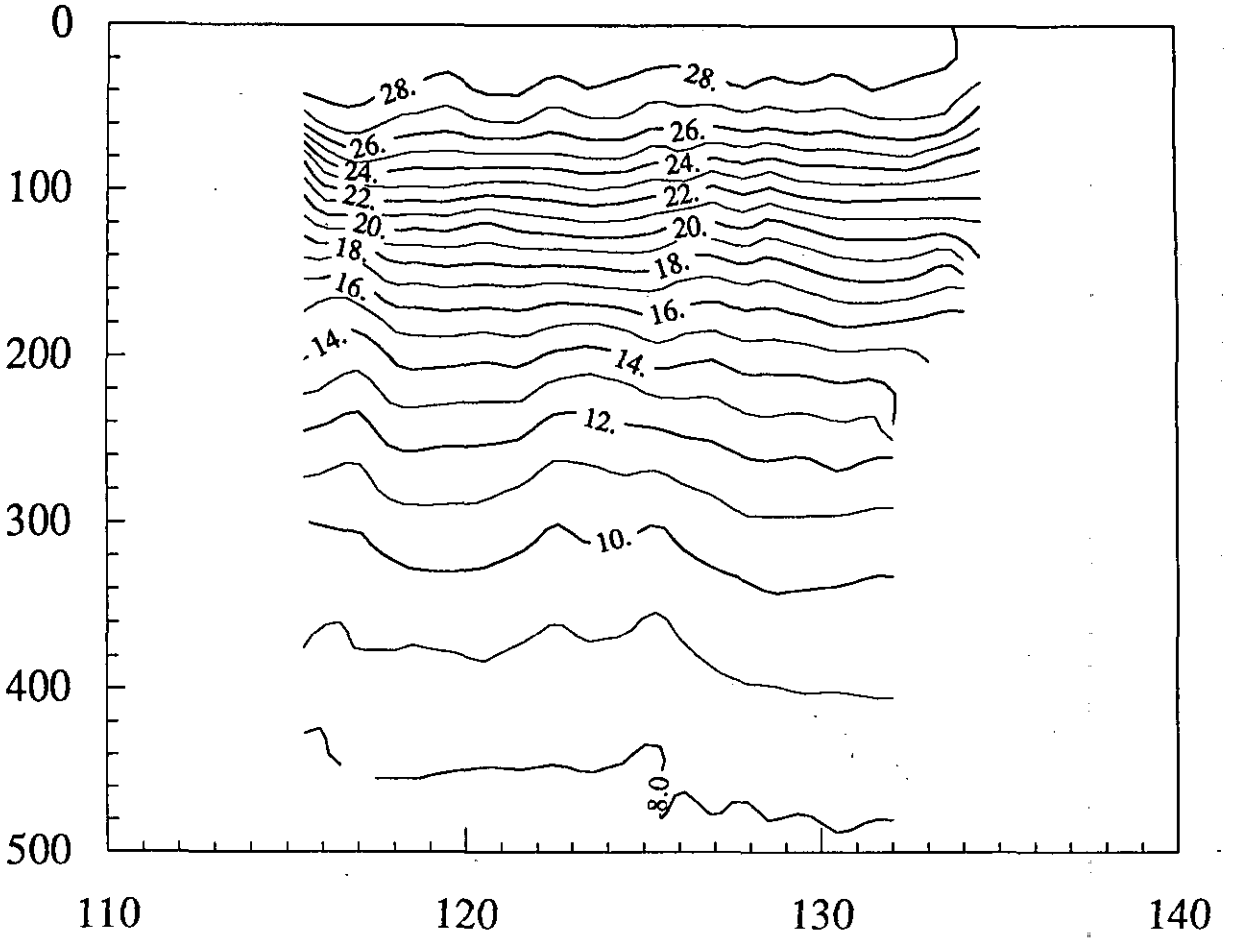

Figure 7A: Mean temperature May 1983–June 1988.
Flores Sea–Banda Sea Track

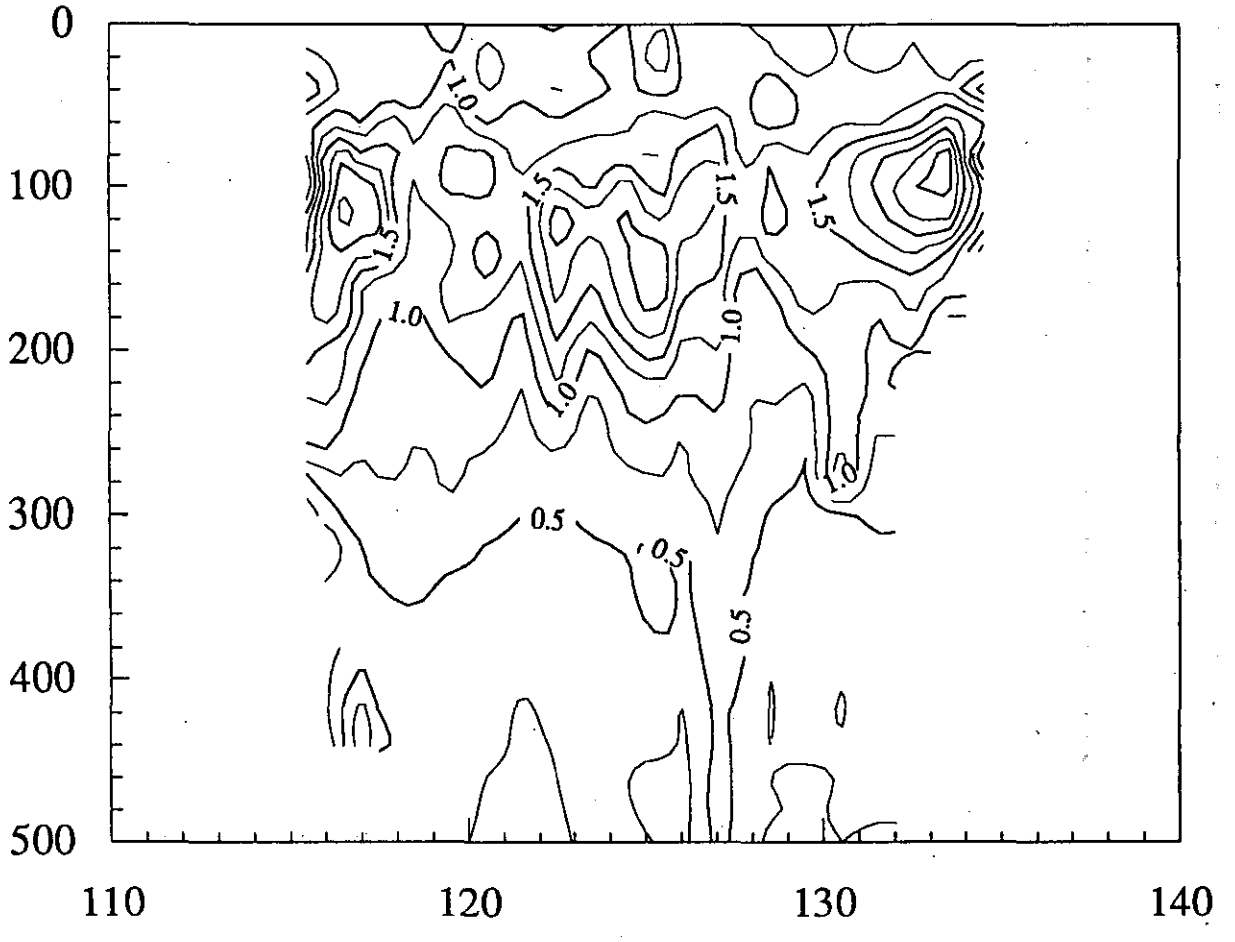

Figure 7B: Standard Deviation May 1983–June 1988.

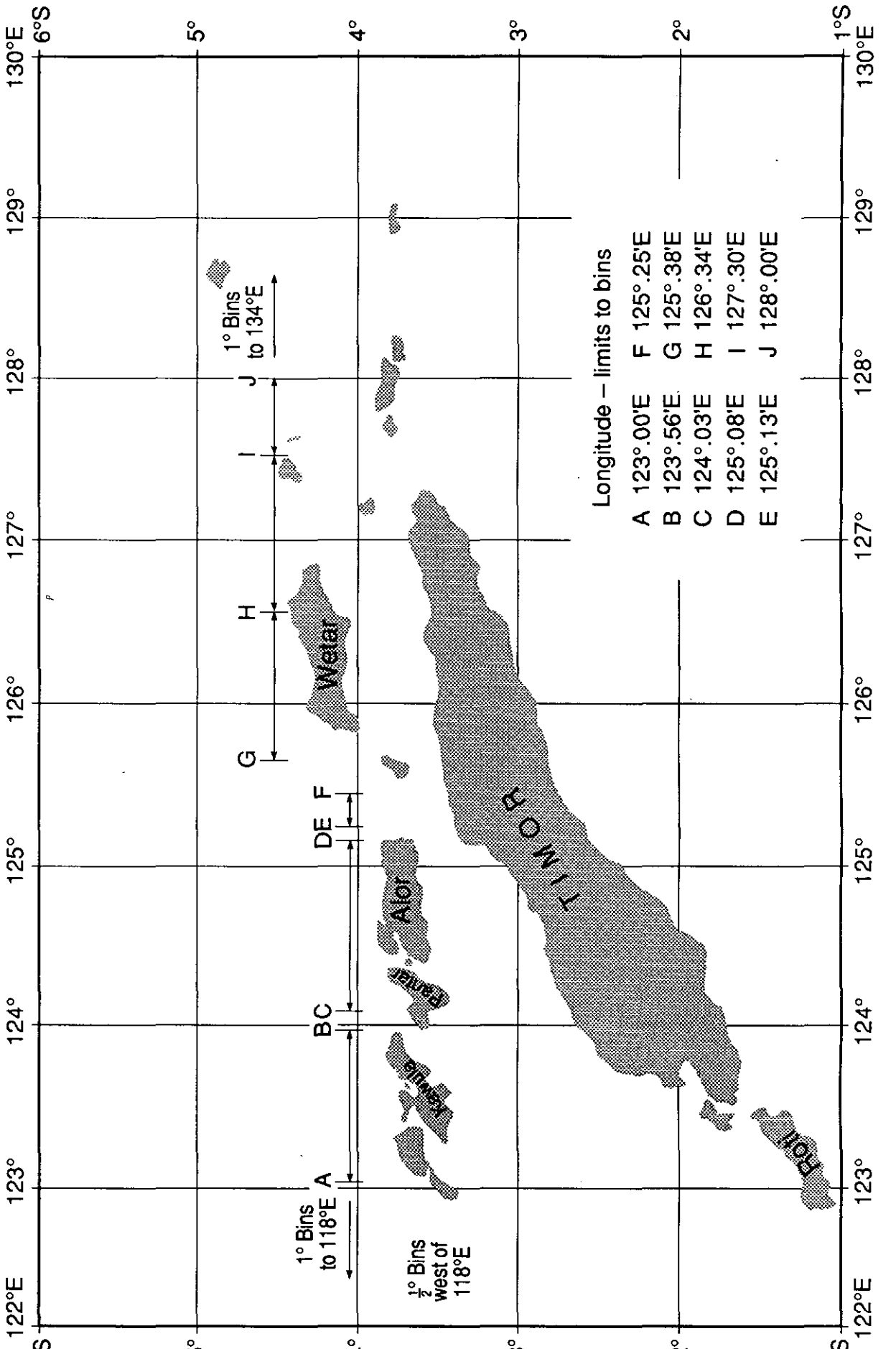

Figure 7C: Distribution of bins along Flores Sea–Banda Sea Track.

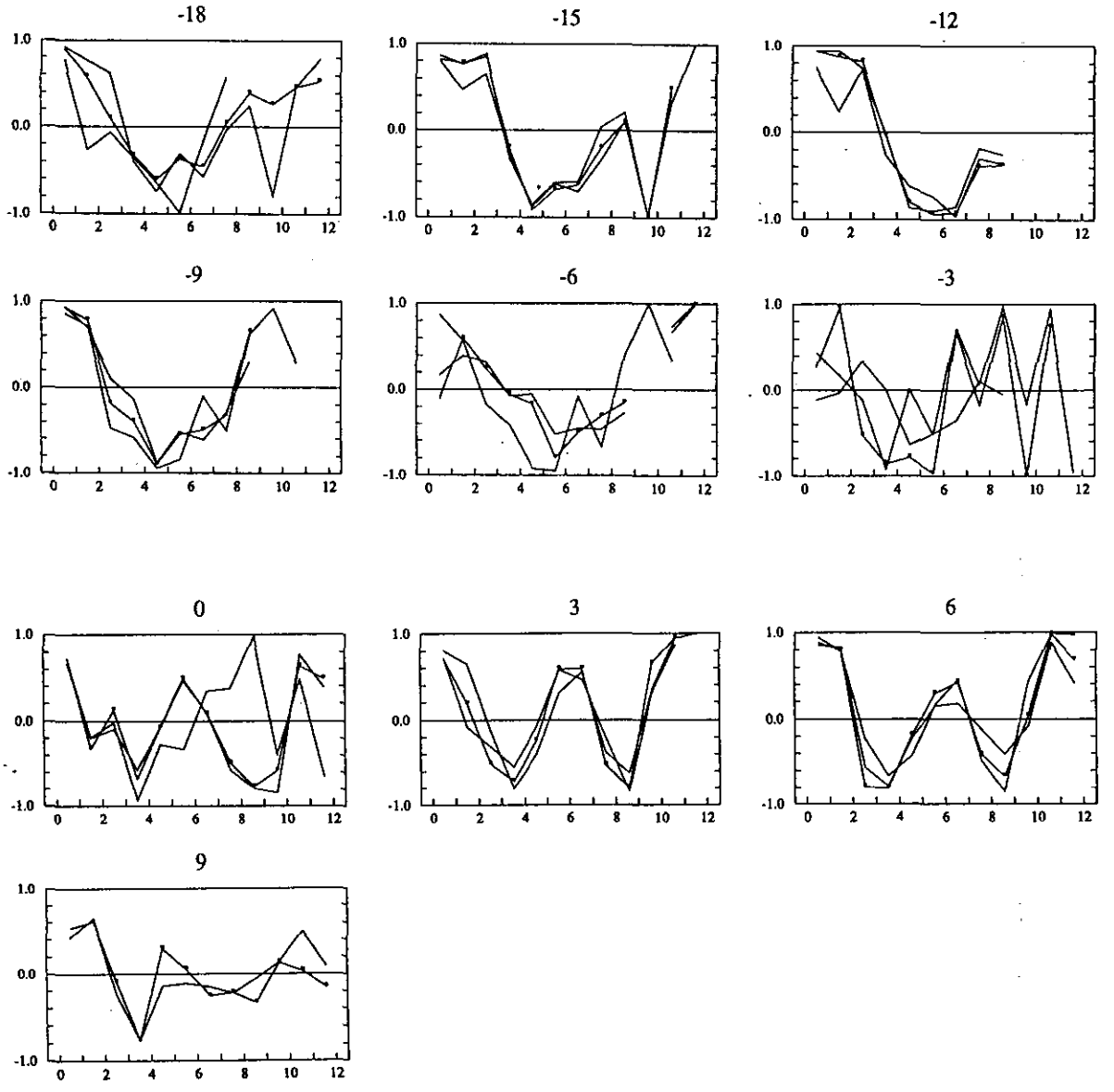

Figure 8A–B: La Réunion–Red Sea Track. Sea surface temperature temporal autocorrelation function, in 3° latitude bands. The central latitude is indicated at the top of each frame and its ACF indicated with dots. Lag is in months.

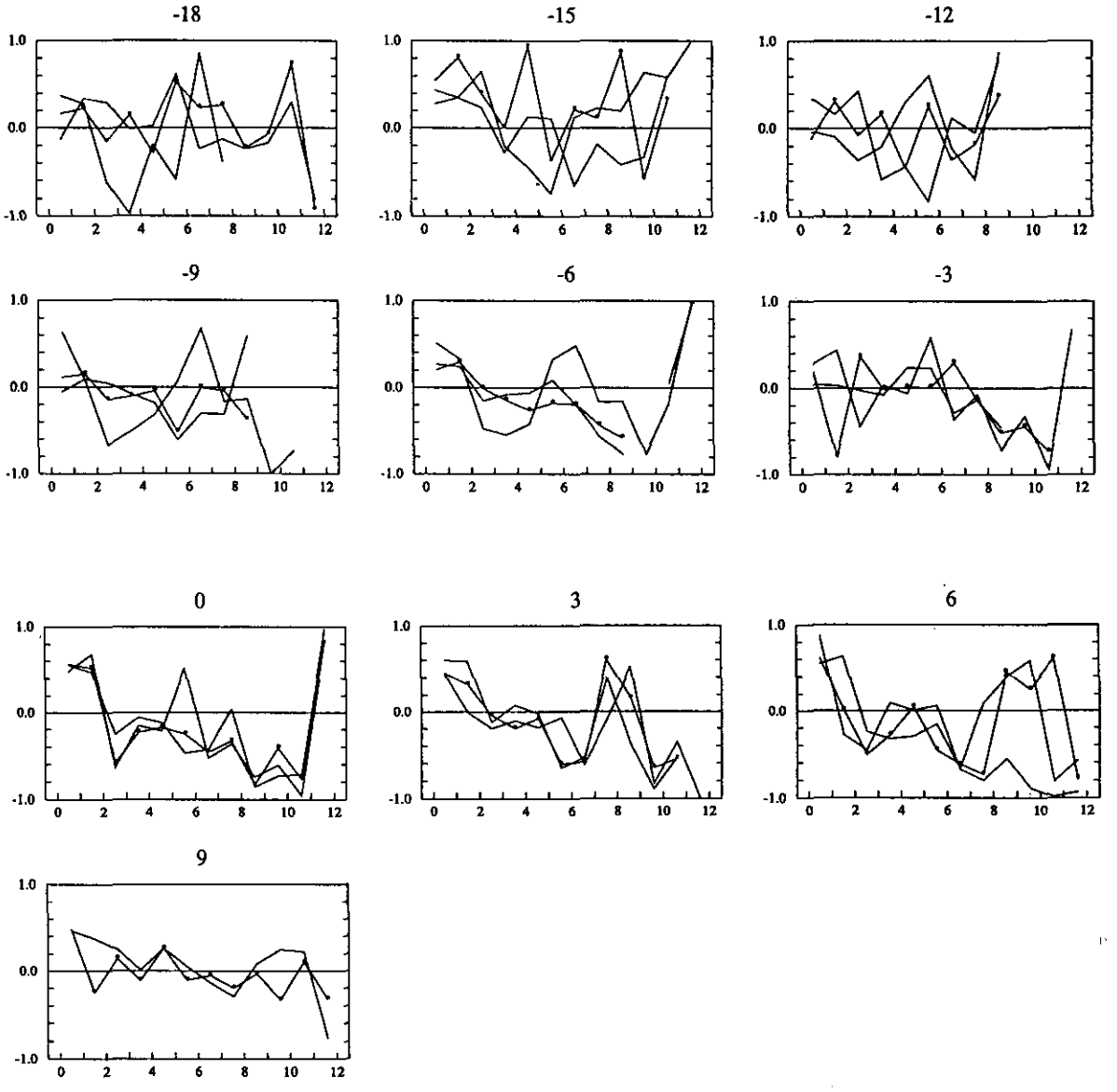

Figure 9A–B: La Réunion–Red Sea Track. Depth of 20°C isotherm temporal autocorrelation function. Details as in Fig. 8.

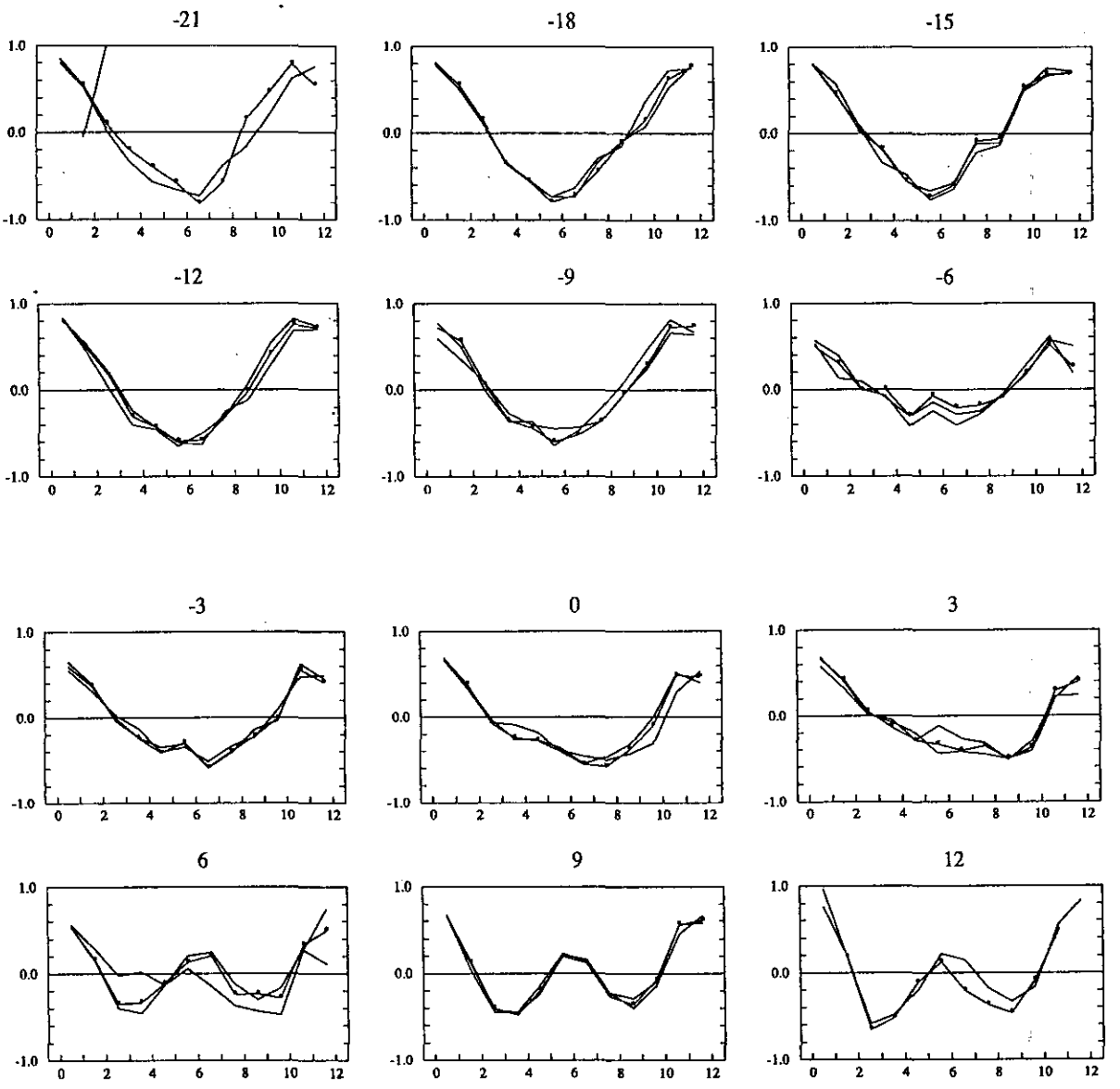

Figure 10A–B: Fremantle–Red Sea Track. Sea surface temperature temporal autocorrelation function. Details as in Fig. 8.

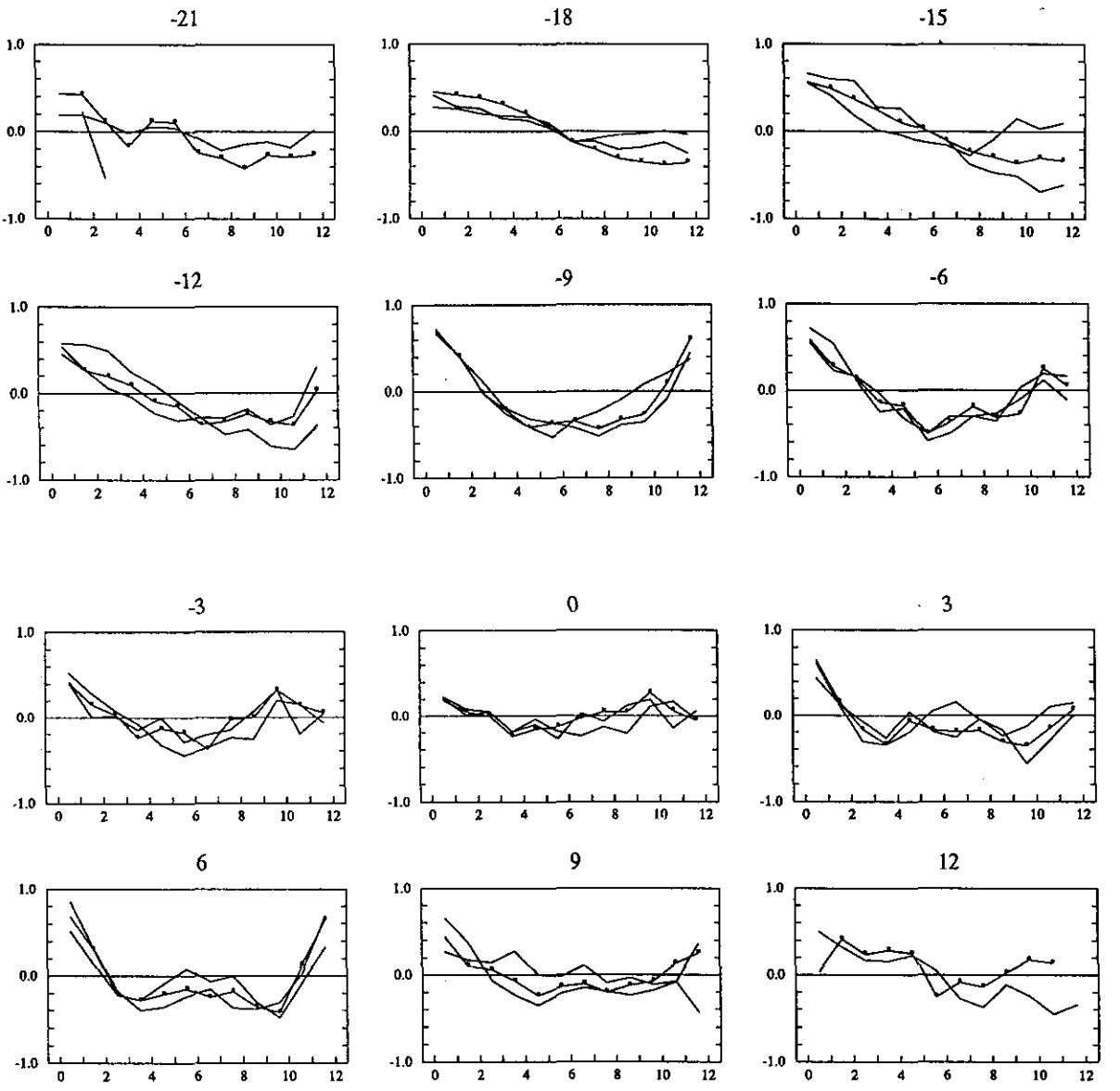

Figure 11A–B: Fremantle–Red Sea Track. Depth of 20°C isotherm temporal autocorrelation function. Details as in Fig. 8.

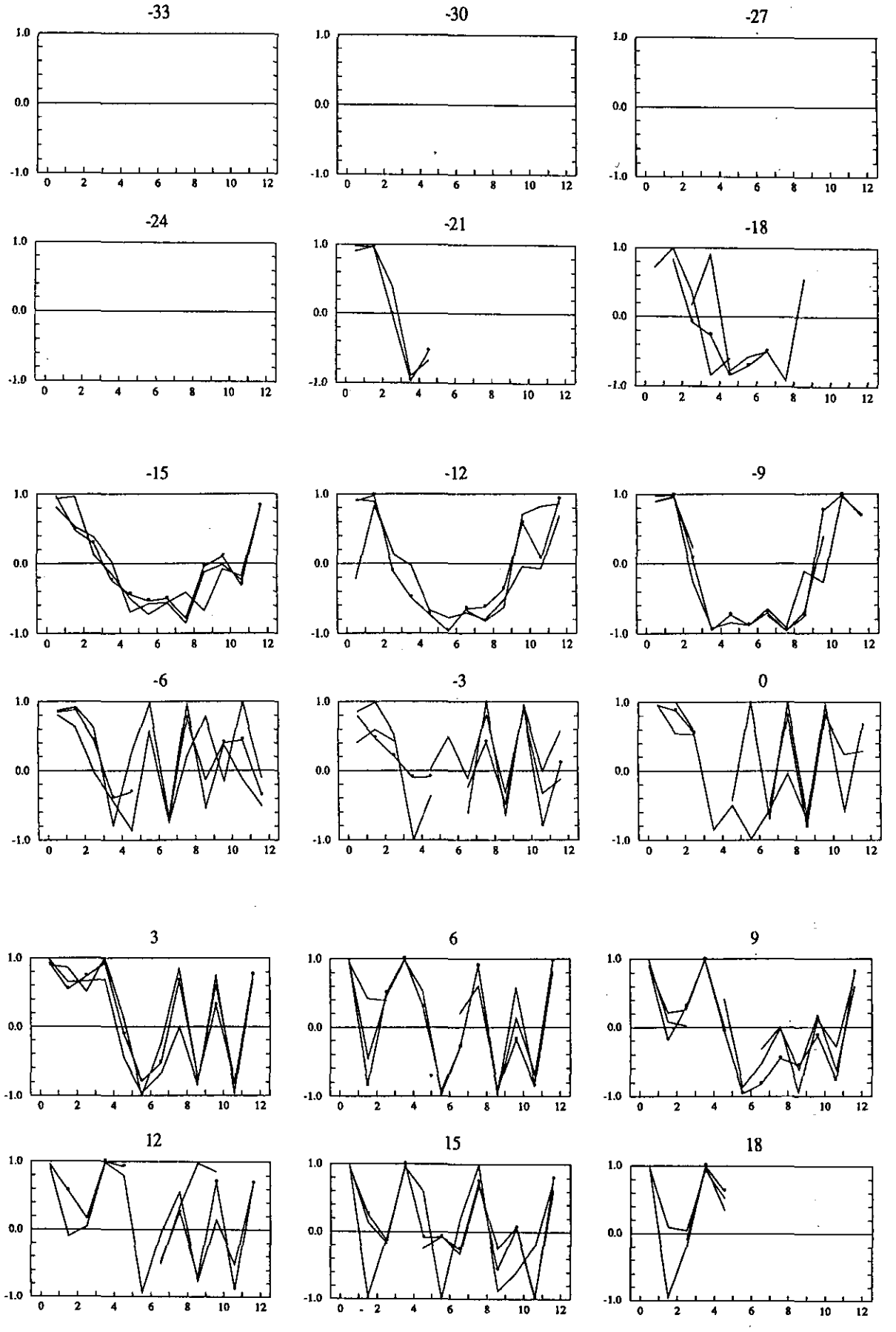

Figure 12A–C: Fremantle–Persian Gulf Track. Sea surface temperature temporal autocorrelation function. Details as in Fig. 8.

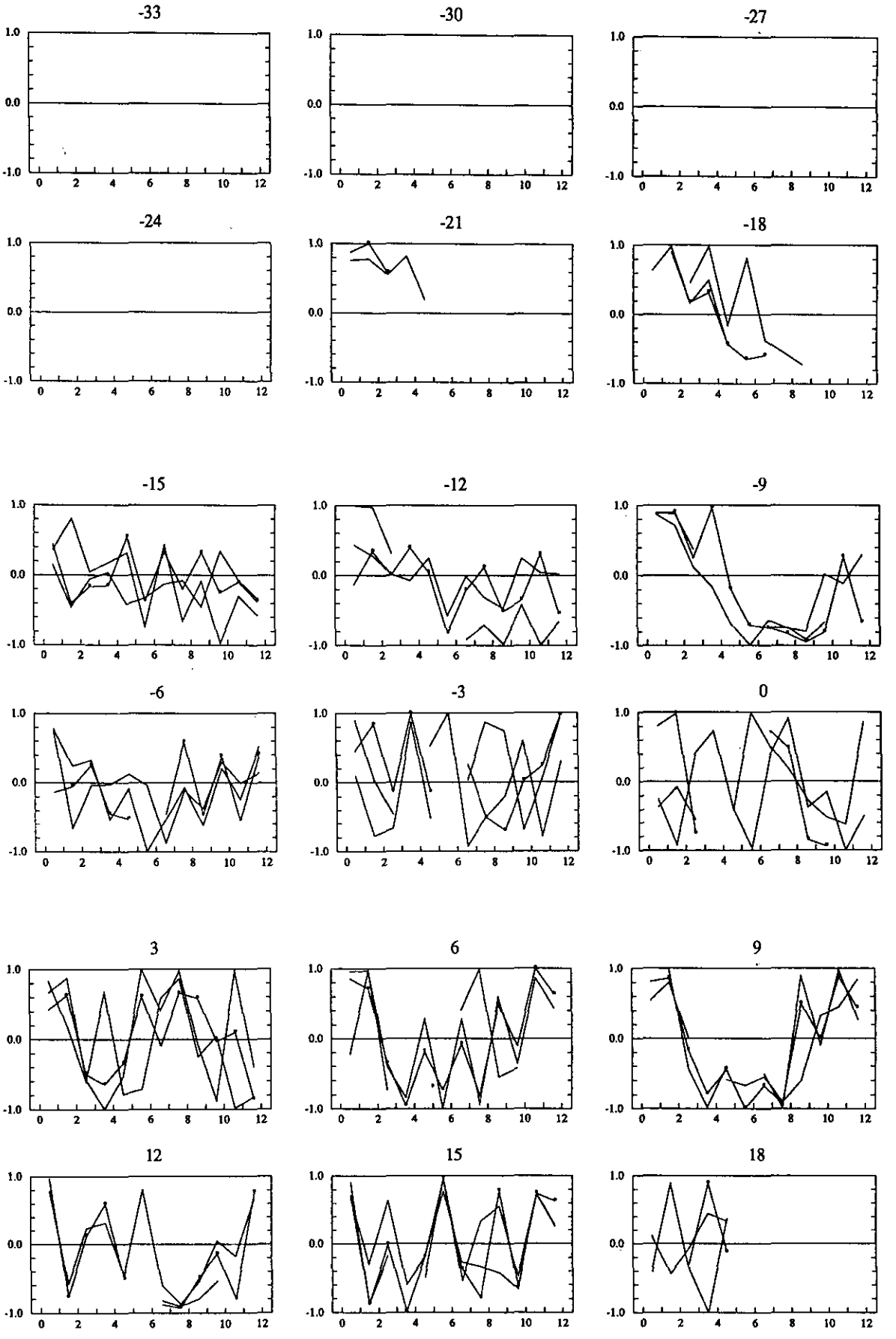

Figure 13 A–C: Fremantle–Persian Gulf Track. Depth of 20°C isotherm temporal autocorrelation function. Details as in Fig. 8.

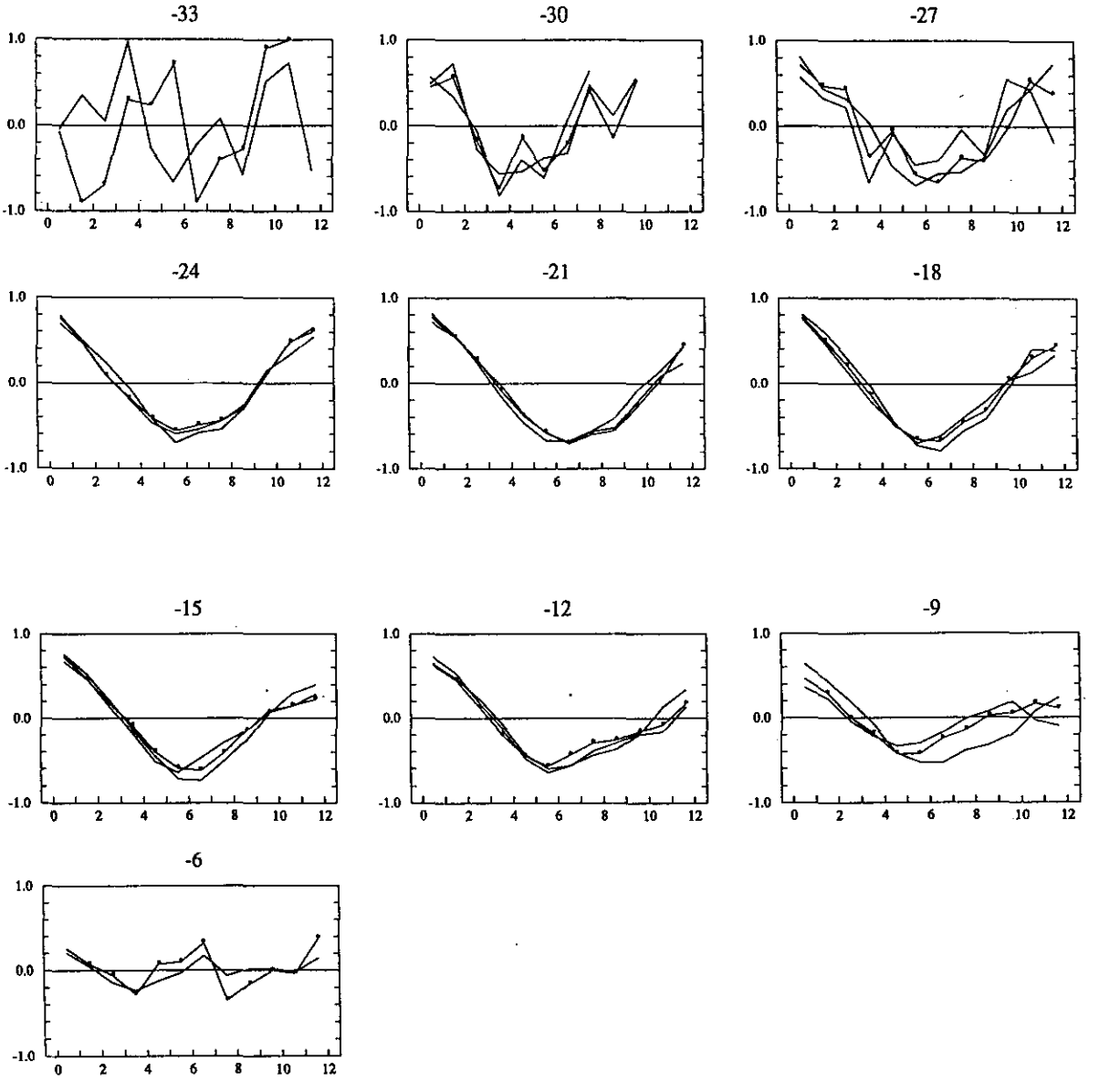

Figure 14 A–B: Fremantle–Sunda Strait Track. Sea surface temperature temporal autocorrelation function. Details as in Fig. 8.

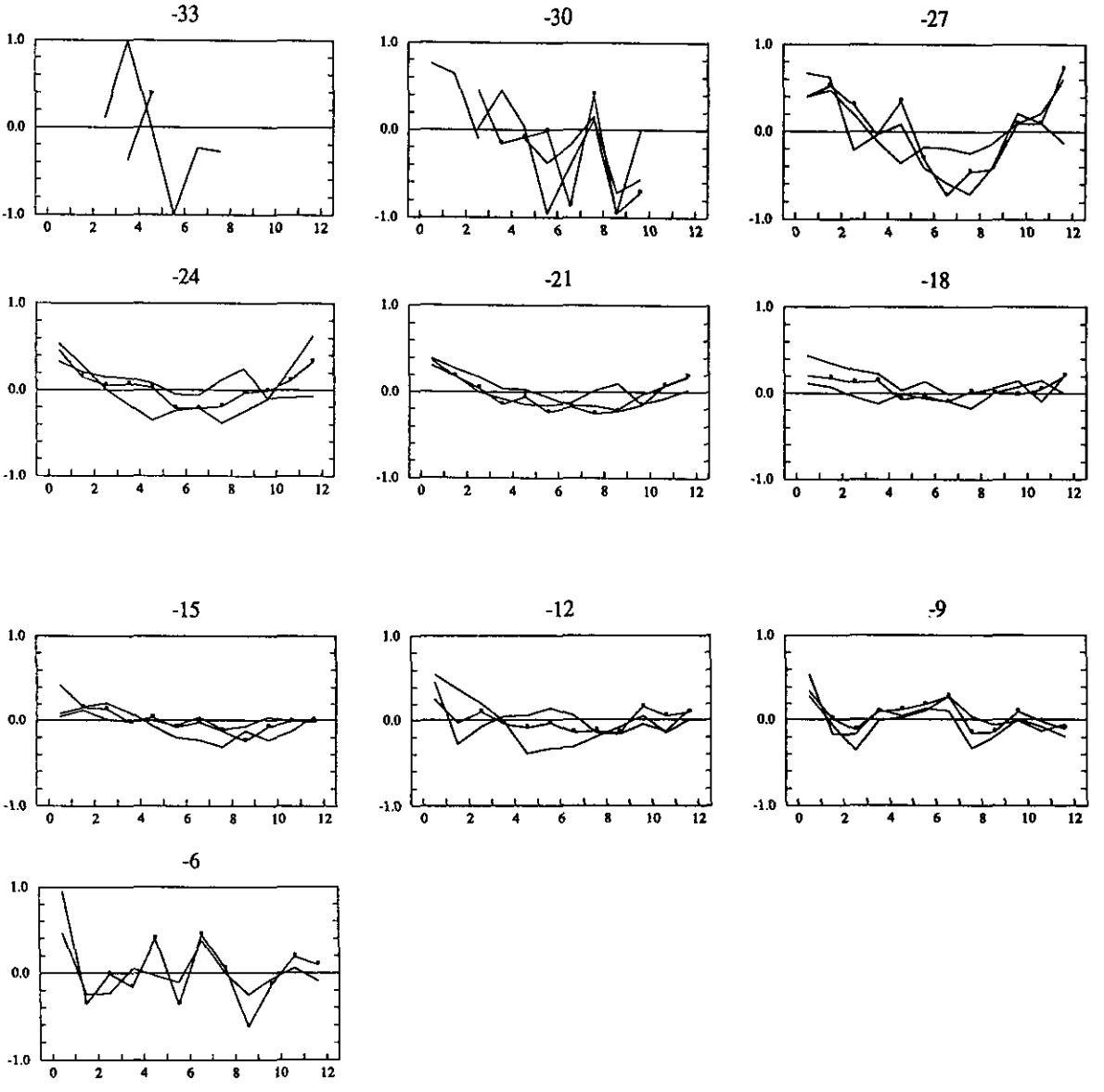

Figure 15A–B: Fremantle–Sunda Strait Track. Depth of 20°C isotherm temporal autocorrelation function. Details as in Fig. 8.

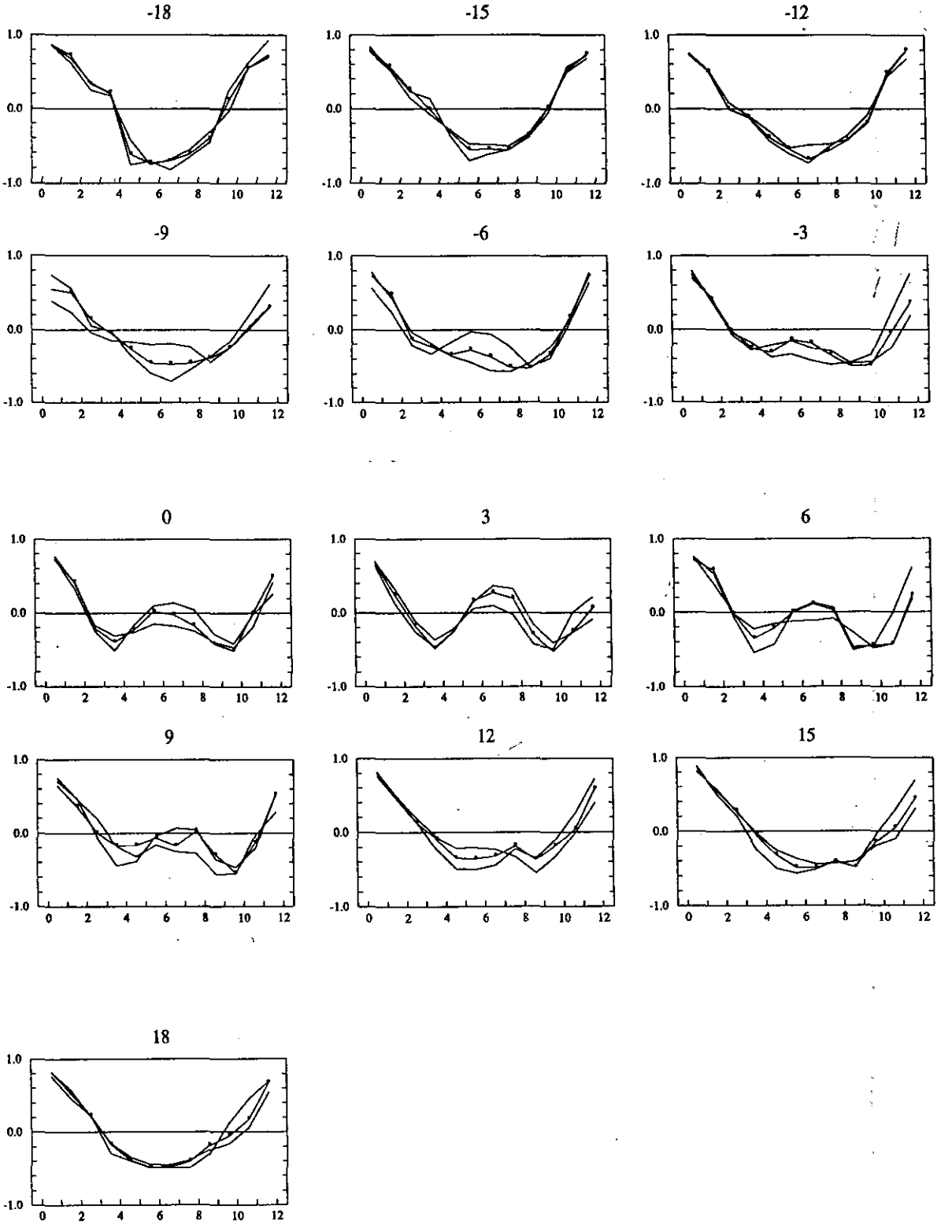

Figure 16A–C: Port Hedland–Japan Track. Sea surface temperature temporal autocorrelation function. Details as in Fig. 8.

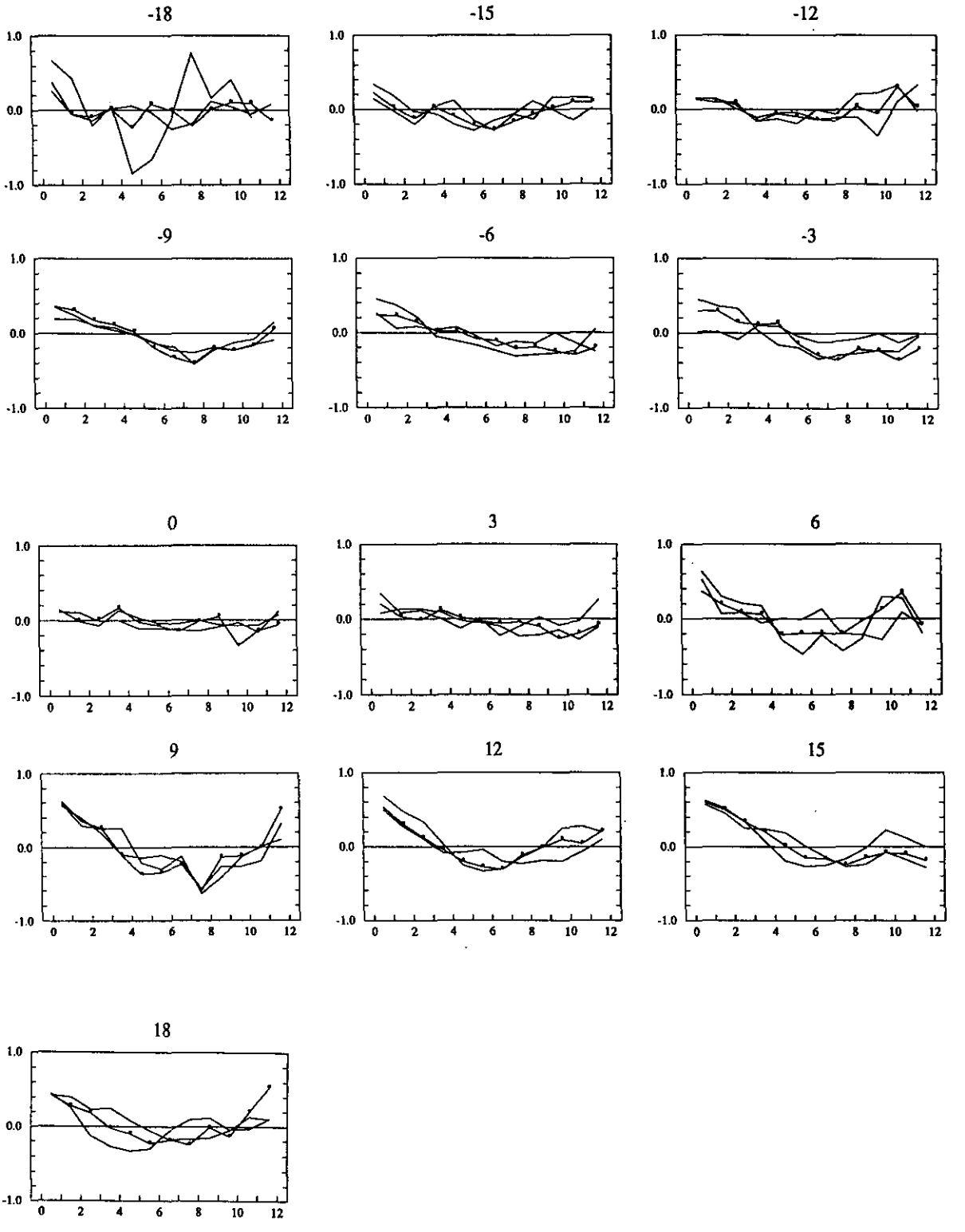

Figure 17A–C: Port Hedland–Japan Track. Depth of 20°C isotherm temporal autocorrelation function. Details as in Fig. 8.

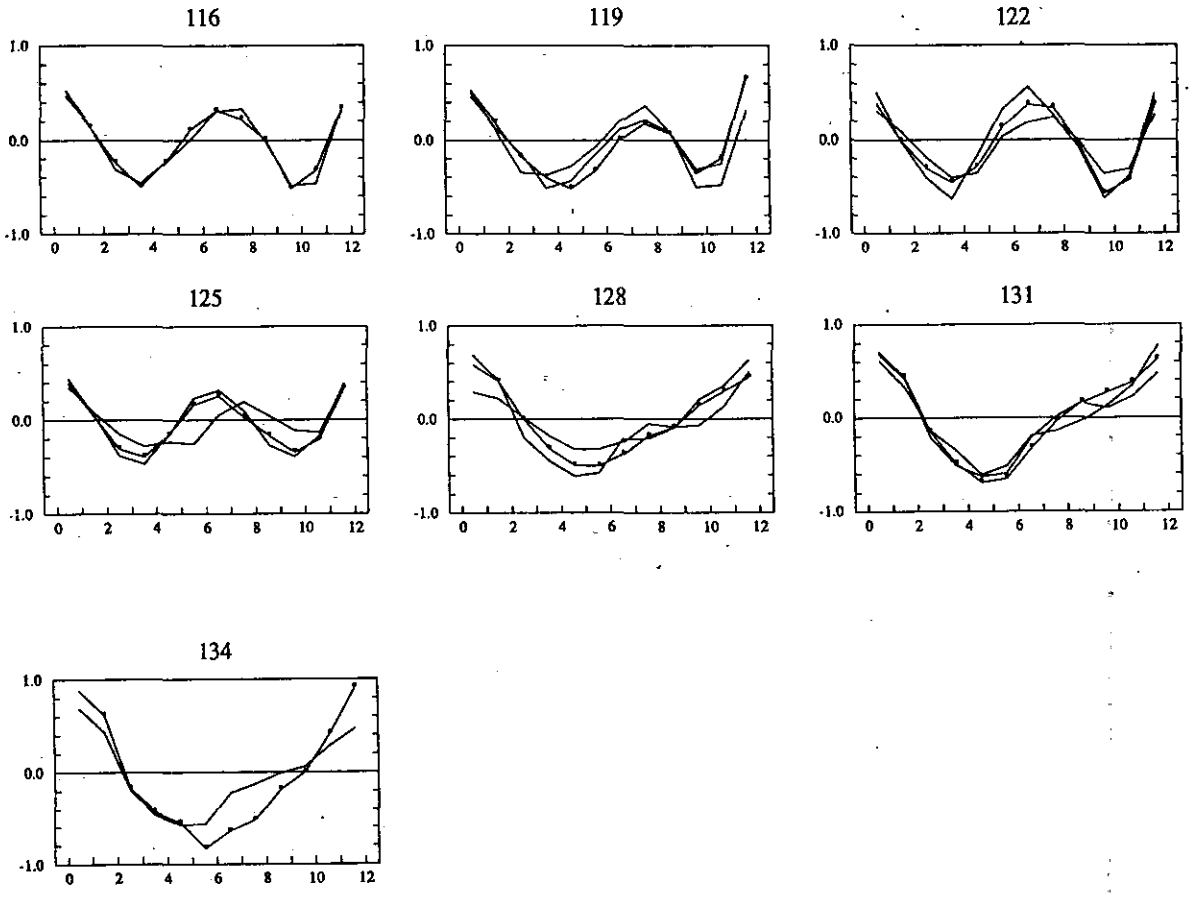

Figure 18A–B: Flores Sea–Banda Sea Track. Sea surface temperature temporal autocorrelation function, in 3° longitude bands. The central longitude is indicated at the top of each frame and its ACF indicated with dots. Lag is in months.

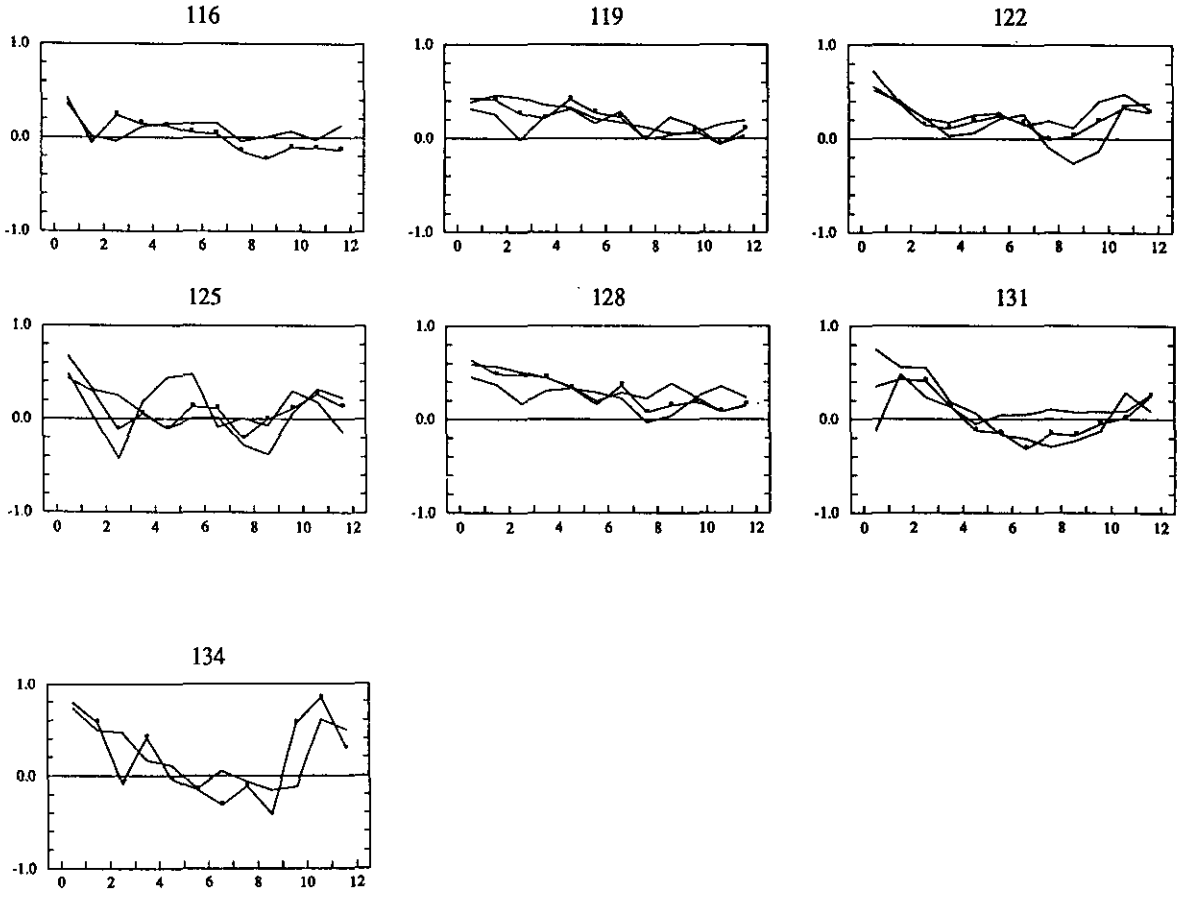

Figure 19A–B: Flores Sea–Banda Sea Track. Depth of 20°C isotherm temporal autocorrelation function. Details as in Fig. 18.

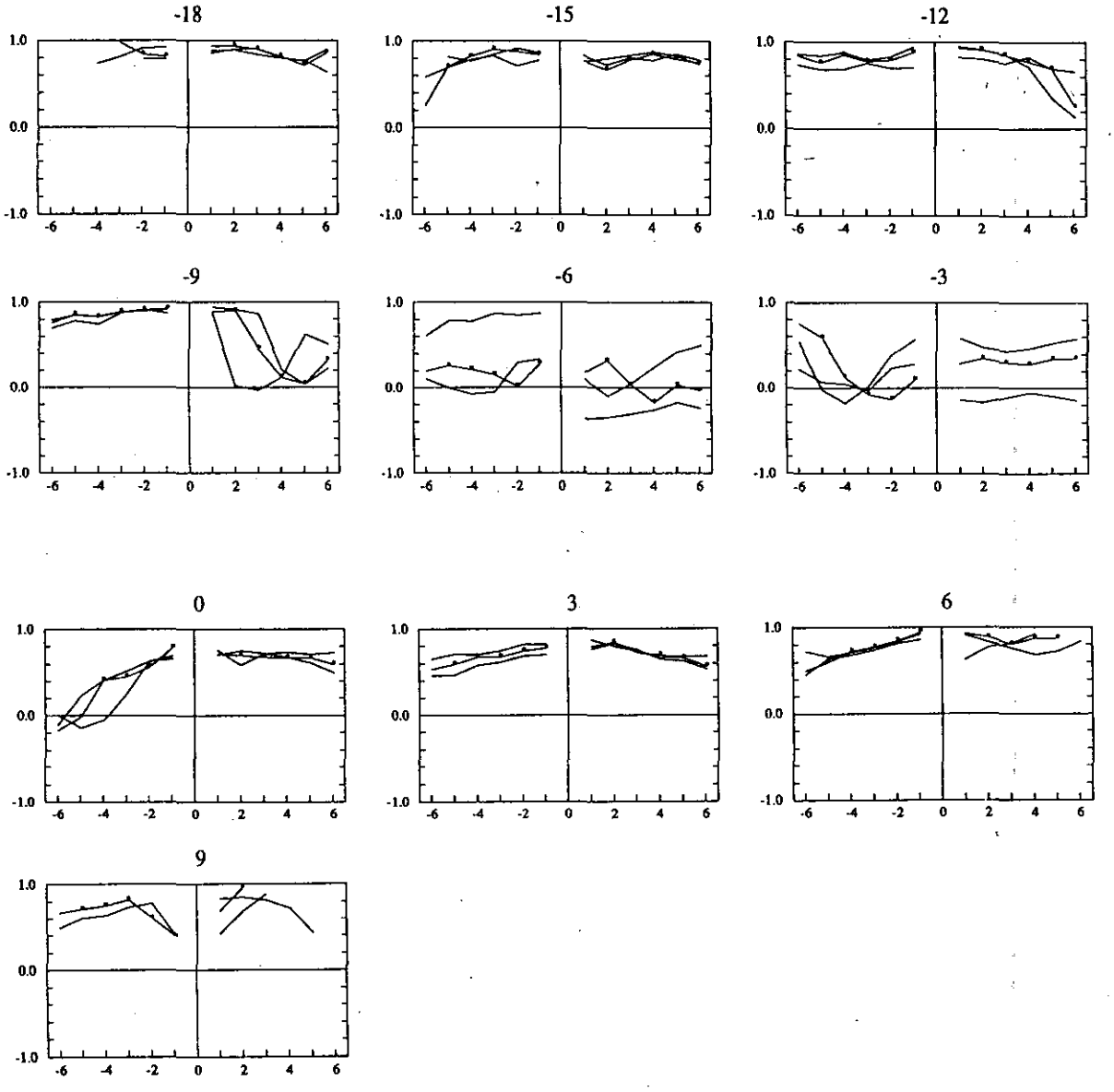

Figure 20A–B: La Réunion–Red Sea Track. Sea surface temperature meridional autocorrelation function, in 3° latitude bands. The central latitude is indicated at the top of each frame, and its ACF indicated with dots. Lag is in degrees latitude; positive indicates northward separation.

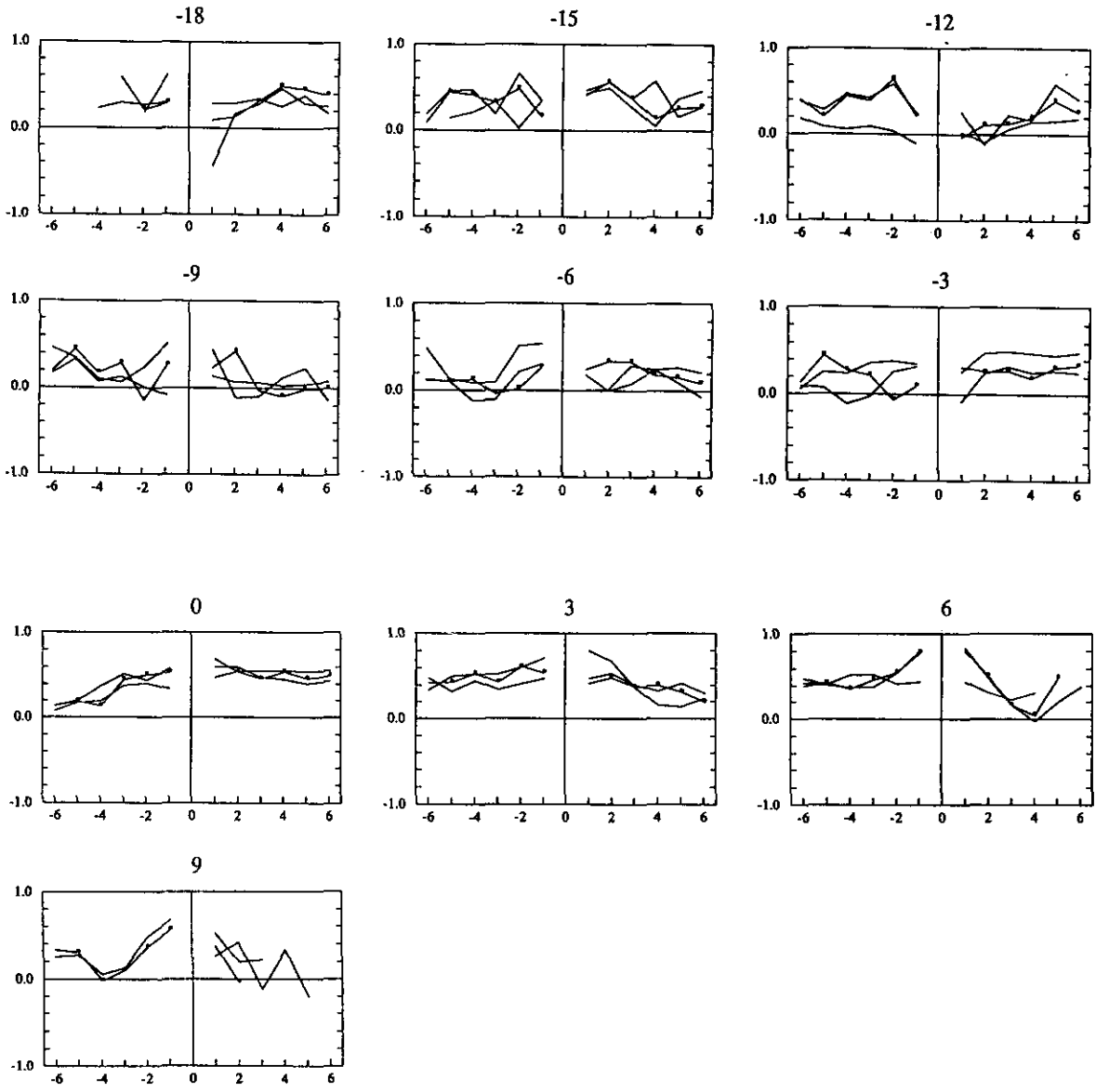

Figure 21A–B: La Réunion–Red Sea Track. Depth of 20°C isotherm meridional autocorrelation function. Details as in Fig. 20.

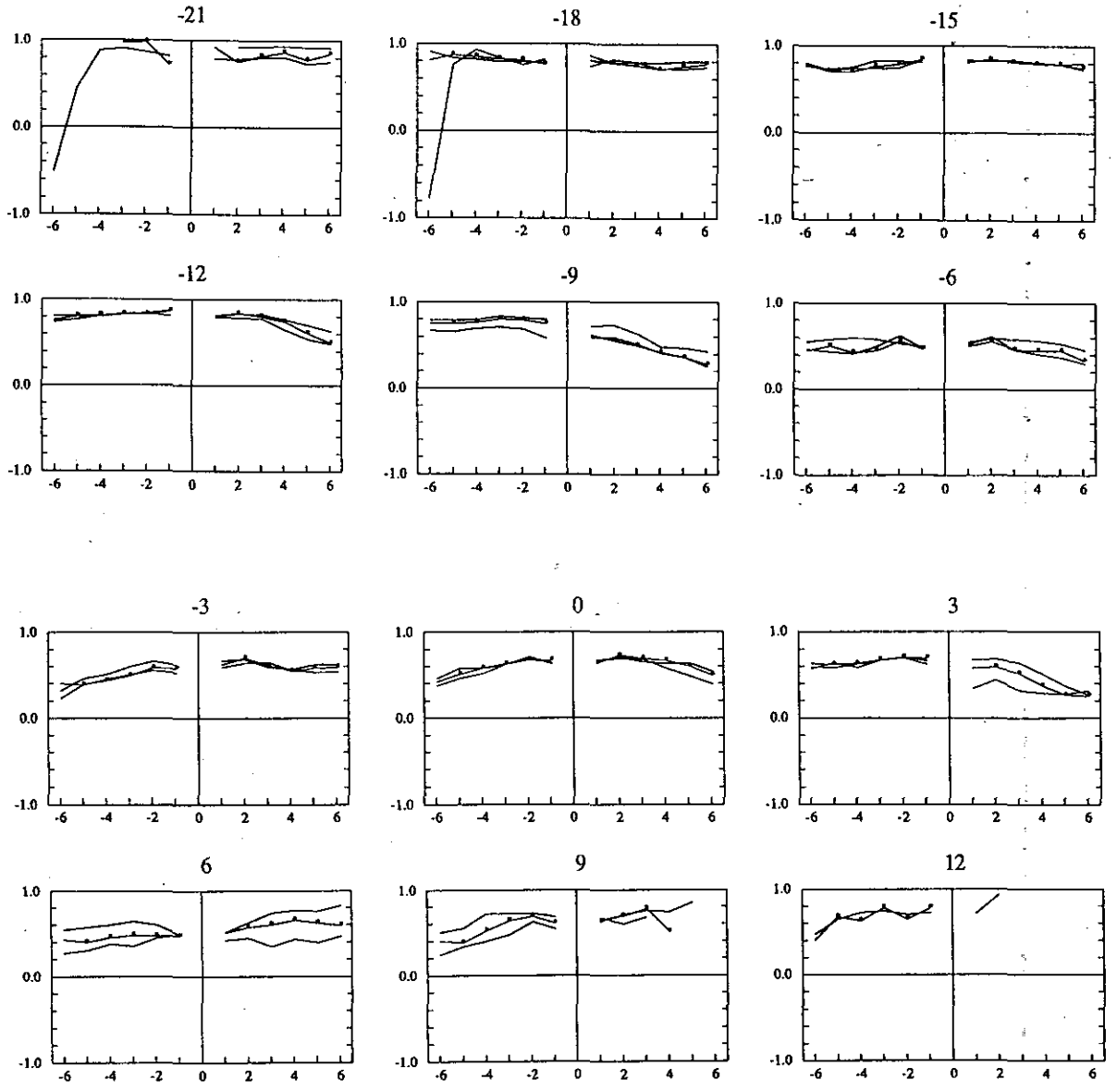

Figure 22A–B: Fremantle-Red Sea Track. Sea surface temperature meridional autocorrelation function. Details as in Fig. 20.

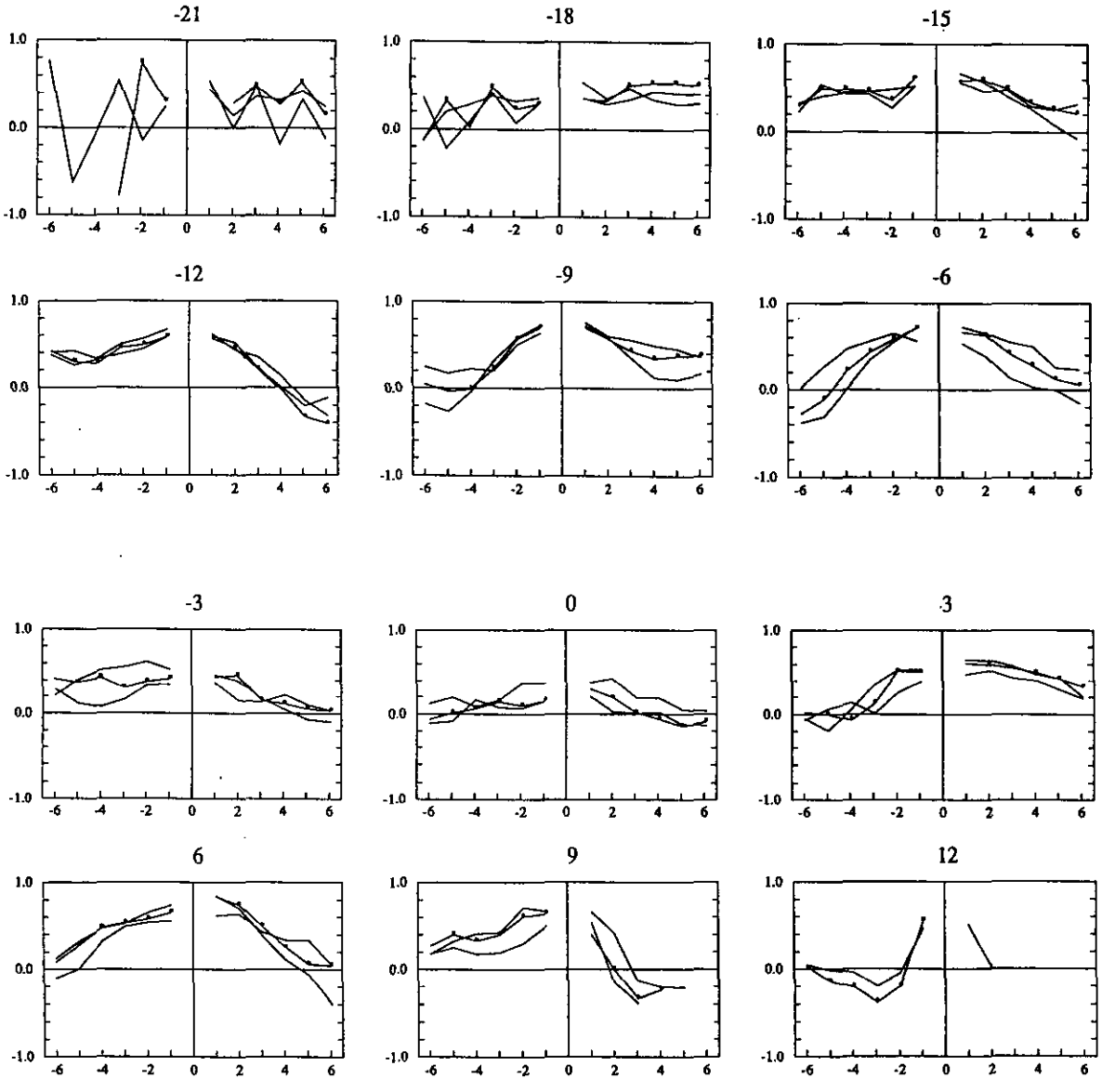

Figure 23A–B: Fremantle–Red Sea Track. Depth of 20°C isotherm meridional autocorrelation function. Details as in Fig. 20.

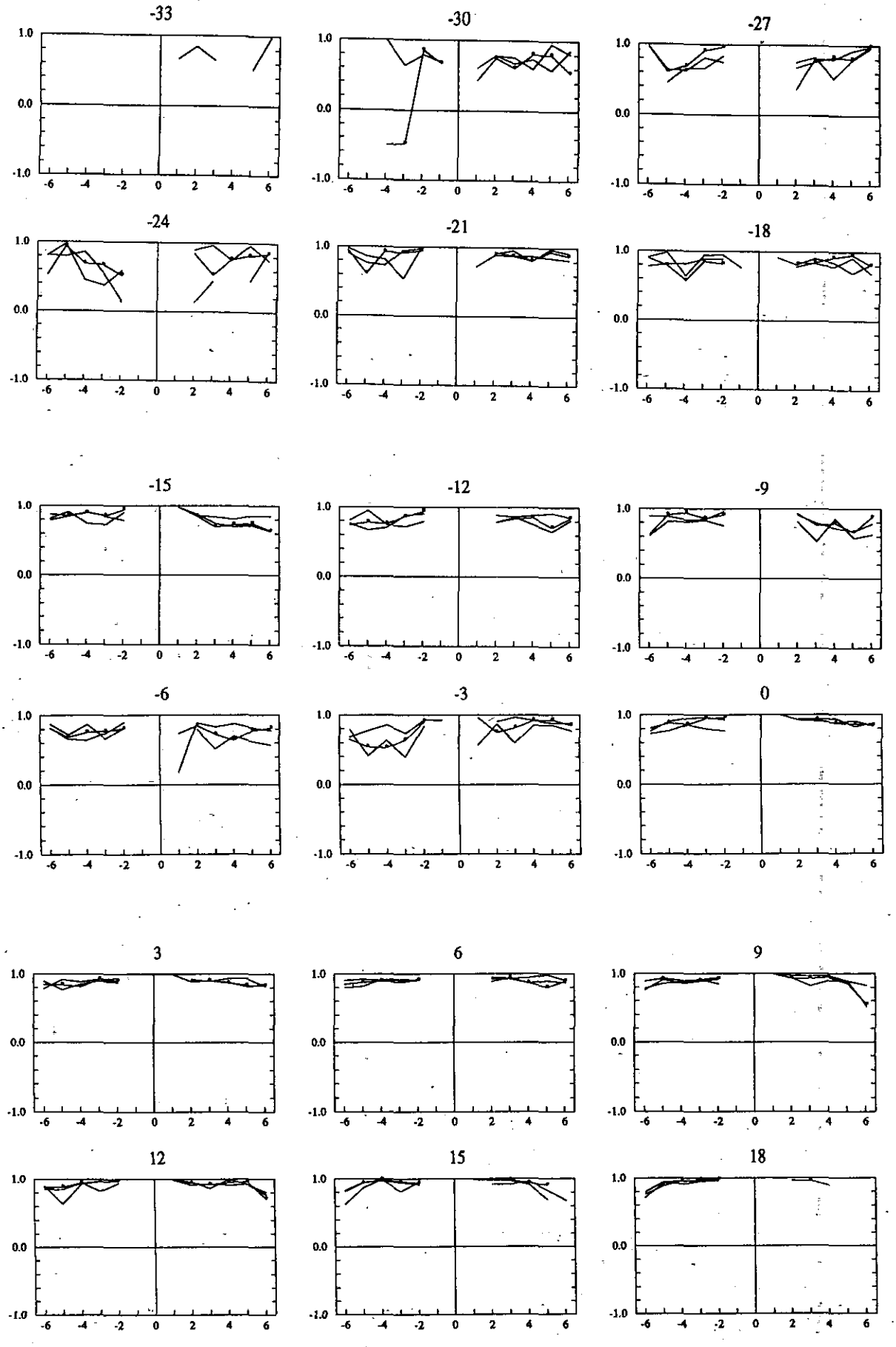

Figure 24A–C: Fremantle–Persian Gulf Track. Sea surface temperature meridional autocorrelation function. Details as in Fig. 20.

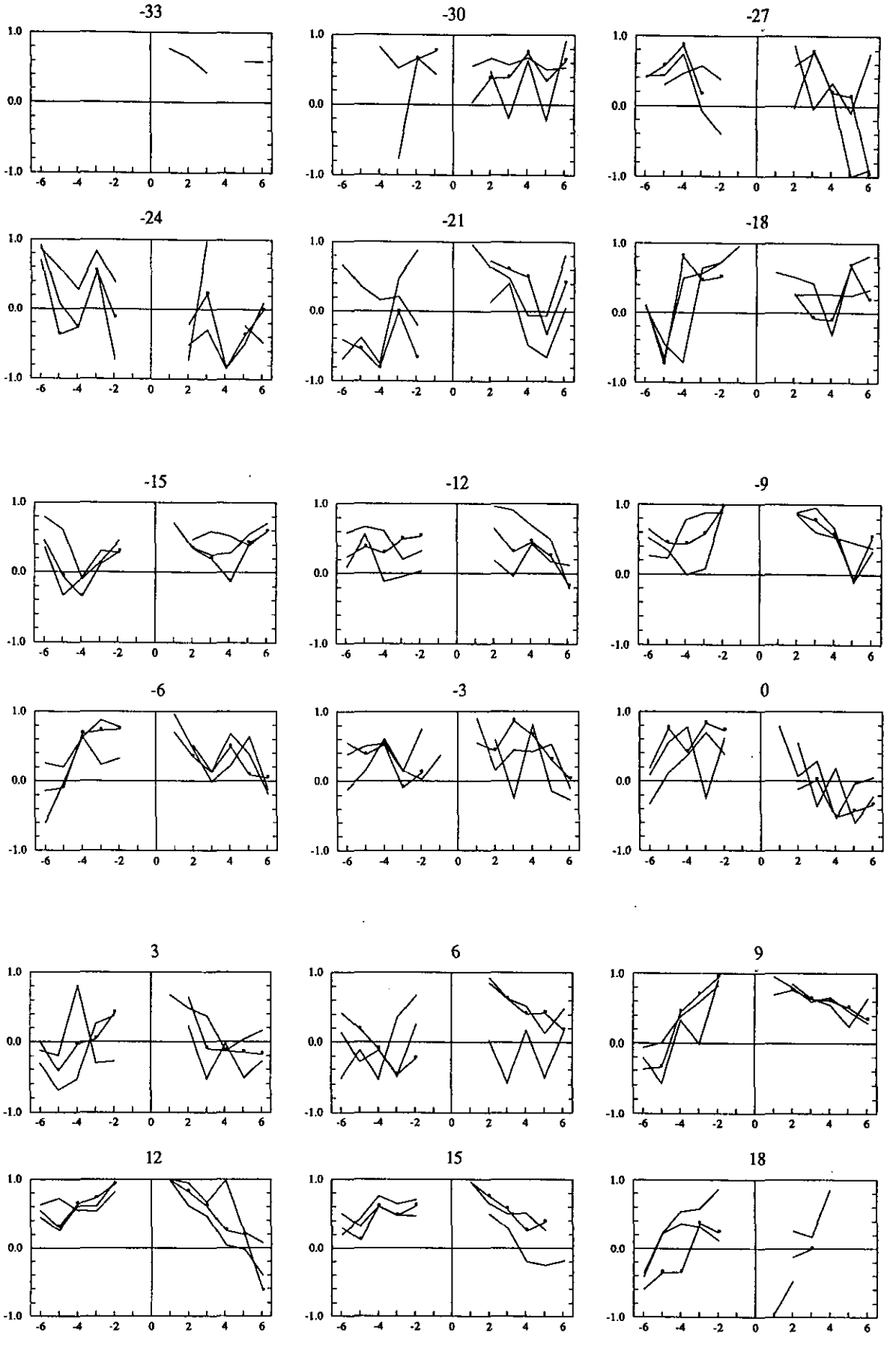

Figure 25A–C: Fremantle–Persian Gulf Track. Depth of 20°C isotherm meridional autocorrelation function. Details as in Fig. 20.

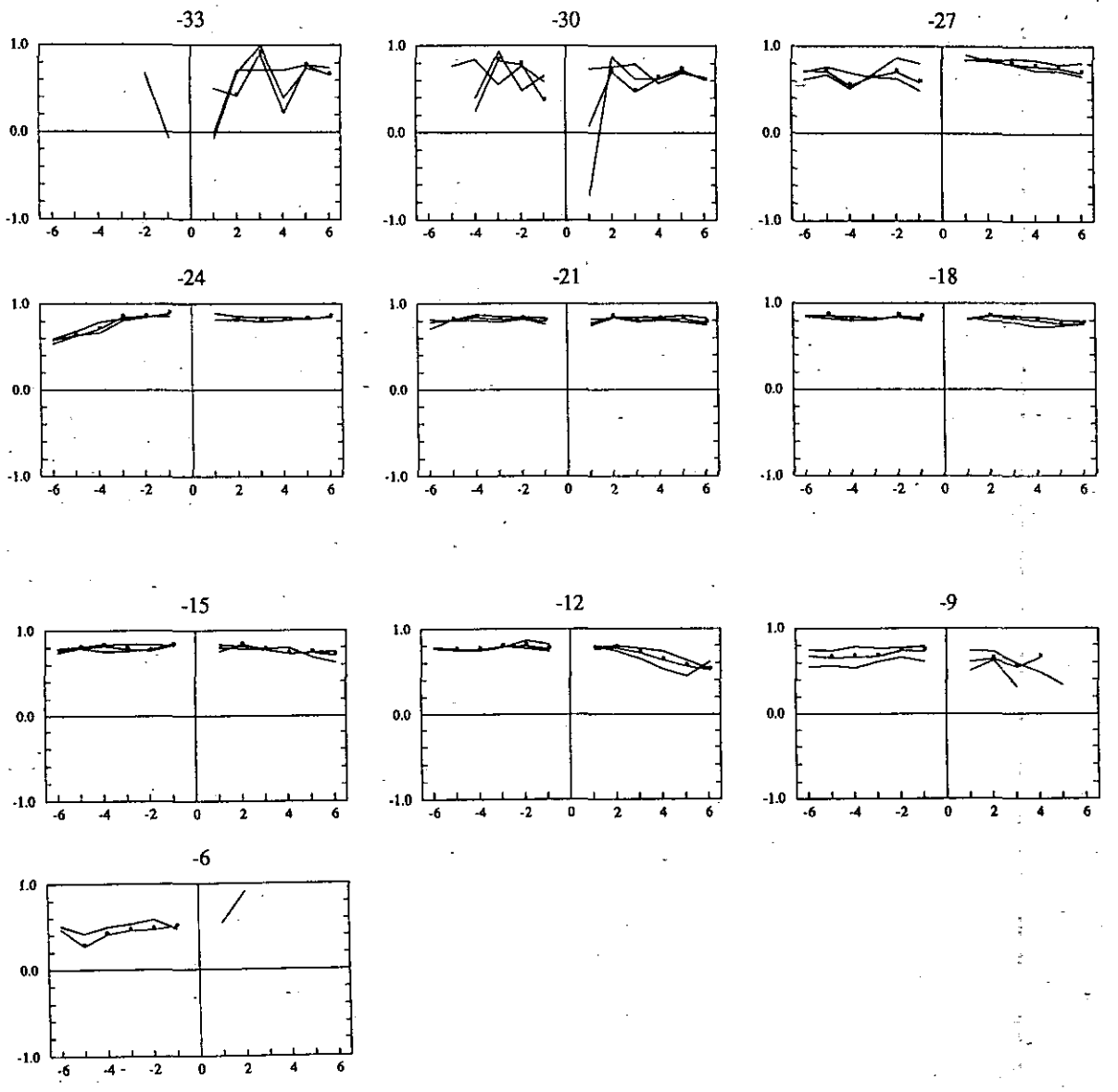

Figure 26A–B: Fremantle–Sunda Strait Track. Sea surface temperature meridional autocorrelation function. Details as in Fig. 20.

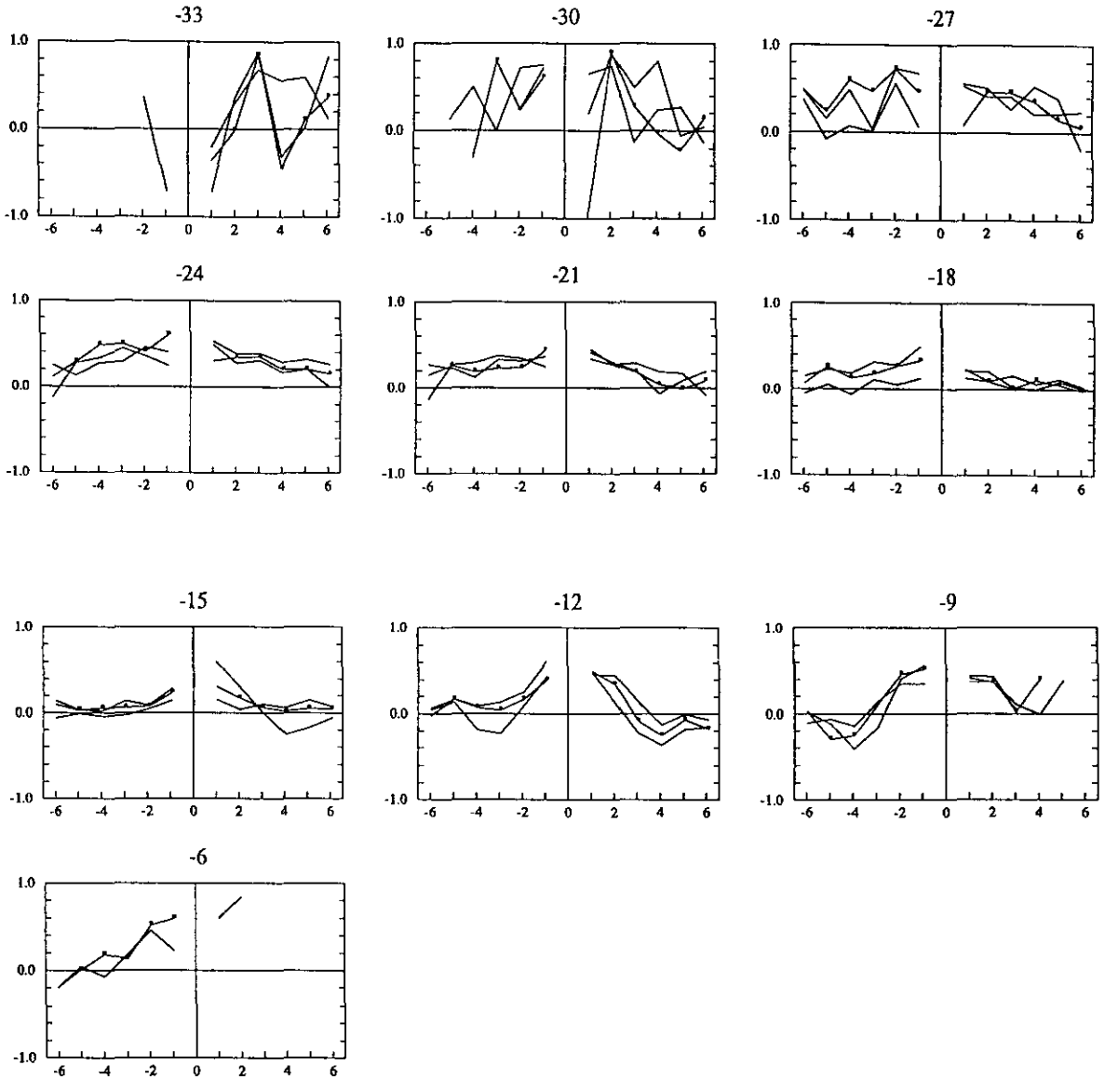

Figure 27A–A: Fremantle–Sunda Strait Track. Depth of 20°C isotherm meridional autocorrelation function. Details as in Fig. 20.

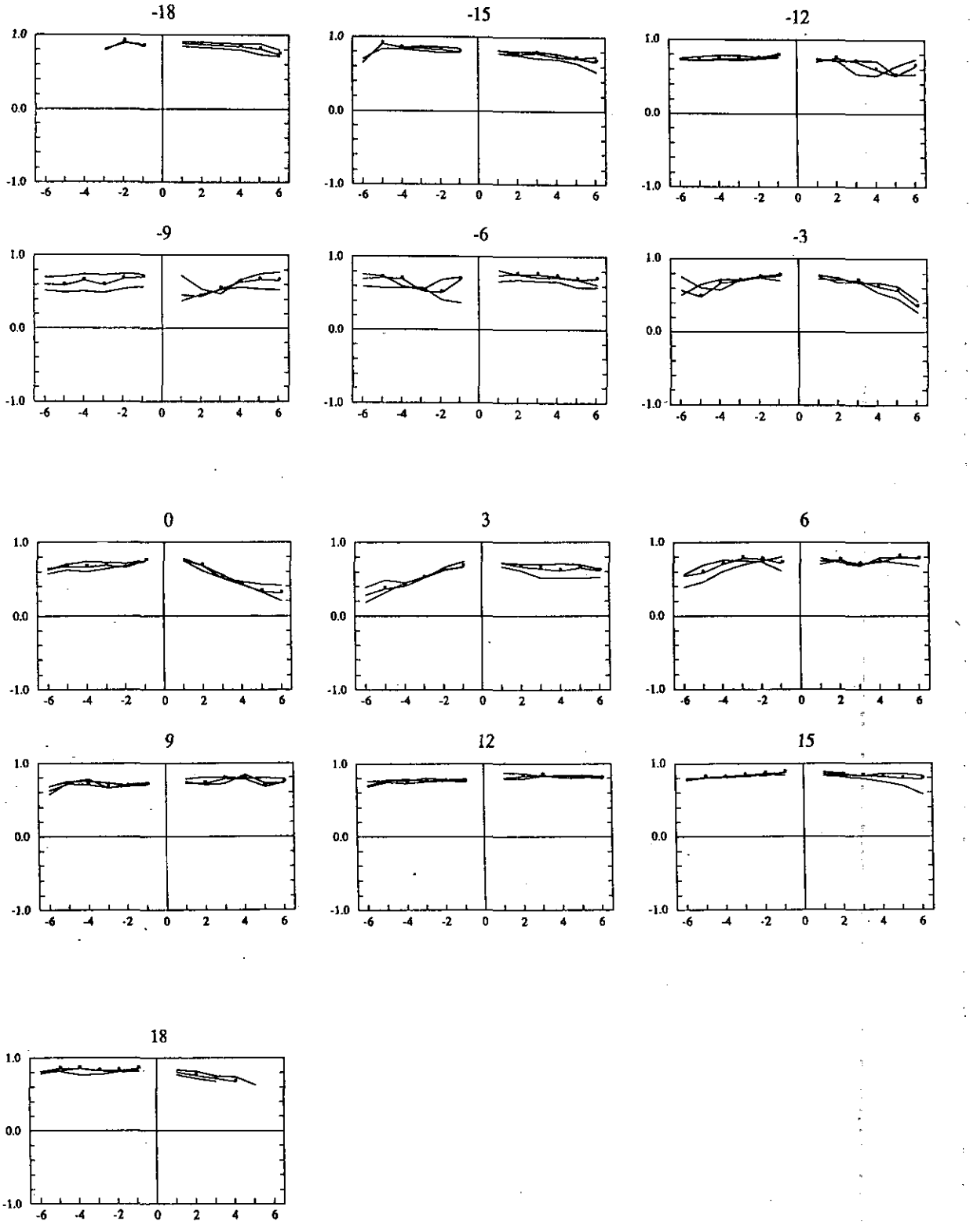

Figure 28A–C: Port Hedland–Japan Track. Sea surface temperature meridional autocorrelation function. Details as in Fig. 20.

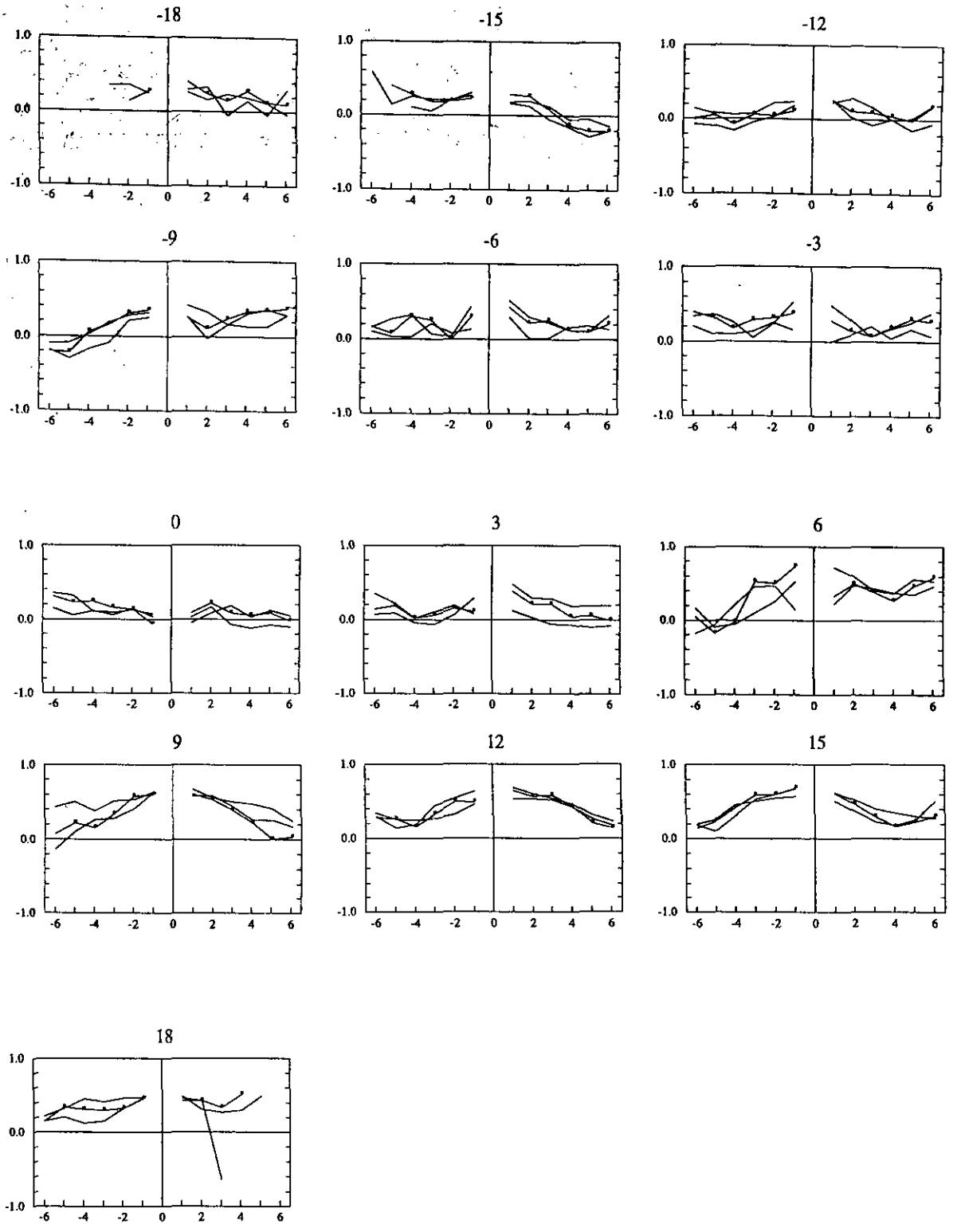

Figure 29A–C: Port Hedland–Japan Track. Depth of 20°C isotherm meridional autocorrelation function.Details as in Fig. 20.

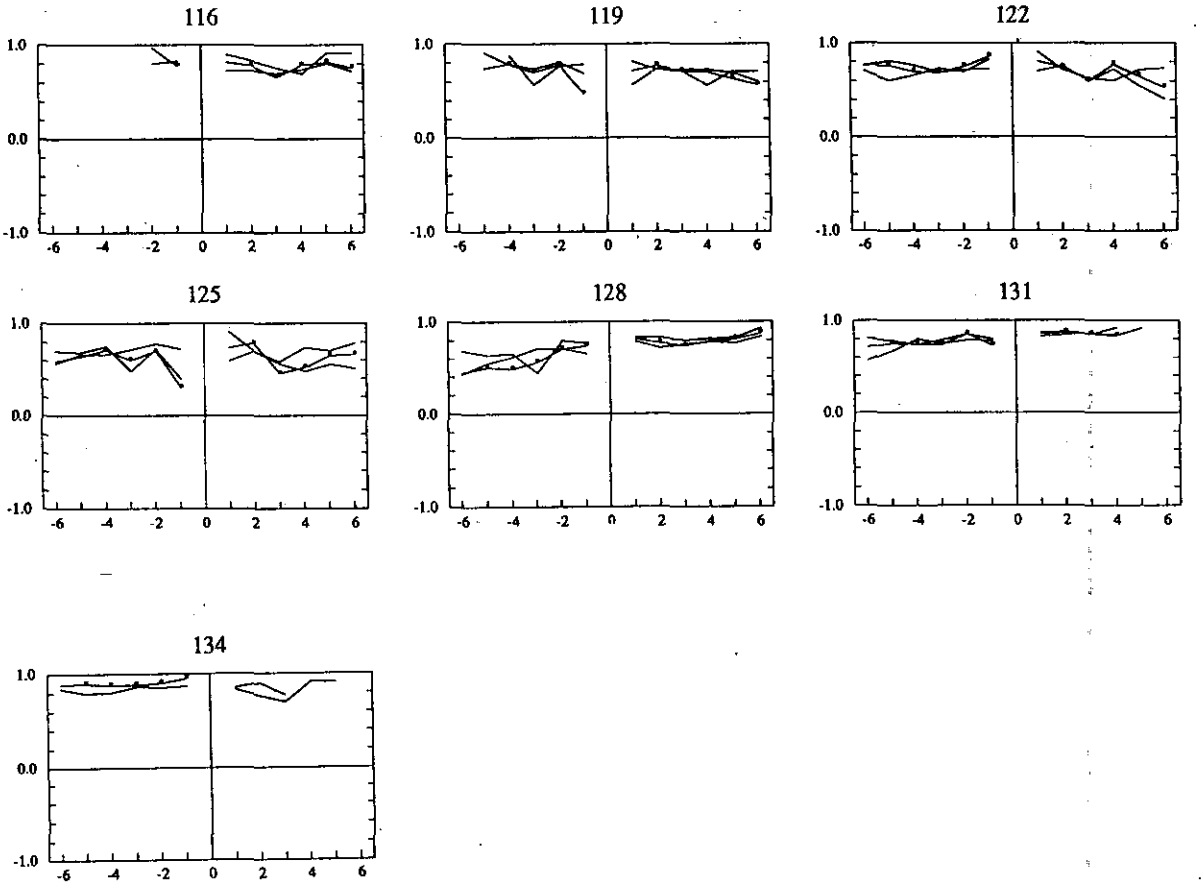

Figure 30A–B: Flores Sea–Banda Sea Track. Sea surface temperature zonal autocorrelation function in 3° longitude bands. The central longitude is indicated at the top of each frame, and its ACF indicated with dots. Lag is in degrees longitude; positive indicates eastward separation.

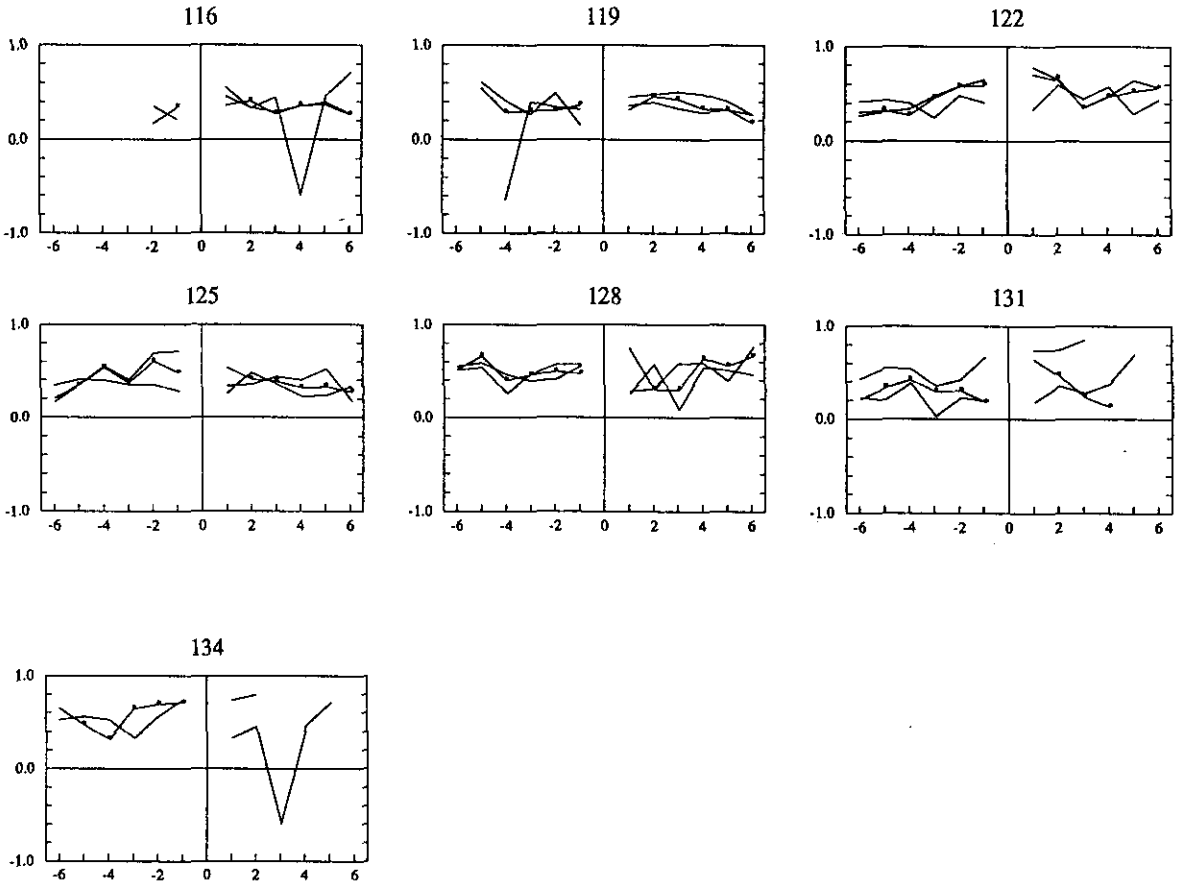

Figure 31A–B: Flores Sea–Banda Sea Track. Depth of 20°C isotherm zonal autocorrelation function. Details as in Fig. 30.

REUNION - RED SEA
FEB 1985 - FEB 1988

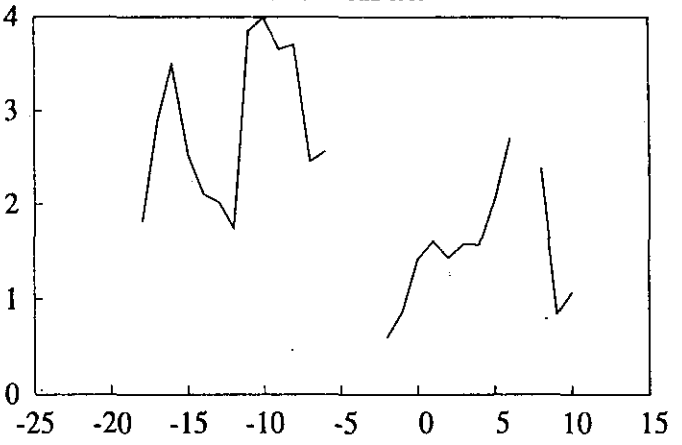

FREMANTLE - RED SEA
AUG 1986 - JUL 1988

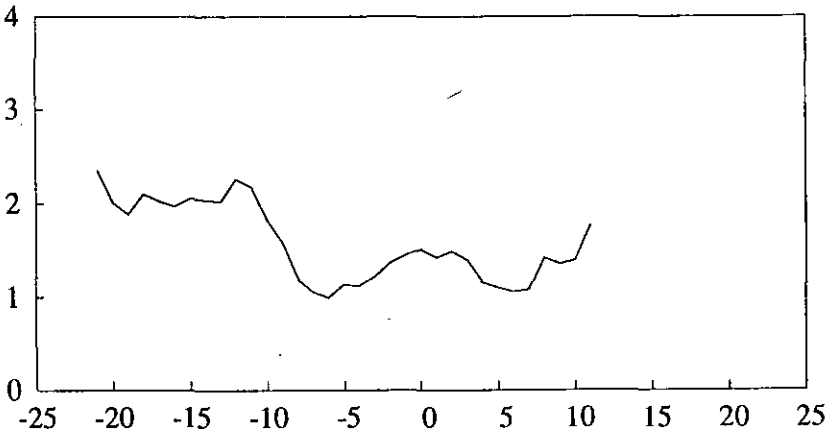

FREMANTLE - PERSIAN GULF
NOV 1985 - DEC 1987

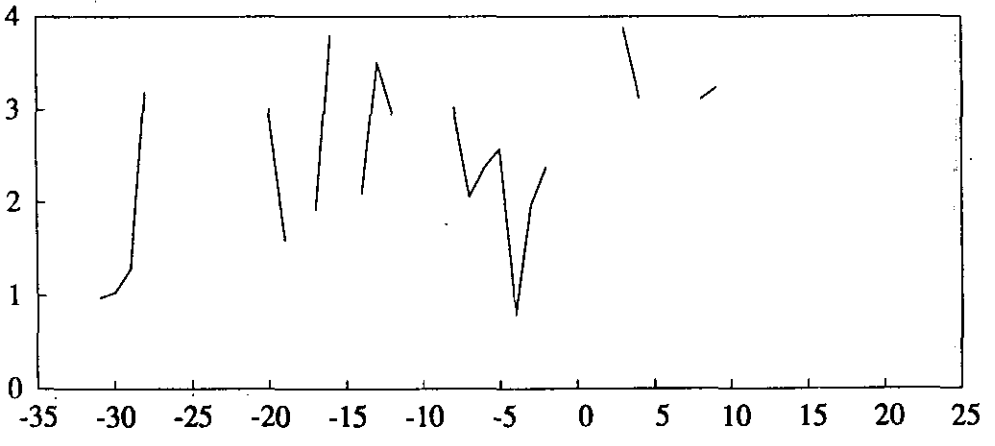

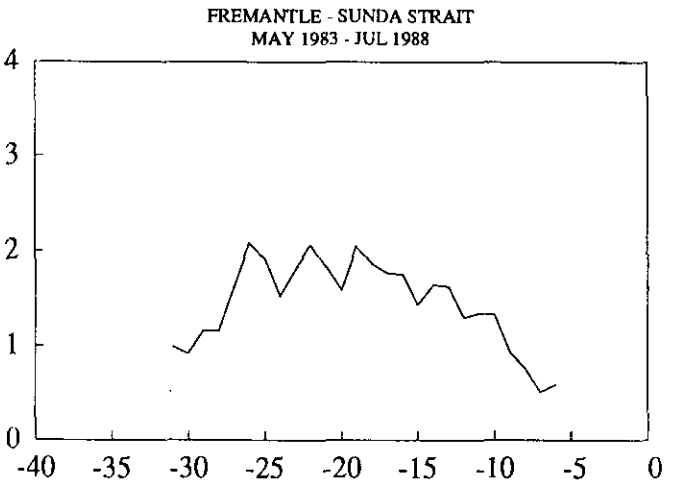

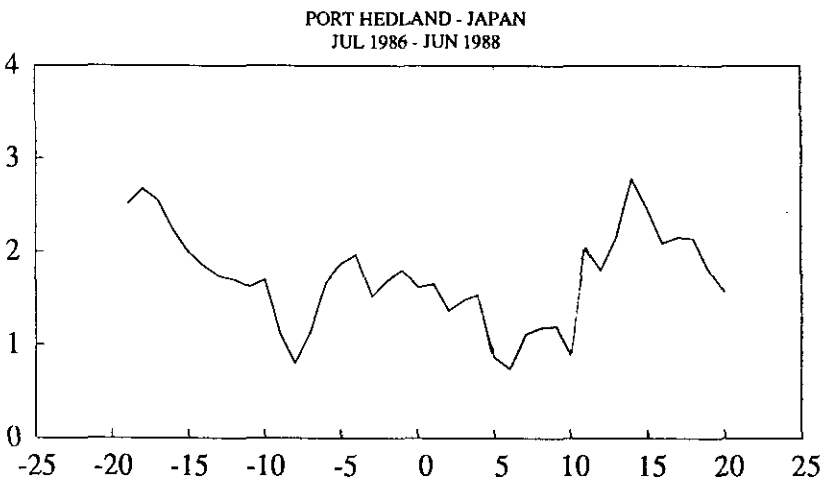

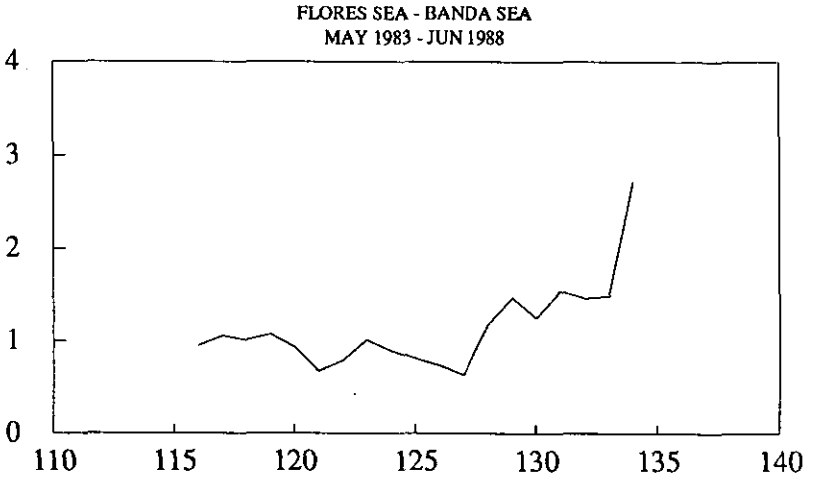

Figure 32 A–F: Signal to noise ratio of SST on the La Réunion–Red Sea (A), Fremantle–Red Sea (B), Fremantle–Persian Gulf (C), Fremantle–Sunda Strait (D), Port Hedland–Japan (E), and Flores Sea–Banda Sea (F) tracks.

REUNION - RED SEA
FEB 1985 - FEB 1988

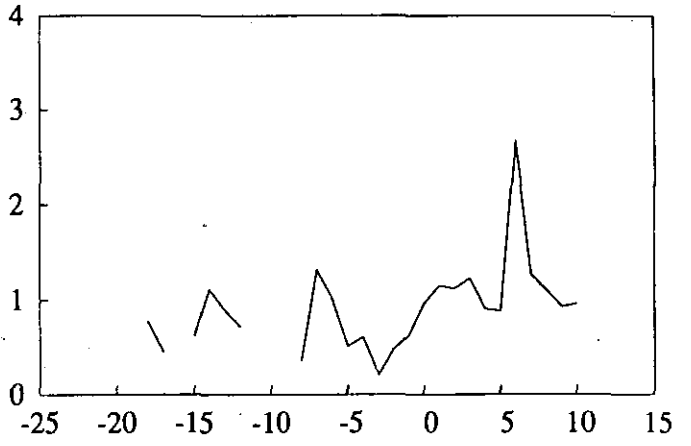

FREMANTLE - RED SEA
AUG 1986 - JUL 1988

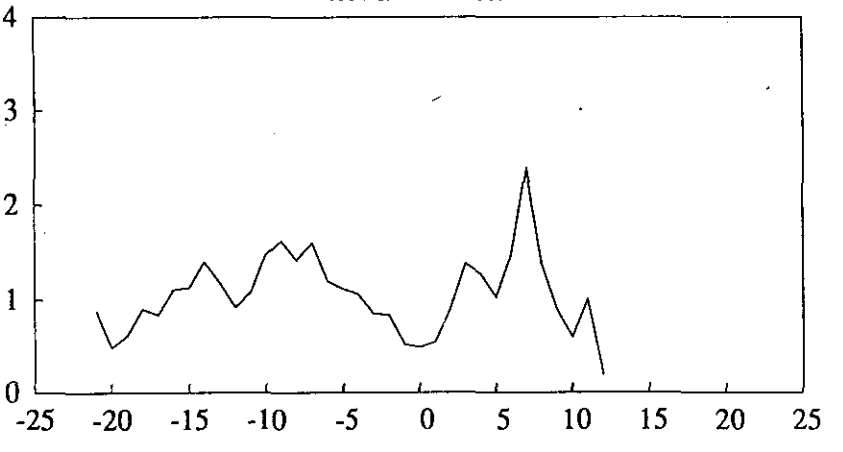

FREMANTLE - PERSIAN GULF
NOV 1985 - DEC 1987

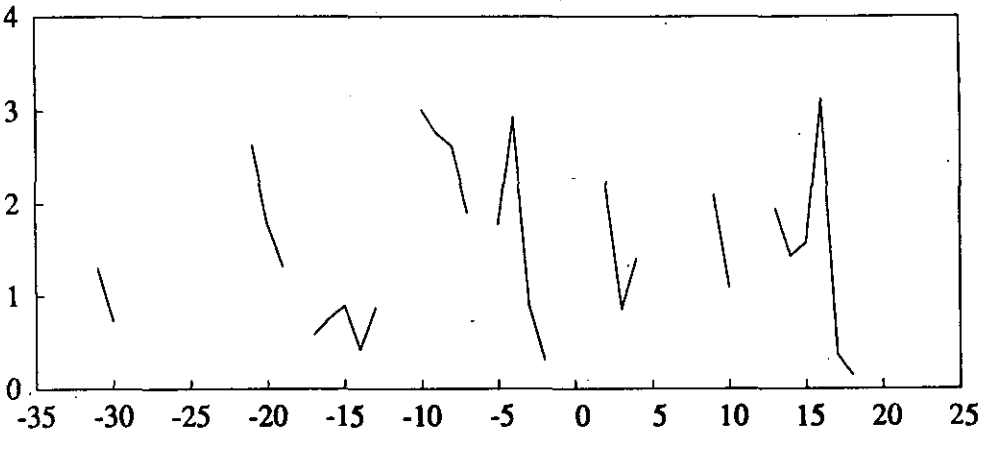

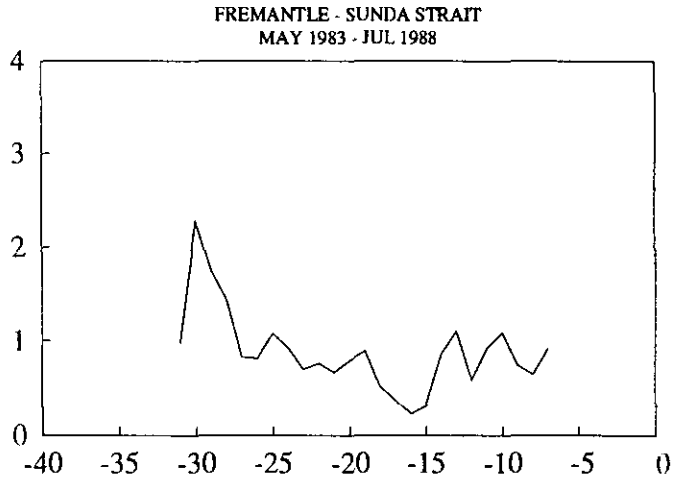

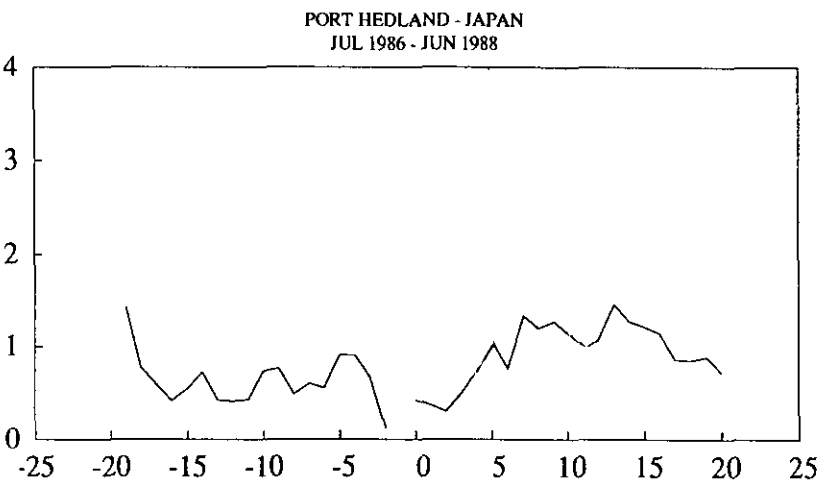

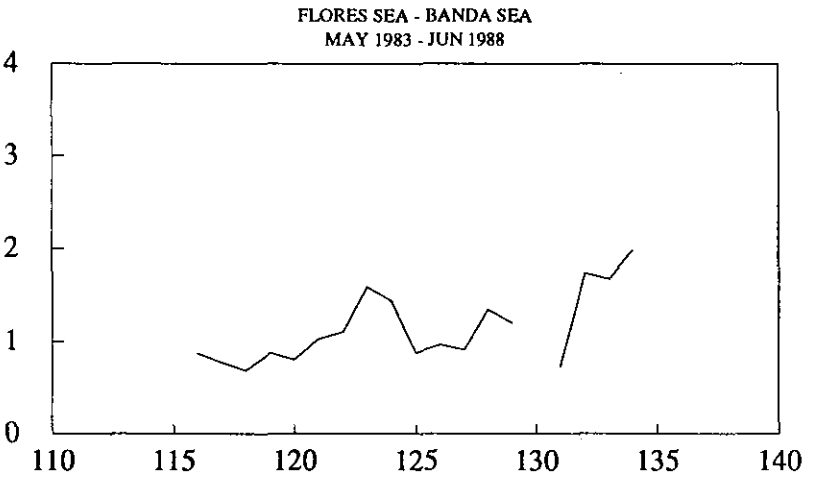

Figure 33A–F: Signal to noise ratio of D_{20} on six tracks as in Fig. 32.

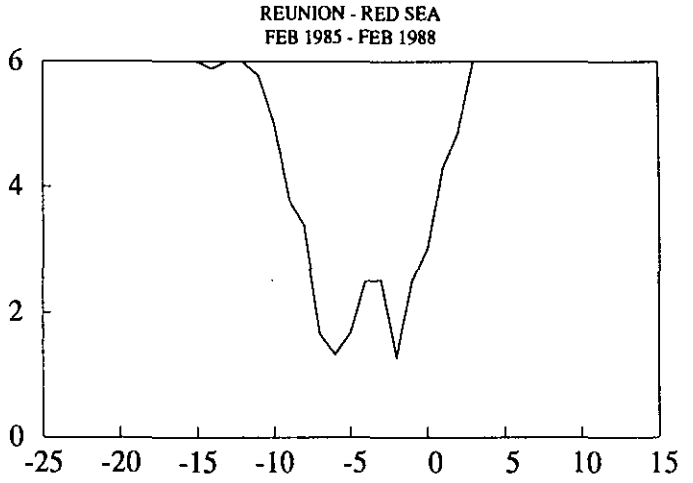
REUNION - RED SEA
FEB 1985 - FEB 1988
6
4
2
0
-25 -20 -15 -10 -5 0 5 10 15

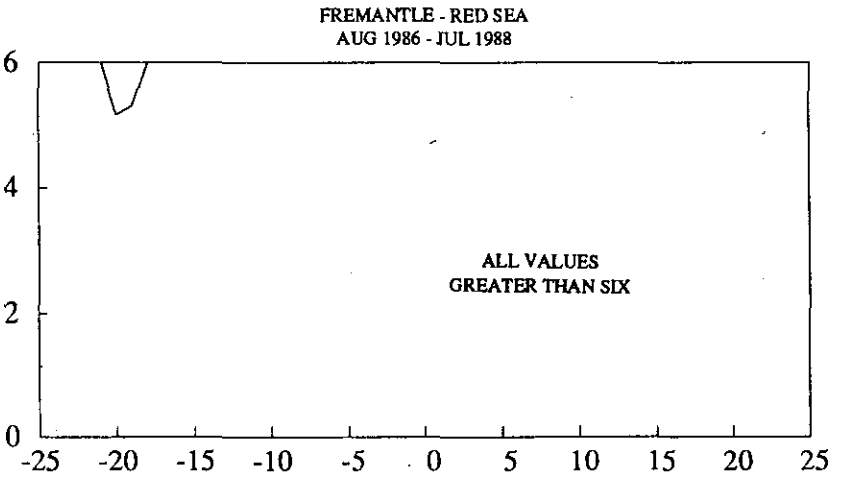
FREMANTLE - RED SEA
AUG 1986 - JUL 1988
6
4
2
0
ALL VALUES
GREATER THAN SIX
-25 -20 -15 -10 -5 0 5 10 15 20 25

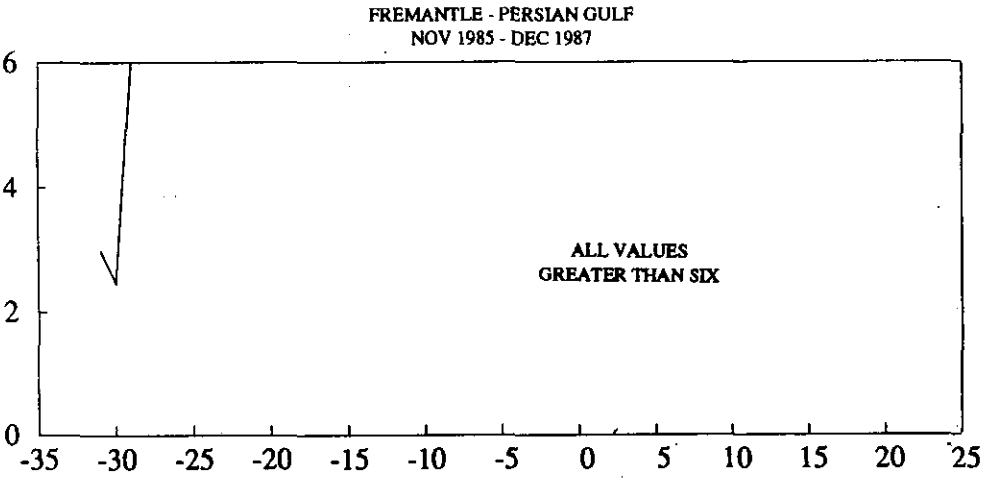
FREMANTLE - PERSIAN GULF
NOV 1985 - DEC 1987
6
4
2
0
ALL VALUES
GREATER THAN SIX
-35 -30 -25 -20 -15 -10 -5 0 5 10 15 20 25

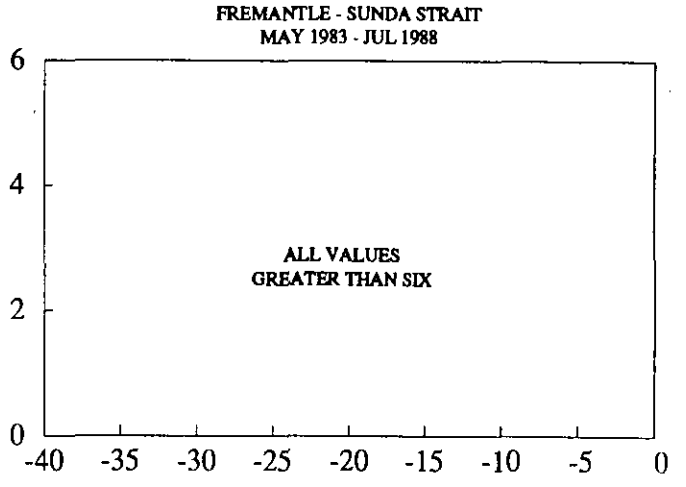

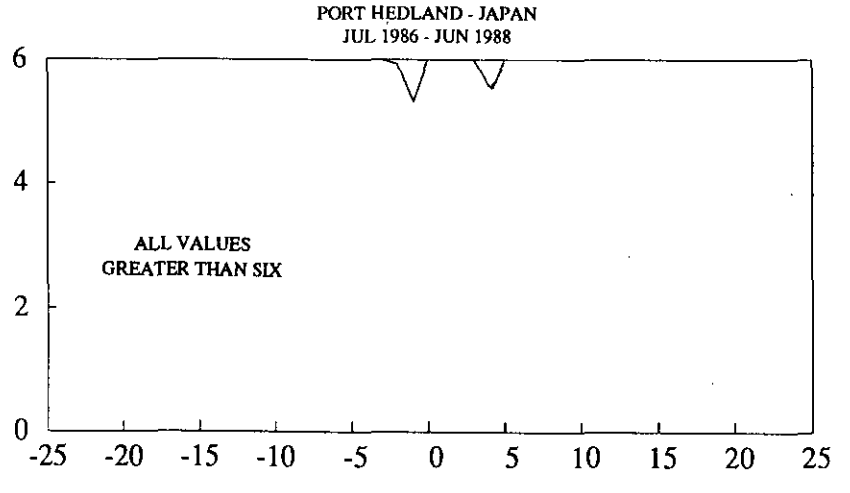

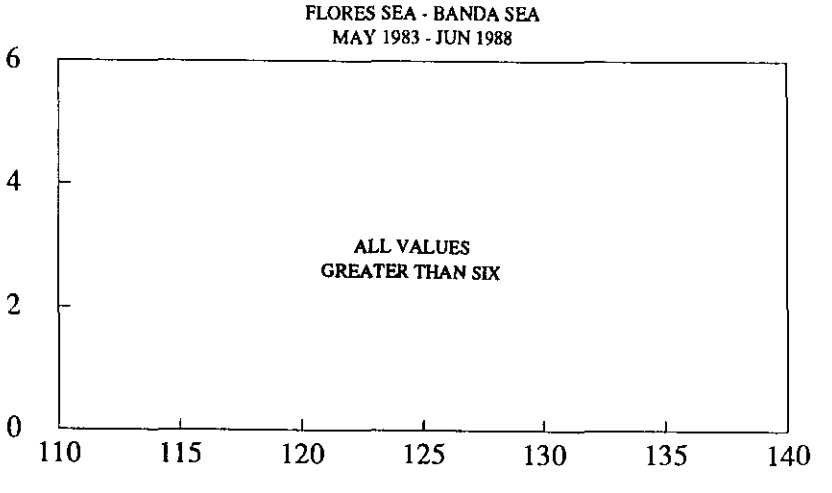

Figure 34 A–F: Meridional decorrelation scale of SST on five tracks (A-E) and zonal decorrelation scale of SST on track F, as in Fig. 32.

REUNION - RED SEA
FEB 1985 - FEB 1988

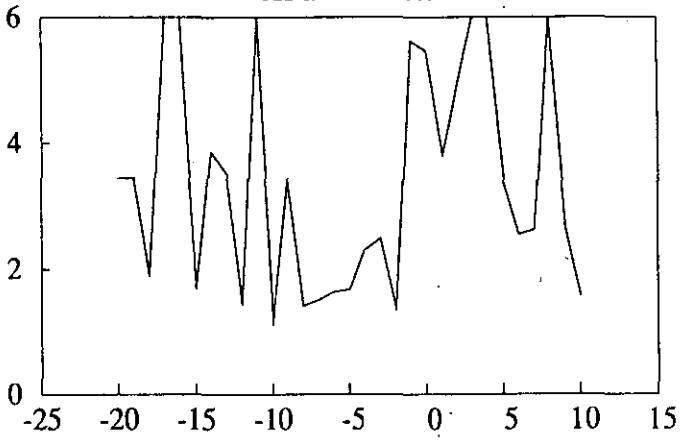

FREMANTLE - RED SEA
AUG 1986 - JUL 1988

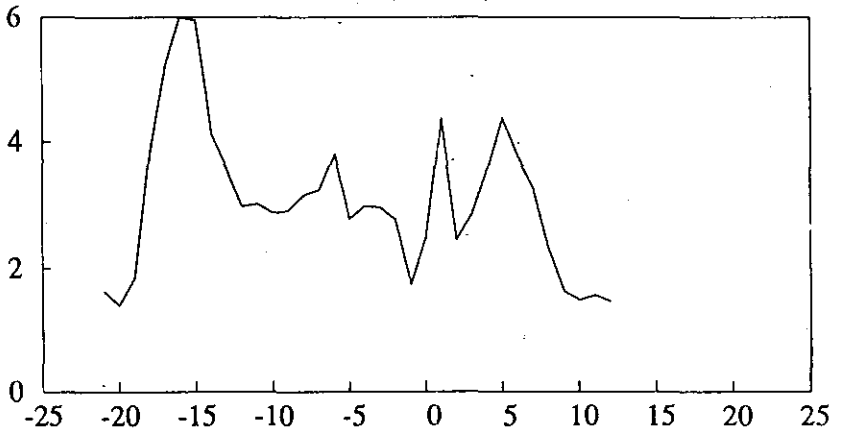

FREMANTLE - PERSIAN GULF
NOV 1985 - DEC 1987

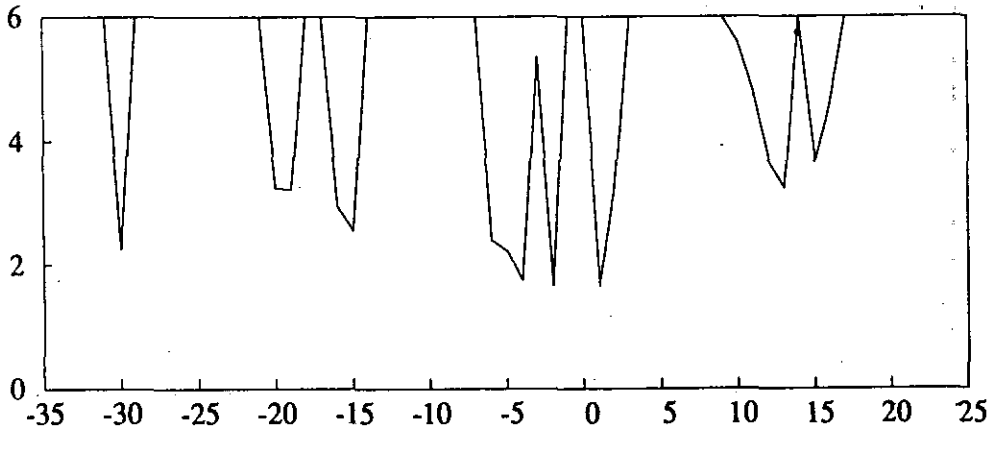

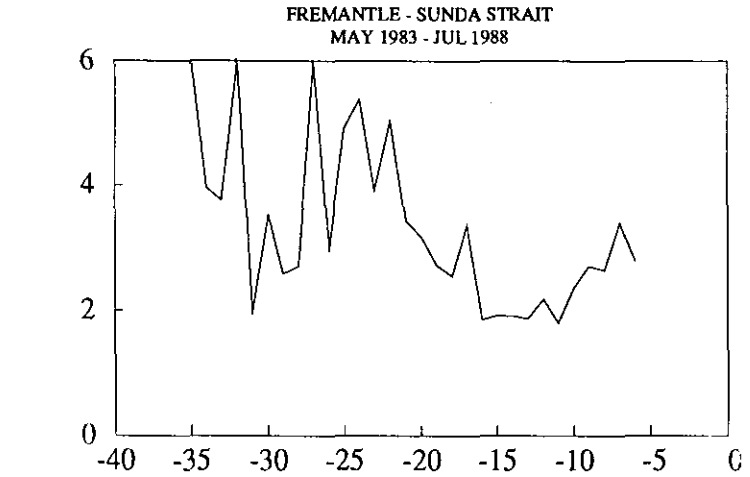

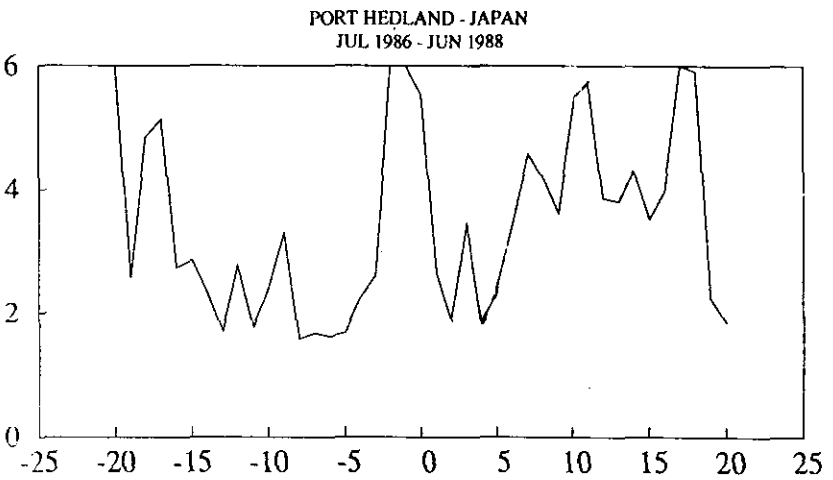

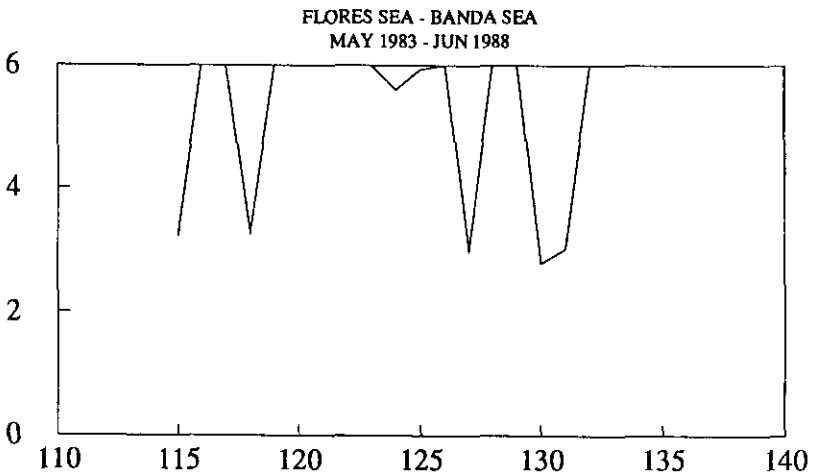

Figure 35A–F: Meridional decorrelation scale of D_{20} on five tracks (A-E) and zonal decorrelation scale of D_{20} on track F, as in Fig. 32.

REUNION - RED SEA
FEB 1985 - FEB 1988

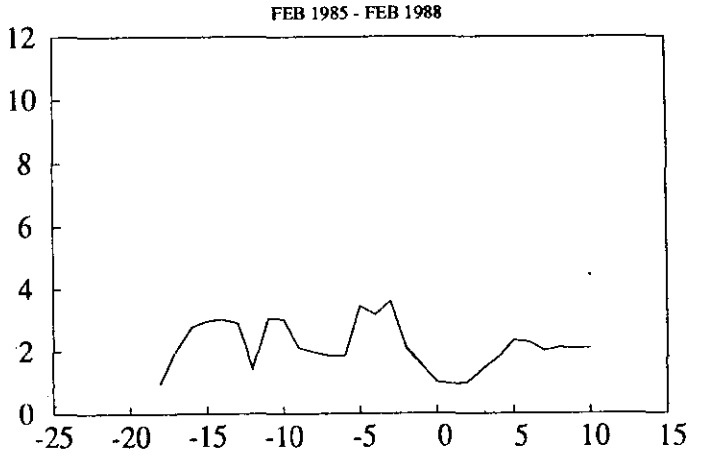

FREMANTLE - RED SEA
AUG 1986 - JUL 1988

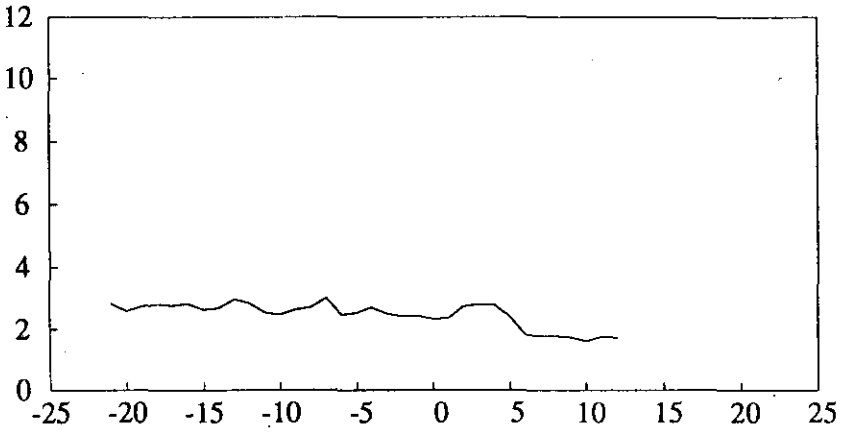

FREMANTLE - PERSIAN GULF
NOV 1985 - DEC 1987

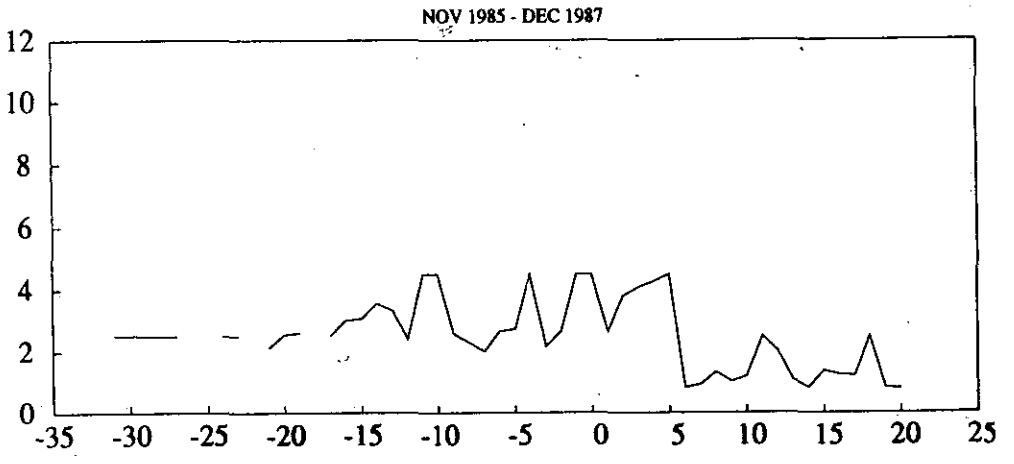

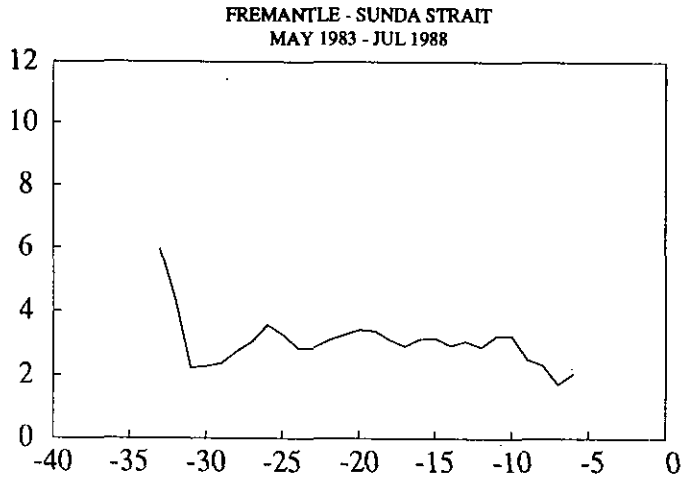

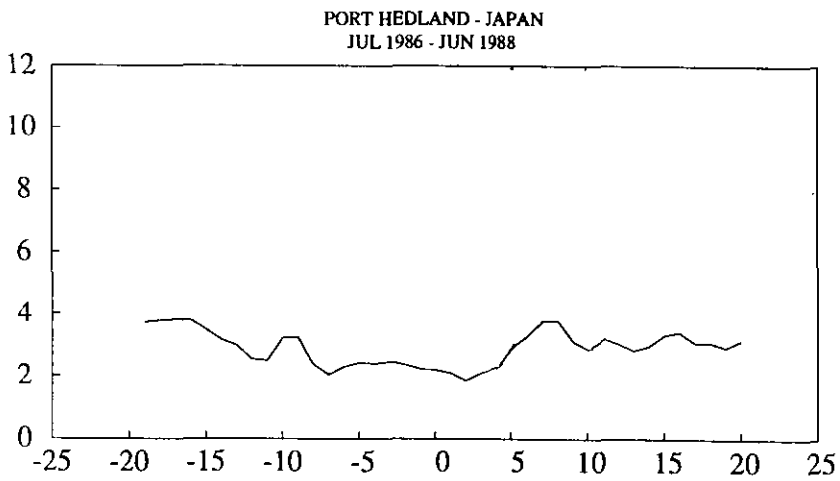

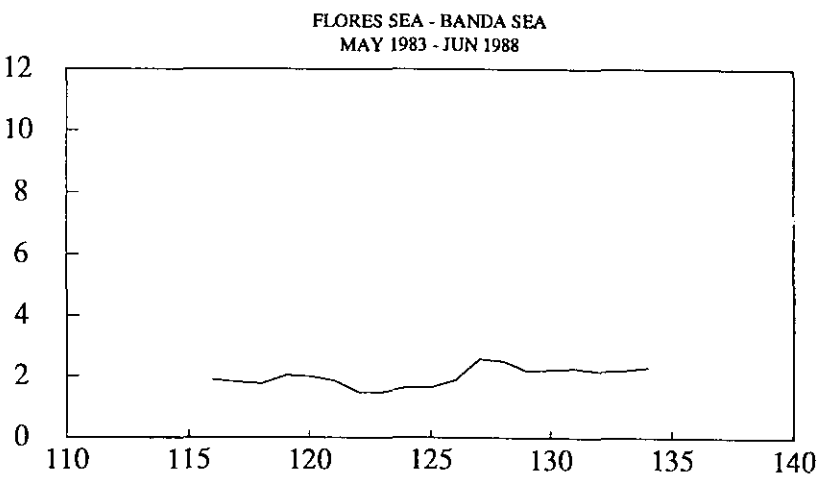

Figure 36A–F: Temporal decorrelation scale of SST on six tracks as in Fig. 32.

REUNION - RED SEA
FEB 1985 - FEB 1988

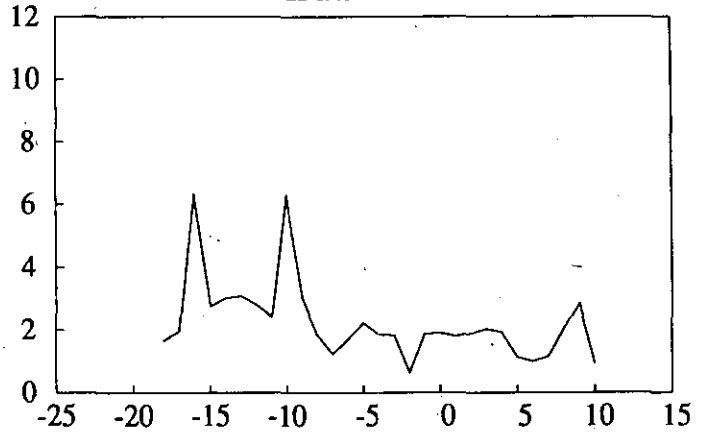

FREMANTLE - RED SEA
AUG 1986 - JUL 1988

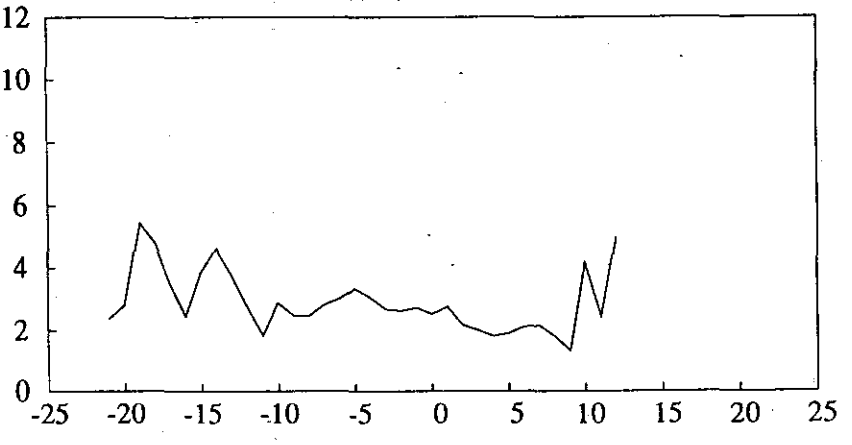

FREMANTLE - PERSIAN GULF
NOV 1985 - DEC 1987

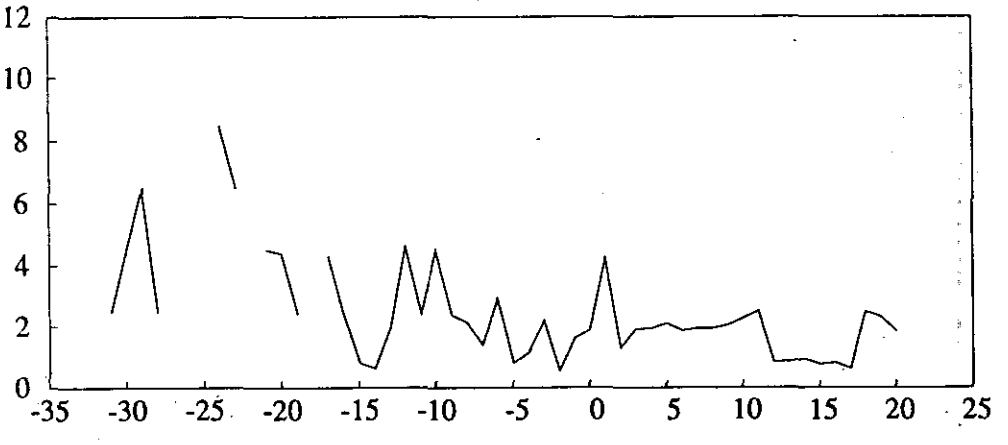

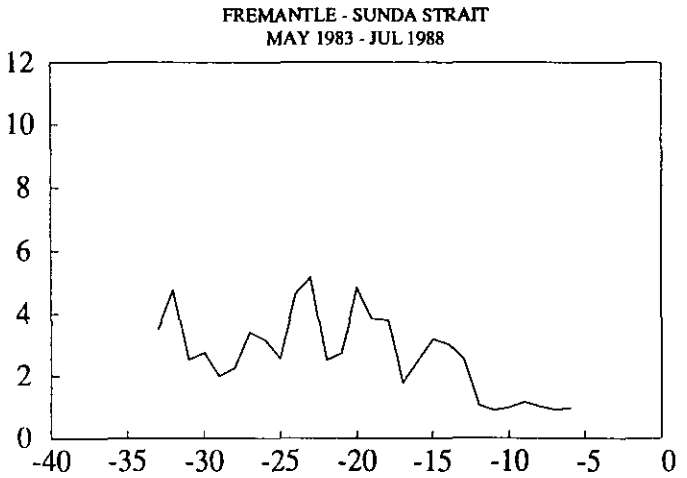

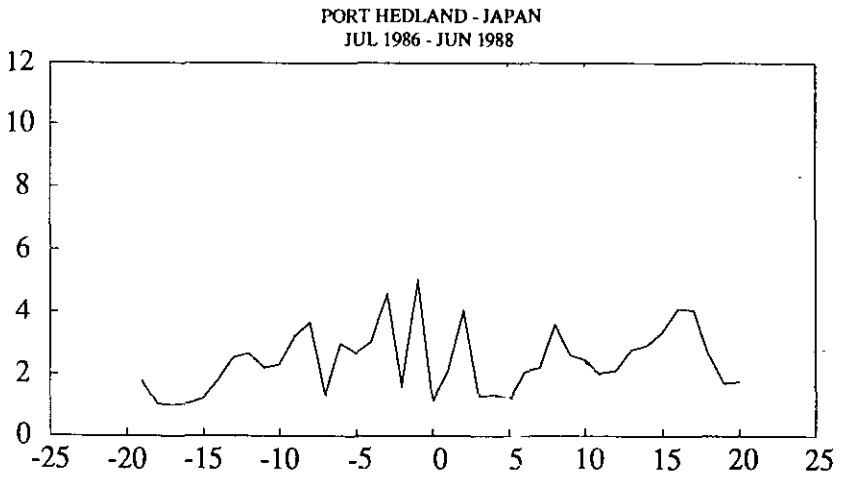

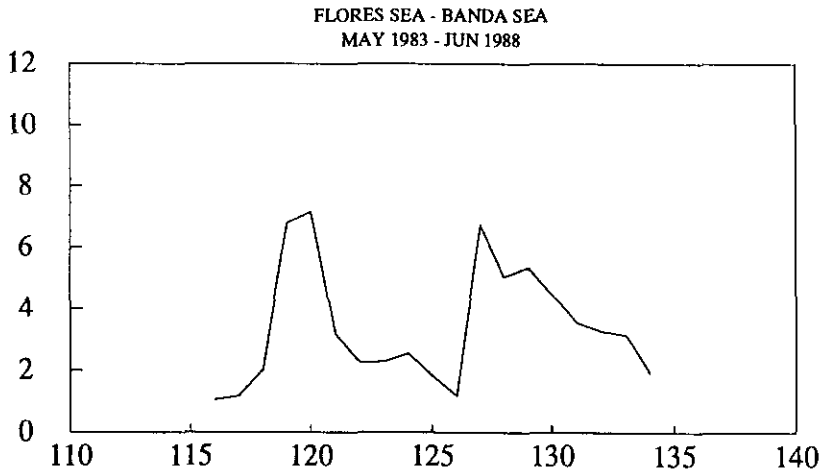

Figure 37A–F: Temporal decorrelation scale of D_{20} on six tracks as in Fig. 32.

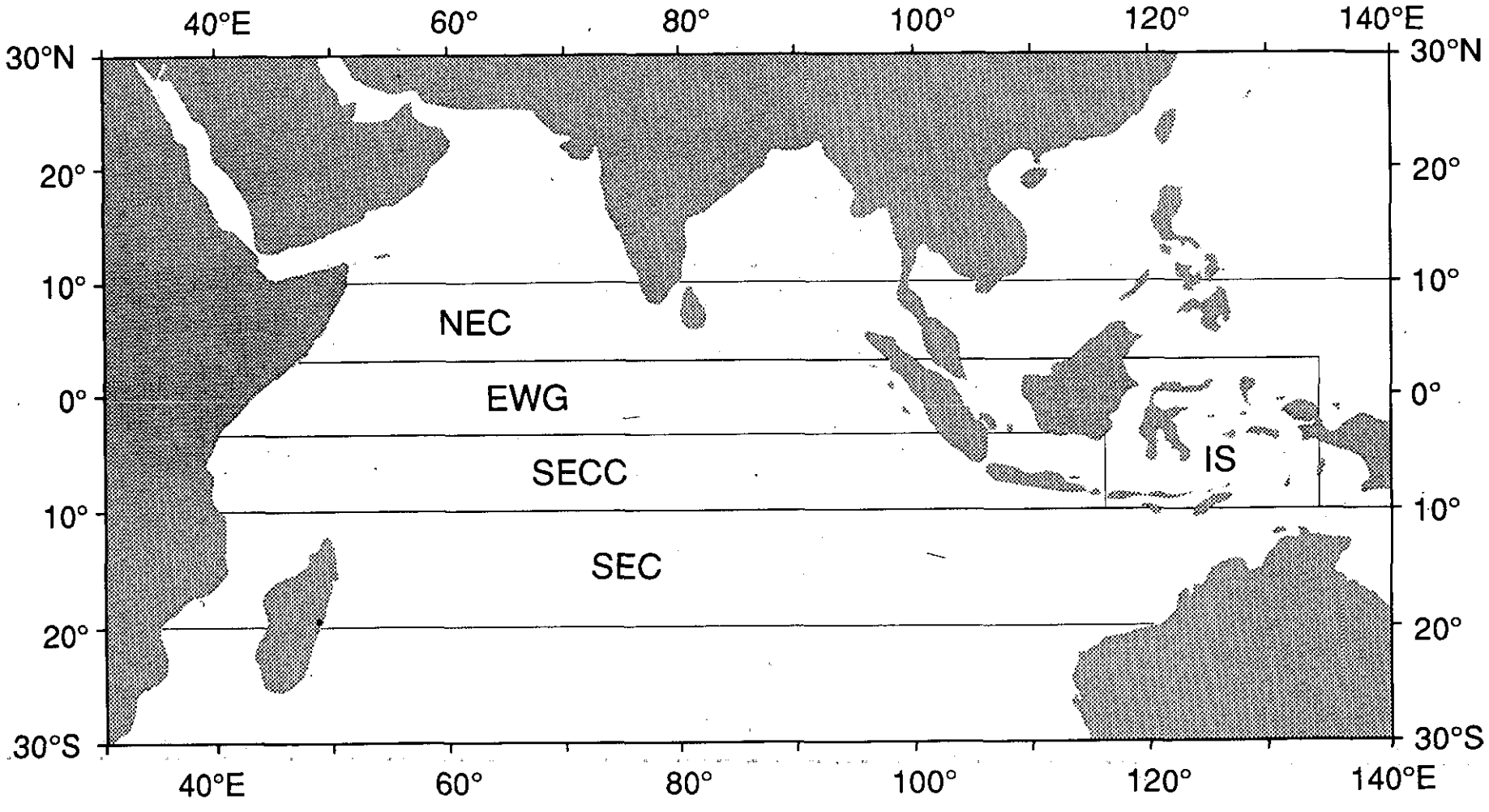

Figure 38: Geographical areas where optimum interpolation statistics were summarised. North Equatorial Current (NEC); Equatorial Wave Guide (EWG); Southern Equatorial Countercurrent (SECC); South Equatorial Current (SEC).

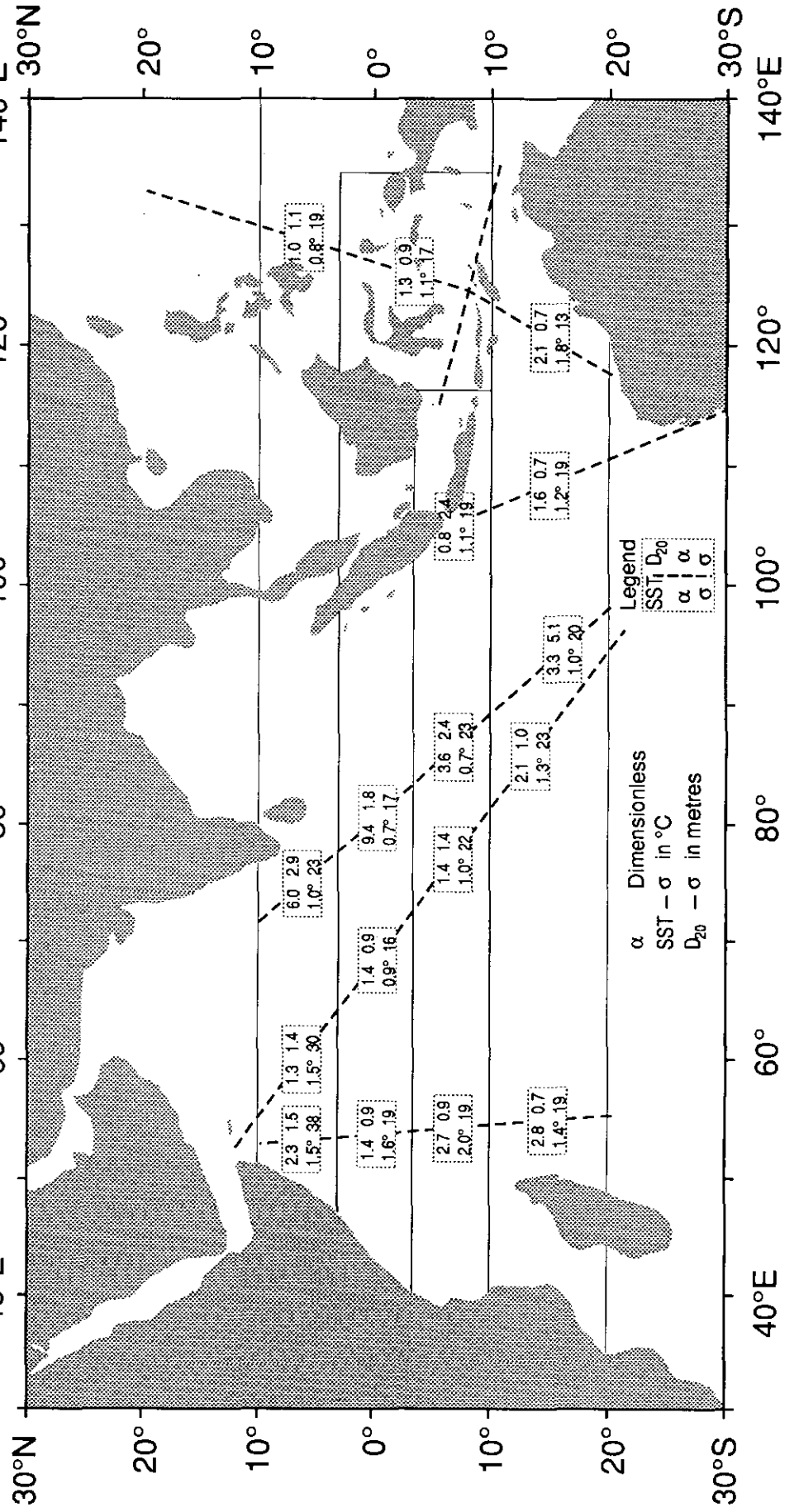

Figure 39: Signal to noise ratio (α), and standard deviation (α). Values for sea surface temperature (SST) and depth of 20°C isotherm (D_{20}) as in legend.

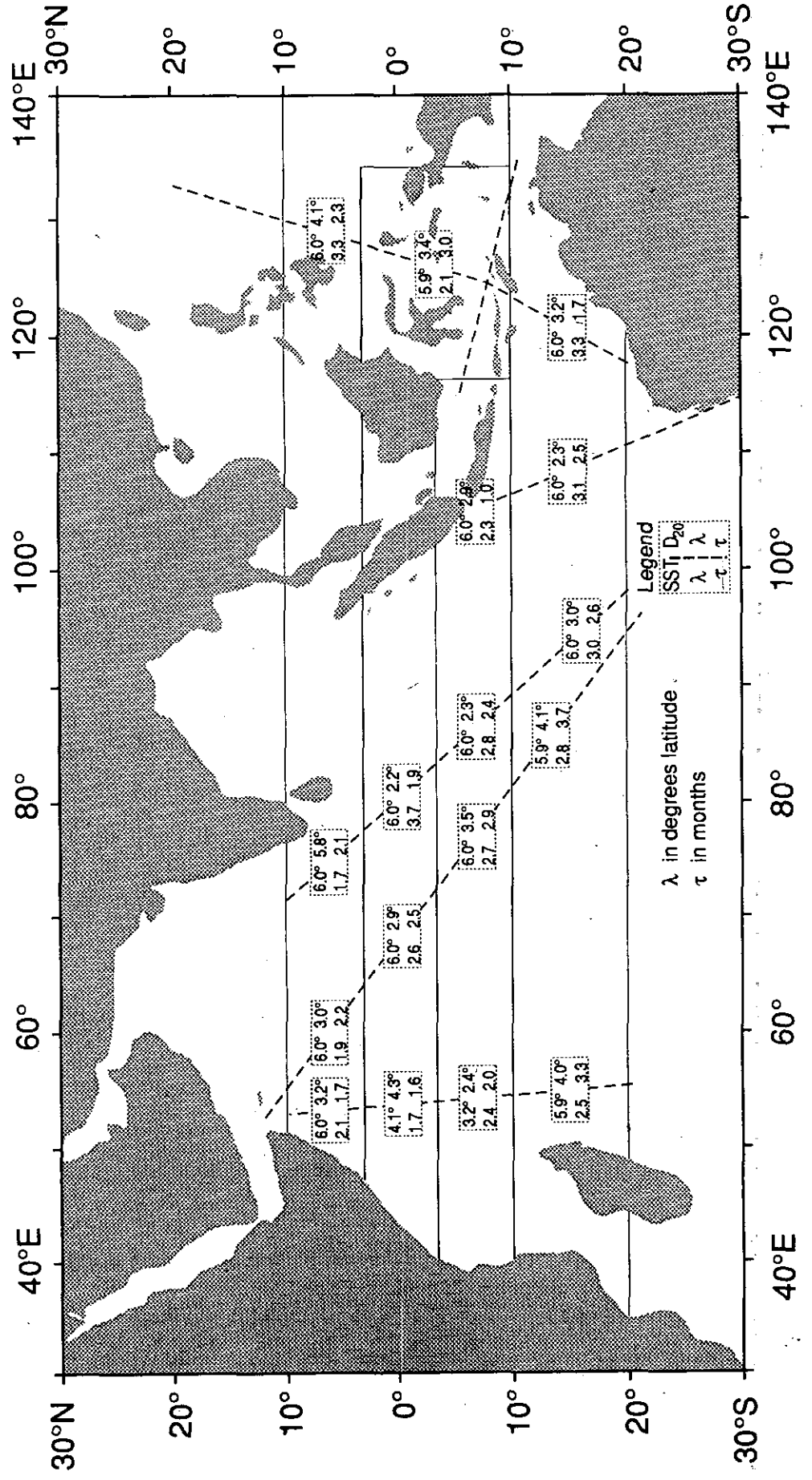

Figure 40: Meridional and temporal decorrelation scales, as in Fig. 39.

CSIRO Marine Laboratories
comprise

Division of Oceanography
Division of Fisheries

Headquarters
Castray Esplanade, Hobart, Tasmania
GPO Box 1538, Hobart, Tas 7001, Australia

Queensland Laboratory
133 Middle Street, Cleveland, Qld
PO Box 120, Cleveland, Qld 4163

Western Australian Laboratory
Leach Street, Marmion, WA
PO Box 20, North Beach, WA 6020

ISBN 0 643 05033 7